

Computer Simulations for Hydrogen Loaded Palladium Clusters

Dissertation
zur Erlangung des Doktorgrades
der Mathematisch-Naturwissenschaftlichen Fakultäten
der Georg-August-Universität zu Göttingen

vorgelegt von

Diana Alejandra Marcano Romero

aus

Caracas

Göttingen 2007

D7

Referent:	Prof. Dr. Helmar Teichler
Korreferent:	Prof. Dr. Reiner Kirchheim
Tag der Disputation:	4.07.2007

Contents

1	Introduction	1
2	Molecular Dynamics Simulation	7
2.1	MD procedure	7
2.1.1	Pressure control	7
2.1.2	Temperature control	8
2.1.3	Integration algorithm	9
2.1.4	Force calculations	10
2.1.5	Conservation of momentum	10
2.1.6	Volume calculation	10
2.2	Monte Carlo-Molecular Dynamics (MC-MD) hybrid program	11
2.2.1	MC-MD algorithm	12
2.3	Physical quantities determined through MD and MC-MD simulations	14
3	Theory	17
3.1	Lattice dilatation and volume change of the metal Lattice due to a point defect	17
3.2	Interaction energy of two point defects	20
3.3	Thermodynamical properties of the H-Pd system	22
3.3.1	Energy of a Hydrogen atom dissolved in a metal	23
3.3.2	Chemical potential of Hydrogen in a metal	24
4	Interaction Potentials	29
4.1	Pd-Pd Interaction Potential	29
4.1.1	Embedded Atom Method potential (EAM)	29
4.1.2	Pair potential I (ppI)	30
4.1.3	Pair potential II (ppII)	32
4.2	H-Pd interaction potential	34
4.3	H-H interaction potential	38
5	Simulations of Hydrogen Loaded Pd	41
5.1	Relative Volume Change in Bulk Pd under H Loading	41
5.2	Binding Energy Calculations	42
5.3	H-H Effective Interaction in Pd	49
5.4	Chemical Potential Calculations of H in Pd	50
5.4.1	Testing of the interaction potentials	50
5.4.2	Solubility isotherms and determination of the solubility limit	59
5.4.3	About the distribution of H atoms in the cluster	63
6	Conclusions	69

7	Summary	71
A	Output of the simulation of bulk Pd with H=2. Example	77
B	Fitting of the Interaction Potentials	81
B.1	Fitting of the Pd-Pd 1 st neighbour interaction model.	81
B.2	Fitting of the Pd-Pd 2 nd neighbour interaction model.	83
C	Electron Gas Term	85

List of Figures

1.1	Isotherms of the system PdH bulk and cluster.	4
2.1	Volume of a Cuboctahedral Cluster	11
2.2	MC Algorithm	13
2.3	MC Algorithm	14
3.1	Kanzaki forces and Displacement field at an octahedral site of a fcc lattice	18
3.2	Radial displacements of the Pd nearest neighbours due to a point defect	20
3.3	Volume change (ΔV) due to a dilatation center	20
3.4	Phase diagram of PdH Bulk	22
3.5	Heat of Solution of H in Pd Bulk as a function of hydrogen concentration. Experimental Results	24
4.1	Pd-Pd EAM Interaction Potential	30
4.2	Pd-Pd pair potential I (ppI)	32
4.3	Pd-Pd pair potential II (ppII).	34
4.4	H-Pd (HPd) Interaction Potential	36
4.5	H-Pd modified (HPd _{mod}) Interaction Potential.	37
4.6	Effect of the HPd modified Interaction Potential on the energy contribution per H atom.	37
4.7	Effect of the HPd modified Interaction Potential on the average distance between H and nearest neighbour Pd atoms.	38
4.8	H-H (HH* and HH* _{mod}) Interaction Potentials	39
4.9	H-H (HH**) Interaction Potential.	40
5.1	Relative volume change $\Delta V/V$ of PdH bulk as a function of hydrogen concentration.	42
5.2	Testing sites at a Pd (100) surface.	44
5.3	Lattice constant in the 923-Pd cuboctahedral cluster.	45
5.4	Testing sites in the 923-Pd cuboctahedral cluster.	46
5.5	Site energies in the 923-Pd cuboctahedral cluster.	47
5.6	Binding energy for H in bulk Pd as function of hydrogen concentration.	48
5.7	H-H elastic interaction in bulk at low H concentrations	49
5.8	H-H elastic interaction in cluster at low H concentrations.	50
5.9	Chemical Potential of H in Pd bulk and cluster - I.	51
5.10	HH direct interaction (using HH* _{mod}) as function of hydrogen concentration.	52
5.11	Chemical potential of H in bulk Pd - II.	53

5.12 HH direct interaction (using HH**) as function of hydrogen concentration.	53
5.13 Effect of the modified Interaction Potential HPd_{mod} on the Binding Energy in bulk.	55
5.14 Effect of the HPd modified Interaction Potential on the Direct H-H Interaction in bulk.	55
5.15 Effect of the HPd modified Interaction Potential on the Chemical Potential and the Binding Energy in bulk.	56
5.16 Chemical potential in bulk and cluster -III.	57
5.17 Fraction of empty bulk- and surface-like sites and site energies in the cuboctahedral cluster as a function of the H concentration.	58
5.18 Binding Energy of H in Pd bulk and cluster using the HPd modified interaction potential.	58
5.19 Vibrational Contribution of the Chemical Potential μ_H in bulk.	59
5.20 Solubility Isotherm of H in Pd in bulk and cluster at low Hydrogen concentrations at 300 K- Experiment.	60
5.21 Solubility Isotherm of H in Pd in bulk and cluster at low Hydrogen concentrations at 300 K.	61
5.22 Sievert's law in Pd in bulk and cluster at 300 K.	62
5.23 Chemical Potential of H in Pd bulk and cluster IV. Maxwell Construction	62
5.24 Energies of the possible configurations in the cluster with $N=5H$	63
5.25 H distributions in cluster. Possible configurations with $N_dH=5$	65
5.26 Fraction of occupied bulk- and surface-like sites in cluster as a function of the H concentration.	66
5.27 H distributions in cluster. Possible configurations with $N_H=230$	67
B.1 Sketch of the pair potential between two metal atoms.	82
C.1 Energy contribution provided by the electron gas term in PdH as a function of hydrogen concentration.	86
C.2 Cohesion energy of PdH bulk as a function of hydrogen concentration.	87

List of Tables

2.1	Berendsen Scaling	8
3.1	Green functions for the fcc lattice	19
3.2	Elastic data for Pd.	19
4.1	Experimental Quantities for bulk Pd	31
4.2	Pd-Pd ppI Interaction Potential parameters	31
4.3	Basic Properties of Bulk Pd described by the ppI potential	32
4.4	Pd-Pd ppII Interaction Potential parameters	34
4.5	Experimental Bulk H-Pd Quantities	35
4.6	H-Pd Interaction parameters	35
4.7	Basic Properties described by the H-Pd Interaction potential	36
4.8	HPd modified Interaction parameters for the ppI interaction model	38
4.9	H-H Interaction parameters for the ppI interaction model.	39
5.1	Binding Energy E_b calculations of H in Pd at a Pd (100) Surface.	43
5.2	Pd (100) Surface Relaxation	44
5.3	Basic Properties of the Pd Cluster described by the ppI potential	45
5.4	Binding Energy E_b calculations in a 923-Pd Cuboctahedral Cluster	48
5.5	H-H interaction in Pd clusters	50
5.6	Chain and shell like H distributions in cluster	66
B.1	Number of Neighbours per shell in the fcc lattice	81

Chapter 1

Introduction

Hydrogen dissolved in metals is a widely studied system due to some particular phenomena found in these hydrides. There is a large solubility of hydrogen in a number of metals, like Pd or Nb, V and Ta, where the H concentration can achieve 100% or more, indicating the formation of a metal mono-hydride. This makes that hydrogen-metal systems are studied as models for mobile energy storage devices, since hydrogen release from the hydride and subsequent oxidation sets free a large amount of energy for further use, e.g. for acceleration of vehicles, like cars or air-crafts [Sch88].

A further peculiarity of hydrogen in metals is its large mobility, which is a necessary prerequisite for energy storage applications, as it allows rapid storage and detracting of hydrogen from the metal hydrides. This large mobility turned out an interesting question by its own, as it is related to quantum mechanical features of hydrogen in metals, that is tunnelling between adjacent positions rather than thermally overcoming the separating potential barriers.

A third point is that hydrogen, in case of large solubility in metals, can be considered as a lattice gas. It is a *lattice* gas, since the hydrogen atoms reside in a space structured by the metallic lattice, and it is a *gas*, since the hydrogen atoms are free to move and to establish the equilibrium distribution in space. While the dynamics of the hydrogen atoms play a minor role for the lattice gas aspects (assuming that the mobility is large enough to establish the equilibrium partition), major contributions come from the local deformations of the lattice holes by the embedded hydrogen atoms, and from the interaction among the H atoms. These indirect and direct coupling between the hydrogen atoms make that the lattice gas can undergo phase transformations, form two-phase mixtures, etc. [Pei78, Fuk04].

The present study considers these lattice gas aspects of hydrogen in metals, where in particular hydrogen in palladium is investigated, and where the main focus is laid on establishing a formal treatment that allows to describe the lattice gas system in case of reduced dimensions, especially in clusters.

Hydrogen (H) dissolves interstitially in bulk fcc-Palladium (Pd) occupying octahedral sites. An H-atom causes local displacements of the Pd atoms from their regular sites. Up to concentrations $x = 0.008 \text{ H/Pd}$ (α phase) there is a continuous macroscopic volume change $\Delta V/V = 0.19 \cdot x$ [Pei78]. At higher x concentrations, the relative volume change is $0.2 \cdot x - 0.0493 \cdot x^2$ [FGG86]. Isotherm p - x curves at different temperatures show that at low concentrations x the amount of absorbed hydrogen is proportional to the square root of the external hydrogen gas pressure. At $x = 0.008 \text{ H/Pd}$, a 'plateau' appears indicating an existence of a miscibility gap where the phases α and α' coexist. At $x \approx 0.6 \text{ H/Pd}$ the curve raises sharply, indicating the entrance into

the α' regime. A special peculiarity is the asymmetry of the isotherms in x and $1 - x$.

A central question in earlier times was the reproduction and interpretation of the p - x isotherms. The first approach is due to LACHER [Lac37]. He derived a theoretical equation containing a term such that the derived isotherm reached a solubility limit at a determined composition ($x = 0.59$). The equation can be derived by assuming that the entropic part of the hydrogen free energy can be modelled by the ideal solution approximation and that the energetic part is due to a finite solution energy for the dilute hydride and an attractive hydrogen-hydrogen interaction. It has the form:

$$k_B T \ln \sqrt{\frac{p}{p_o}} = \mu_H = k_B \ln \frac{x}{x_o - x} + (\kappa_2 - \kappa_1 x) \quad (1.1)$$

LACHER uses $x_o = 0.59$ and proves that the properly selection of the parameters κ_1 and κ_2 , allows to reproduce fairly well the $p - x$ isotherm up to $x = 0.59$.

GRIESSEN ET AL [FGG86] use this model with $x_o=1$ but they assume that there is in the chemical potential an additional term due to the increased number of electrons in the PdH system with increased H content. In a rigid band model, the additional electrons fill up the band structure of the material. Also they carried out p - x isotherm measurements above the critical point, as well as in the α and α' phase regions at lower temperatures in Pd bulk. They obtained the following form for the heat of solution

$$\Delta H(x) = -0.066 - 0.549 \cdot x + 0.487 \cdot x^2. \quad (1.2)$$

GRIESSEN ET AL [GD84] found empirically that the heat of formation of binary hydrides is related to the characteristic electron band energy parameter ΔE ,

$$\Delta H(x) = \frac{n_s}{2}(\alpha \Delta E + \beta) \quad (1.3)$$

where $\Delta E = E_F - E_S$. E_F is the Fermi energy, E_S is the center of the host metal electronic band with a strong s character at the interstitial sites occupied by hydrogen, n_s is the number of electrons per atom in the lowest s -like conduction band of the host metal, and α and β are constants. Eq. (1.2) was interpreted using the semiempirical band structure model for the heat of formation, and the hydrogen concentration dependence of $\Delta H(x)$ can be written as [FGG86],

$$\frac{d\Delta H(x)}{dx} = \frac{-B(x) \cdot V_H^2(x)}{V_m(x)} + \frac{\alpha}{N(E_F(x))} \quad (1.4)$$

where $B(x)$ is the bulk modulus, $V_H(x)$ is the partial volume of hydrogen, $V_m(x)$ is the volume of the host metal, α is an empirical constant and $N(E_F)$ is the density of states in PdH_x above the Fermi level in pure Pd. The first term of the RHS of Eq.1.4 is called the elastic contribution and the second term is called the electronic contribution, because it describes the rise of E_F due to the extra hydrogen electrons. The sign reversal that Eq.1.2 shows at $x \approx 0.55$ is a result of the filling of d -band states. Also the reduction of the elastic term at higher concentrations is equally important.

With a thermodynamical analysis, FLANAGAN [FL75], using the p - x isotherm measurements of WICKE AND NERNST [WN64], calculated the heat of solution ΔH of hydrogen in palladium, derived from $d(\ln(\sqrt{p})/d(1/T))$ as function of x and obtains also a dependency similar as the one from GRIESSEN ET AL.

SALOMONS [Sal90] carried out atomistic computer simulations for the bulk PdH system with a set of interaction models proposed by GILLAN [Gil86]. This set describes the Pd-Pd interaction with a sixth order polynomial yielding an equilibrium lattice constant of $a=4.0 \text{ \AA}$ for pure Pd, a H-Pd first neighbour model fitted to reproduce the frequency of hydrogen in Pd and an H-H first neighbour interaction repulsive model, which predicts that nearest neighboring (N) H atoms, interact through $V(N_{\text{distance}})=0.005 \text{ eV/pair}$. Using Widom's method [Wid63] within a molecular dynamics simulation, he determined for the bulk PdH system μ_{H} at 600, 800 and 1000 K. His calculation was based on the formalism of WAGNER AND HORNER [Pei78] which is a statistical model that assumes that the entropic part of the hydrogen free energy can be modelled by the ideal solution approximation and that the energetic part is due to a finite solution energy for the dilute hydride, the vibrational energy contribution and an attractive hydrogen-hydrogen described with the mean field approximation, that is:

$$\mu_{\text{H}} = E_{\text{b}} + u_{\text{elastic}} + u_{\text{directHH}} + k_{\text{B}}T \ln \frac{x}{1-x} + \mu_{\text{vib}} + pV_{\text{H}} \quad (1.5)$$

From the μ_{H} calculation at 600 K, the presence of a α - α' phase transition was established. However, using these interaction models, at a constant concentration x , μ_{H} increases with decreasing temperature, contrary to experimental results. This discrepancy was attributed to the missing electronic band structure effects. After obtaining μ_{H} from the MD simulation, assuming values for μ_{vib} , $-k_{\text{B}}T \cdot \ln(x/1-x)$, pV_{H} and u_{directHH} (in the mean field approximation), $E_{\text{b}}+u_{\text{elastic}}$ was estimated and resulted in discrepancy to the model of WAGNER AND HORNER [Pei78].

In PdH_{*x*} clusters, *p-x* isotherm measurements [Sul03, SA01a] indicate that in the α phase region, the solubility is enhanced compared to bulk Pd. There also exists a two-phase region, which is narrowed compared to bulk. The two phase field region has a plateau with a small slope. The assumption of additional occupation of surface and subsurface sites explains the enhanced solubility in the α phase. It also explains, the narrowing of the miscibility gap. The pressure of the miscibility gap is the same in bulk and in cluster, indicating that bulk-like sites in cluster are similar to sites in bulk. The slope cannot be explained so far. A sketch of the isotherm curves of bulk and cluster is shown in Fig. 1.1, to illustrate the difference between the two curves.

CALVO AND CARRE [CC06] investigated the hydrogen loading of 147 atoms Pd cluster (and bulk Pd) by molecular dynamics and monte carlo calculations. They use the Pd-Pd interaction potential from REY ET AL [RGGR⁺93] and the H-H, H-Pd interaction potentials taken from the work by TOMANEK ET AL [TSL91]. For pure Pd bulk, they obtain good agreement with the experimental cohesion energy E_{coh} (3.89 eV), however, at an equilibrium lattice constant $a=3.6 \text{ \AA}$ which is nearly 10% lower than the experimental value. By introducing single H atoms, they determine the binding energy E_{b} , of hydrogen in palladium as $E_{\text{b}}=-2.413 \text{ eV}$. In their work, the PdH cluster was investigated using a cuboctahedral and an icosahedral structure with 147 Pd, aimed at studying structural changes under hydrogen loading. They used a combined monte carlo-conjugate gradient local minimization procedure. For both clusters there is a hydrogen concentration by which E_{b} has a minimum value. It is to be observed that for finite x concentration, they use Eq. 3.33 instead of Eq. 3.36 for the binding energy calculations. In the MC calculations, they use a rigid Pd structure, neglecting the lattice relaxation when inserting hydrogen atoms. This means a rather severe approximation, as the energy gain due to the relaxation is large compared with $k_{\text{B}}T$.

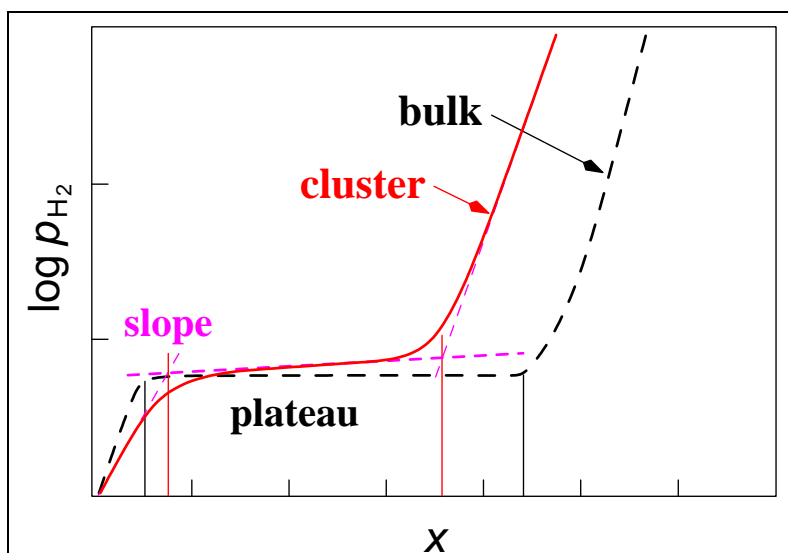


Figure 1.1: Isotherms of the system PdH bulk and cluster. It is shown the differences of the isotherm curves in bulk and cluster.

In the present work, the central aspect is the use of a novel expression for the chemical potential of H in bulk Pd and in clusters, which is a straightforward result from the partition function of the system and follows from an extension of Widom's [Wid63] particle insertion method. The novel expression has the simple form of a phenomenological approach that uses the ideal solution model for the configuration entropy part for the chemical potential, it involves an interaction expression for the coupling between the particles, and it contains a vibration part, i.e.,

$$\mu_{\text{H}} = k_{\text{B}}T \ln \left(\frac{x}{1-x} \right) + \langle \epsilon(x) \rangle + \mu_{\text{vib}} \quad (1.6)$$

The quantity $\langle \epsilon(x) \rangle$ is well defined from basic statistical physics and is accessible to numerical computation within a hybrid monte carlo - molecular dynamics (MC-MD) procedure. It involves direct hydrogen-hydrogen interactions, the deformations of the lattice by the absorbed hydrogen atoms and, in particular, the energy gain from lattice relaxation, the so-called self-trapping energy from the dilute hydrogen limit up to large hydrogen concentrations. The main approximation in the derivation of $\langle \epsilon(x) \rangle$ lies in the neglect of transition state (that means saddle point) contributions to the equilibrium partition function of the system. The used approach is applicable to all kinds of crystalline homogeneous substitutional and interstitial alloy systems, also to spatially structured arrangements with internal or external boundaries, and to systems with reduced dimensions like layer-structures or clusters. In the present work it will be used to analyse aspects of the chemical potential of hydrogen in bulk Pd and in a 923 Pd-atoms cuboctahedral cluster, where the latter question combines the statistical mechanics of a many-body system with the problem of spatially varying site energies.

This work is organized as follows: In chapter 2, an introduction to molecular dynamics and monte carlo simulations is given, together with their implementation to the calculations made in this work. In chapter 3, a brief description of the elastic interaction of the H atoms in the metal is presented and its relationship to the relative volume change under H loading, which is important for the development of the H-Pd interaction potential. Also there are presented thermodynamical properties of the

system PdH bulk, such as the free energy F and the chemical potential of H in the metal, μ_{H} . Chapter 4, describes the interaction models used in this work. For the Pd-Pd interaction several models were tested, which include a first, second or third shell of neighbours. The H-Pd interaction is a first neighbour model. For the H-H interaction model, a next neighbour model and next nearest neighbour model are compared. In chapter 5, results of the simulations in PdH-bulk and PdH-cluster are presented, compared with the experimental results, and discussed. Finally, in chapter 6, conclusions are given.

Chapter 2

Molecular Dynamics Simulation

In this work the binding energy (E_b) and the chemical potential (μ_H) of H in a Pd cluster are determined, using a molecular dynamics (MD) simulations and a combined monte carlo - molecular dynamics (MC-MD) approach, respectively. The present chapter (section 2.1) explains the basic concepts involved in a MD simulation and the steps used. Section (2.2) describes the main elements of the MC-MD procedure.

2.1 MD procedure

By the MD method [AT87, FS05, Rap04] the trajectories $\vec{r}_i(t)$ of atoms i are determined by means of numerical integration of Newton's equations:

$$m_i \cdot \ddot{\vec{r}}_i = \vec{f}_i \quad (2.1)$$

where the total force \vec{f}_i acting on the atom i is determined from the potential energy $U(r_1, \dots, r_N)$ between atom i and the other j particles in the system as:

$$\vec{f}_i = -\vec{\nabla}_i V(r). \quad (2.2)$$

Newton's third law implies that $\vec{f}_{ji} = -\vec{f}_{ij}$. So each atom pair needs to be examined only once. The numerical integration is done with a Predictor-Corrector algorithm of 5th order where the integration step was chose to resolve the thermal vibrations of an atom with mass m_i and frequency ω . The simulations were performed in an NPT ensemble (number of particles (N), pressure (P) and temperature (T) constant).

2.1.1 Pressure control

At each integration step the pressure in the system is calculated through the atomic virial (v) expression:

$$v = -\frac{1}{3} \sum_i \sum_{j>i} \vec{r}_{ij} \cdot \vec{f}_{ij}(r), \quad (2.3)$$

and the instantaneous pressure P_i is:

$$P_i \cdot V = v + \frac{N \cdot 2 \cdot E_{\text{kin}}}{3}, \quad (2.4)$$

Table 2.1: Parameters used by the Berendsen Scaling. Time constants for the Berendsen thermostat and barostat are shown. Instead of using the isothermal compressibility the ratio C/τ_P was adjusted together with τ_{T1} and τ_{T2} to deliver a faster relaxation of the system. τ_{T1} (H) and τ_{T2} (Pd) are chosen different because of the different masses of the atoms.

C ($\text{\AA}^3/\text{eV}$)	τ_P (fs)	τ_{T1} (fs)	τ_{T2} (fs)
0.000046	0.02	10	100

where V is the volume and E_{kin} is the total kinetic energy of the system. The instantaneous pressure P_i is used afterwards to scale the box length (Box) and the position (\vec{r}_i) of the atoms. In the MD simulations the scale factor λ_P is

$$\lambda_P = \frac{(P_i - P_d)\xi + Box}{Box}, \quad (2.5)$$

where ξ is a friction coefficient and in this work the value $\xi = 1/100 \text{ \AA}^4/\text{eV}$ was used. If λ_P is < 0.99 , λ_P is set to 0.99. If λ_P is > 1.01 , λ_P is set to 1.01. In this way λ_P is chosen close to 1. For a current integration step:

$$Box_{\text{current}} = Box_{\text{previous}} \times \lambda_P \quad (2.6)$$

and

$$\vec{r}_i = \vec{r}_{i,\text{previous}} \times \lambda_P, \quad (2.7)$$

where the index *previous* stands for a previous integration step.

For the MC-MD simulations the Berendsen barostat [BPvG⁺84] was used. In this case the scale factor λ_P is given by:

$$\lambda_P = \left[1 + \left(\Delta t \frac{C}{\tau_P} \right) \cdot (P_i - P_d) \right]^{1/3} \quad (2.8)$$

where Δt is the integration step, C is the isothermal compressibility of the system and τ_P is a time constant. The values used in this work are given in table 2.1. τ_P controls how fast the desired P_d is achieved. Afterwards the box length and the atomic positions are given by Eq. (2.6) and Eq. (2.7).

2.1.2 Temperature control

At each integration step an instantaneous temperature (T_i) is calculated through the kinetic energy E_{kin} of the system

$$\frac{3}{2}k_B T_i = \frac{1}{N} \sum_{i=1}^N \frac{1}{2} m_i \cdot \dot{r}_i^2. \quad (2.9)$$

The temperature is maintained constant rescaling the velocities of each atom. In the MD simulations this was done by using a simple rescaling where the scale factor λ_T is given by

$$\lambda_T = \sqrt{T_d/T_i}, \quad (2.10)$$

where T_d is the desired simulation temperature and T_i is calculated using Eq. (2.9). The velocities in the current integration step ($\vec{v}_{i,\text{current}}$) are rescaled as

$$\vec{v}_{i,\text{current}} = \vec{v}_{i,\text{previous}} \times \lambda_T, \quad (2.11)$$

where the index *previous* stands for a previous integration step.

In the MC-MD simulation a Berendsen thermostat was used. In this thermostat the scale factor is given by

$$\lambda_T = \sqrt{\left[1 + \left(\frac{\Delta t}{\tau_T}\right) \cdot \left(\frac{T_d}{T_i} - 1\right)\right]}, \quad (2.12)$$

where Δt is the integration step and τ_T is a constant which describes the strength of the coupling of the system to a hypothetical heat bath. The larger τ_T the weaker the coupling and it takes longer to achieve a given T_d after a previous T_i . The values used are given in table 2.1. Since the H and Pd atoms have masses in a ratio $\approx 1:100$, the values of τ_T were chosen different for each atom type. Afterwards the velocities were scaled according to Eq. (2.11).

2.1.3 Integration algorithm

The simulation program used in this work was already available in the group and it was written in Fortran 77. It was modified in order to include the interaction potentials, the Berendsen scaling, to account for surface effects, to include a MC procedure and to calculate after a given number of integration steps physical quantities with the corresponding fluctuations. The program was structural rearranged in order to optimize the simulation time.

As mentioned before, the equations of motion are solved numerically by means of a modified Predictor-Corrector algorithm [Tei96, Rap04]. The algorithm is called predictor-corrector because it makes use of information computed at earlier time step. The goal is to solve the second order differential equation:

$$\ddot{x} = g(x, \dot{x}, t) \quad (2.13)$$

The predictor step $P(x)$ for time $t+\Delta t$ is an extrapolation of values computed at earlier times t , that is

$$P(x) : x(t + \Delta t) = x(t) + \Delta t \cdot \dot{x} + \frac{\Delta t^2}{24} \cdot [19 \cdot \ddot{x}(t) - 10 \cdot \dot{x}(t - \Delta t) + 3 \cdot \ddot{x}(t - 2\Delta t)]. \quad (2.14)$$

With this predictor value $x(t + \Delta t)$ the forces on the individual atoms -and therefrom $\ddot{x}(t + \Delta t)$ - are calculated and corrected values for $x(t + \Delta t)$ are determined through

$$C(x) : x(t + \Delta t) = x(t) + \Delta t \cdot \dot{x} + \frac{\Delta t^2}{24} \cdot [3 \cdot \ddot{x}(t + \Delta t) + 10 \cdot \ddot{x}(t) - \ddot{x}(t - \Delta t)], \quad (2.15)$$

$$C(\ddot{x}) : \ddot{x}(t + \Delta t) = \ddot{x}(t) + \frac{\Delta t}{12} \cdot [5 \cdot \ddot{x}(t + \Delta t) + 8 \cdot \ddot{x}(t) - \ddot{x}(t - \Delta t)]. \quad (2.16)$$

2.1.4 Force calculations

Interaction potentials such as tight binding potentials (TB), embedded atom method (EAM) and Finnis- Sinclair potentials (FS) have similar analytical forms:

$$U_{\text{TOT}(i)}(r) = \sum_{j \neq i} U_{\text{P}}(r) + U_{\text{N}(i)}(r), \quad (2.17)$$

where the contribution of atom i to the total energy (U_{TOT}) is given by a pair contribution U_{P} and a many body term (or local density) given by U_{N} . The many body term is a nonlinear function of the separation r between atoms and it is generally written as:

$$U_{\text{N}(i)} = -C \cdot \sum_{j \neq i} \sqrt{\rho_i(r)}. \quad (2.18)$$

The total force \vec{f}_i^{TOT} on an atom i derived from this potential is:

$$\vec{f}_i^{\text{TOT}}(r) = - \sum_{j \neq i} \left[\frac{\partial}{\partial r} U(r) - \frac{C}{2} \frac{\partial}{\partial r} (\rho_i^{1/2} + \rho_j^{1/2}) \right] \cdot \frac{\vec{r}}{r}. \quad (2.19)$$

In the case of simple pair potentials where only the pair contribution U_{P} is available the force is calculated as:

$$\vec{f}_i^{\text{TOT}}(r) = - \sum_{j \neq i} \left[\frac{\partial}{\partial r} U(r) \right] \cdot \frac{\vec{r}}{r}. \quad (2.20)$$

In a MD simulation the most time consuming part of each integration step is the force calculation. In order to reduce the amount of work required for the interaction and force calculation, a neighbours list was used in order to restrict the force calculations to atom pairs with relevant interactions. This list was updated every 10 integration steps. The cutoff radius of the neighbours list was chosen different for each interaction potential. It was set to $\approx 1.5 \times$ cutoff radius of the interaction.

2.1.5 Conservation of momentum

In the absence of external forces at each integration step and after the corrector step the total momentum of the system is set to zero in order to suppress translations of the overall system. In clusters, the periodic boundary conditions are removed and additionally degrees of freedom are introduced, in order to avoid rotations of the system around its center of mass.

2.1.6 Volume calculation

In bulk the usual way to calculate the pressure is using Equation (2.4) where the volume is determined by the box length. In bulk, the volume is calculated with the previous knowledge of the shape of the system. If the simulation cell is cubic then the volume is simply:

$$V = \text{Box}^3 \quad (2.21)$$

There is a difficulty with the concept of volume when simulating a cluster in an NPT ensemble. In the literature, there are given at least four ways to define the volume of a system consisting of N atoms: using the fact that the volume is an

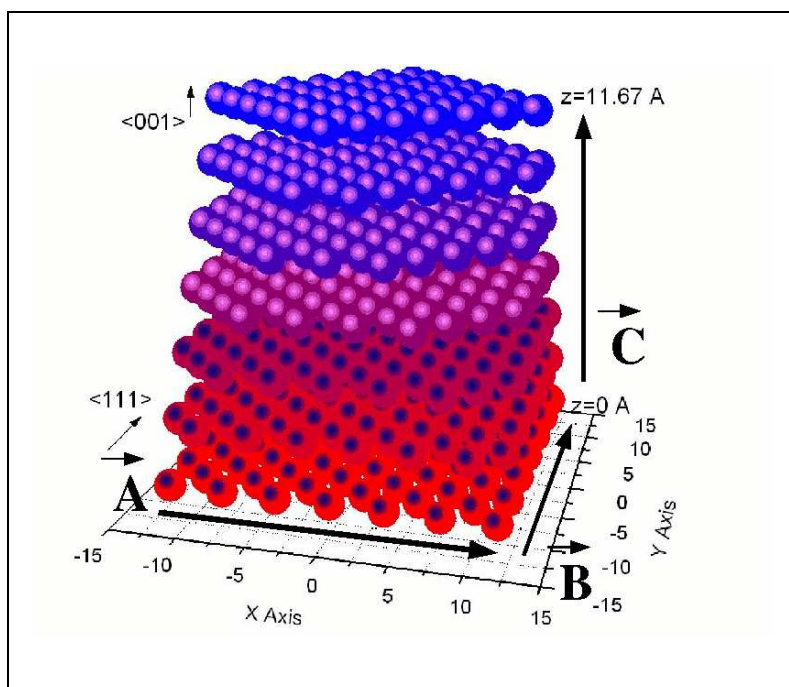


Figure 2.1: Volume of the Cuboctahedral Cluster. It is shown the upper part of a 923 Pd unrelaxed cluster. The length $|\vec{A}|$ of the innermost layer (at $z=0.0$), which has the largest number of atoms, is taken as the *Box* length.

additive quantity which can be written as a summation of the volume of individual atoms [SG02], spherical approximation [CXWB92] where the cluster is assumed to be a sphere of radius R , whose center is defined as the center of mass of all atoms, using a Voronoi cell whose interior consists of all points in 3Dim which are closer to a particular lattice point than to any other [Rap04] and using the convex hull algorithm [BDH96] where the convex hull from a set of points is determined and the volume of this hull is calculated. In this work, due to the simulation temperature used ($T=0.05K$), the cluster does not experience any deformation. Therefore, it was chosen, to take the box length (see figure 2.1) of an unrelaxed cluster as an initial condition. Then at each integration step this box length and the position of the atoms were rescaled according to Eq. (2.8), Eq. (2.6) and Eq. (2.7). In this way no *real volume* is needed for the rescaling of positions. However, in Eq. (2.4) the volume is taken approximately as the scalar triple product of three vectors \vec{A} , \vec{B} , \vec{C} :

$$V = 2 \cdot |\vec{A} \cdot (\vec{B} \times \vec{C})|. \quad (2.22)$$

2.2 Monte Carlo-Molecular Dynamics (MC-MD) hybrid program

In classical statistical mechanics context [AT87], a system of N particles at temperature T will have an average energy $\langle U \rangle$ given by the thermal average of the potential energy $U(\vec{r}_N)$:

$$\langle U \rangle = \frac{1}{Z} \int d\vec{r}^N U(\vec{r}^N) \exp \left[-\frac{U(\vec{r}^N)}{k_B T} \right], \quad (2.23)$$

where Z is the partition function and the integral concerns N , that means $3N$ configurational degrees of freedom. Only an extreme small area in the $3N$ -space of energetic favourable configurations contributes to the integral, while most of the space gives only a negligible contribution to the integral due to the large values $U/k_B T$. By the monte carlo procedure with importance sampling such as the Metropolis method, the *main* contributions to the integral are selected by restricting the integral to configurations that have sufficient low energy from the actual configuration. Usually the MC simulations follows the following scheme:

- Choose an atom (or more) at random
- Move it at a random amount and generate by this from a counted configuration a test configuration. The displacement should allow to sample the configuration space as efficiently as possible.
- Calculate the acceptance probability Π caused by the random shift, where

$$\Pi = \exp \left[-\frac{\Delta E}{k_B T} \right], \quad \Delta E = U(\vec{r}^N)_{test} - U(\vec{r}^N)_{old} \quad (2.24)$$

- Accept or reject the test configuration (Metropolis algorithm):
 - If $\Delta E < 0$, accept the test configuration and count it as the new configuration
 - If $\Delta E > 0$, accept the test configuration if a random number between 0 and 1 is smaller than Π
 - Otherwise, reject the test configuration, count the old configuration once again and choose new test configuration
- Repeat many times for making averages. Averaging over the counted configurations means an ensemble average with canonical probability $\exp(-U_i/k_B T)$ of the configurations.

In this work, a hybrid Monte Carlo procedure was used. Each MC step is followed by a 5000 MD steps. Instead of moving an atom, different configurations α with N_H H atoms were generated. With this procedure one move in the configuration space consists in integrating the system (MD part) through phase space for a fixed time. After this using the metropolis algorithm the configuration is accepted or rejected (MC part). The aim of using a MC procedure is to sample the whole available energy landscape by means of comparing two successive configurations using the metropolis algorithm. In this way different energetic favourable configurations at a temperature T_{MC} will be found, see figure 2.2. We were interested in obtaining statistical averages of energy gains in the system when adding an extra H atom to the already generated MC configurations. In the following section the the whole procedure is explained in detail.

2.2.1 MC-MD algorithm

In what follows, a state α consists of a 923 Pd atoms cuboctahedral cluster (or of 864 Pd atoms in the fcc lattice) and N_H , H atoms randomly distributed over octahedral sites. Different states α corresponds to different random H distributions with the

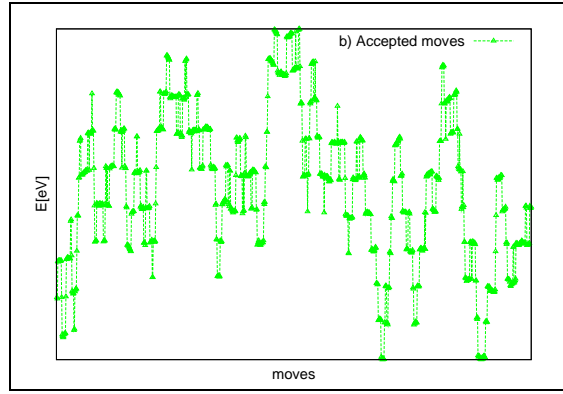


Figure 2.2: MC simulation using the metropolis algorithm. Energetic favourable configurations at a temperature T_{MC} are found. For T_{MC} , different states α corresponding to different H distributions are generated.

same number N_H . Starting with N_H H atoms it is required to generate different states α each with energy E_α . The first part of the algorithm follows the scheme:

- A first state is generated by randomly choosing a number N_H of octahedral sites and setting H atoms at these sites.
- 5000 MD integration steps allows the system to relax at $T_{MD}=0.05$ K. Averages are computed over the last 1000 MD integration steps where E_α is taken as the total potential energy average, over the last steps.
- The metropolis algorithm is used to accept or to reject an α state. In either case a new configuration is generated by choosing randomly one occupied site to be emptied and randomly one empty site to be occupied.
- All the above is repeated. Altogether 1000 MC steps \times 5000 MD steps are carried out.

The energy E_α is the configurational energy of the state which comprises two contributions,

$$E_\alpha = E_{vib} + E_{IE}, \quad (2.25)$$

where E_{vib} is the vibrational energy of all atoms and E_{IE} is the interaction energy contribution. At $T \rightarrow 0$, E_{vib} is negligible and the configurational energy reduces to only the interaction potential contribution.

The second part of the algorithm consists of obtaining the energy gain, from adding one extra H atom to the system. The following scheme is performed:

- We chose 10 $X_{N_H}^\alpha$ configurations with energy E_α as initial states.
- Taking a $X_{N_H}^\alpha$ configuration, a new state $X_{N_H+1}^\gamma$ is generated by selecting 1 empty octahedral site and setting at this site a H atom. The system has now $(N_H + 1)$ H atoms.
- 5000 MD integration steps are used to relax the system at $T_{MD}=0.05$ K. Averages are computed over the last 1000 MD integration steps where $E_{N_H+1}^\gamma$ is taken as the total potential energy average.

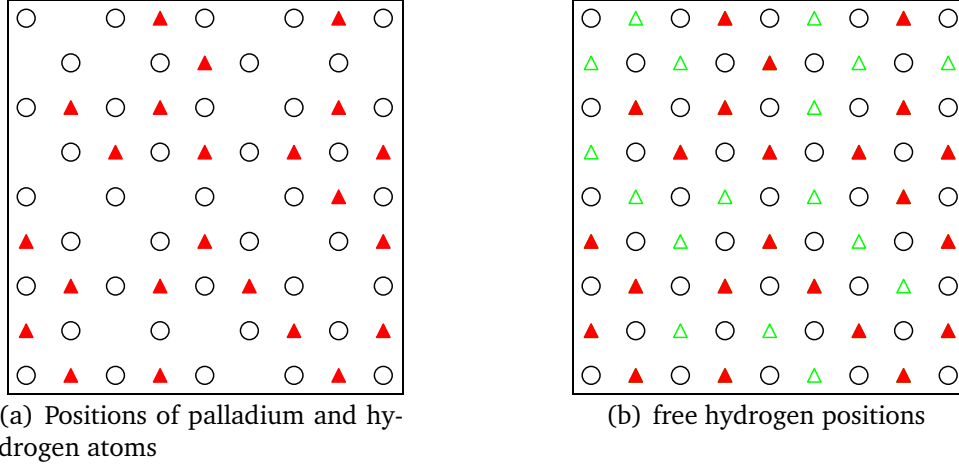


Figure 2.3: Energy gain by adding 1 extra H atom. Starting with a configuration with N_H hydrogen atoms (\blacktriangle) in a palladium lattice (\circ) see part (a), all different empty sites (\triangle) are tested with an additional H atom in order to determine the energy gain at a temperature T_{MC} .

- All the above is repeated. Altogether $N_o - N_H$ steps \times 5000 MD steps are carried out, where $N_o - N_H$ is the number of available unoccupied sites (See figure 2.3).

The energy gain of the system $\langle \epsilon(x) \rangle$ is a function of the H concentration x ¹ and it is the statistical average of the energy difference between states α belonging to a MC-chain and γ states:

$$\langle \epsilon(x) \rangle = -k_B T \ln \left(\frac{1}{N_\alpha} \sum_\alpha \frac{1}{N_\gamma} \sum_\gamma \exp[-\Delta E_\alpha^\gamma / k_B T] \right), \quad (2.26)$$

where N_α is the number of configurations α , N_γ is the number of available unoccupied sites ($N_o - N_H$) and ΔE is given by

$$\Delta E = U_\gamma(N_H + 1) - U_\alpha(N_H) \quad (2.27)$$

As deduced in Section 3.3.2, the chemical potential μ_H is:

$$\mu_H = k_B T \ln \left(\frac{x}{1-x} \right) + \langle \epsilon(x) \rangle + \mu_{\text{vib}}(x) \quad (2.28)$$

where $\mu_{\text{vib}}(x)$ describes vibrational contributions of the H atoms.

2.3 Physical quantities determined through MD and MC-MD simulations

Using MD, two different sets of simulations were made. In bulk, to prove the adaptability of the interaction potentials, and in the cuboctahedral clusters to estimate their chemical potential. The simulations in bulk use periodic boundary conditions, those in Clusters without periodic boundary conditions in order to account for surface effects. Simulations performed on pure Pd were carried out by using an integration

¹ $x = N_H / N_{Pd}$ in bulk. $x = \tilde{x} = N_H / N_\sigma$ in cluster. N_σ : number of available sites

step $\Delta t = 2.0$ fs and on Pd loaded with H by using an integration step $\Delta t = 0.26$ fs in order to resolve the movement of the H atoms which have 100 times less mass than the Pd atoms. For each simulation an equilibration run is allowed before taking averages. When determining binding energies the simulation temperature was chosen to be 0.05K. In this way the system relaxes faster because of the small vibrations of the Pd atoms around their equilibrium positions. Quantities such as kinetic (E_{kin}) and potential energy (E_{pot}) per atom, cohesion Energy (E_{coh}) of Pd as a function of H concentration x , the binding energy (E_{b}) of H in Pd as a function of the concentration x , the change in lattice energy and relative volume changes under H loading are calculated.

The MC-MD procedure was used to simulate H loaded bulk and clusters. After 1000 MC steps \times 5000 MD steps the binding energy of H in Pd as a function of the concentration x , $E_{\text{b}}(x)$, the average energy gain $\langle\epsilon(x)\rangle$ and the chemical potential of H at $T = 300$ K, $\mu_{\text{H}}(x)$ is determined.

In both MD and MC-MD simulations, the initial velocities are generated using random directions and Gaussian distribution of the absolute values with variance adapted to the desired simulation temperature. They are adjusted to ensure that the center of mass of the system is at rest. The system is then allowed to relax. The identification of a fully relaxed system follows an empirical rule. It is assumed that the system is fully relaxed when the change of E_{pot} between two successive steps is about 0.001 eV because of the proper comparison with experimental results which have an error of ± 0.01 eV. In Bulk-MD simulation, Pd alone was allowed to equilibrate for 200 ps before loading it with H followed by approximately 80 ps. Afterwards averages of quantities were taken within the next 2.6 ps. For the MC-MD simulations an already relaxed system was taken as the initial condition. After an MC step the system was allowed to relax for 1.3 ps. Averages of energies with their respectively fluctuations [AT87] were calculated. In the Appendix A it is given as an example the output of the simulation of Bulk Pd with 1 H atom.

Chapter 3

Theory

Regarding the origin of the interaction between the H atoms in a metal, it is known that there are two contributions: A short range repulsive interaction which comprises the electrostatic interaction of the screened H protons and also the induced polarization of the electronic cloud and an elastic interaction mediated by the metal lattice, which is long range and attractive. An interstitial H atom deforms the host lattice and creates a long ranged strain field which is felt by other H atoms. It is accepted that the H-H interaction in the metal causes the plateau in the solubility isotherm of H in Pd. In this chapter a brief description of the elastic interaction is given. We begin in section 3.1 by describing the relationship between local lattice deformation and macroscopic volume changes. The material presented here was adopted from the work of LIEBFRIED [LN78]. In section 3.3 some basic thermodynamical properties of the system Pd-H are presented, followed by a description of how to calculate the chemical potential of hydrogen in a metal. In this work we used a modified approach of Widom's method.

3.1 Lattice dilatation and volume change of the metal Lattice due to a point defect

A Hydrogen atom will induce a distortion of the metal lattice at the absorption site. The displacement field due to the distortion can be represented by virtual forces (the Kanzaki forces, see figure 3.1) applied to each lattice atom to reproduce the actual displacement of the metal atom. The Kanzaki force distribution is describable by a multipole expansion of which the first relevant term is the dipole term P_{ij} , where

$$P_{ij} = \sum_m \kappa_j^m x_i^m \quad (3.1)$$

where κ^m is the Kanzaki force applied to the m 'th atom situated at a distance x^m from the hydrogen atom. i, j label cartesian coordinates. Because the octahedral sites of the fcc lattice provide six metal atoms equidistant from the occupying hydrogen atom, P_{ij} is isotropic, that is $P_{ij} = P_o \delta_{ij}$. P_{ij} describes the dilating/contracting action of the force distribution and has the dimension of an energy.

In the lattice, the induced displacement field S_i^m of atom m' is given by:

$$S_i^m = \sum_{m'} G_{ik}^{mm'} \kappa_k^{m'}, \quad (3.2)$$

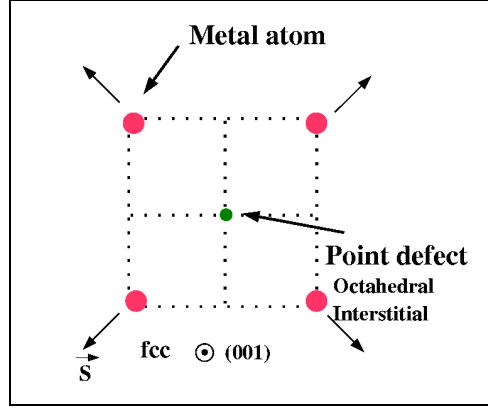


Figure 3.1: Kanzaki forces and displacement field at an octahedral site of a fcc lattice. \vec{S} is the displacement field caused by the point defect. In the perfect harmonic lattice the same displacements \vec{S} are produced by the virtual Kanzaki forces \vec{f} .

where $G_{ik}^{mm'}$ is the static Green's function evaluated at the separation distance between the sites m and m' . The static Green's function $G_{ik}^{mm'}$ represents the displacement of atom m in i -direction when a unit force in k direction is applied at site m' . For an infinite and isotropic medium the Green's function from linear elasticity theory is:

$$G_{ij}(r) = \frac{1}{16\pi(1-\nu)\mu} \left[(3-4\nu)\delta_{ij} + \frac{x_i x_j}{r^2} \right] \frac{1}{r}, \quad (3.3)$$

where $r = (x_i x_i)^{\frac{1}{2}}$ denotes the distance from the force center, μ ($\mu = C_{44}$) is the shear modulus and ν is poisson's ratio of the isotropic elastic medium. Eq. (3.3) can also be written as

$$G_{ij}(\vec{x} - \vec{x}') = \frac{1}{4\pi\mu} \frac{\delta_{ij}}{|\vec{x} - \vec{x}'|} - \frac{1}{16\pi\mu(1-\nu)} \frac{\partial^2}{\partial x_i \partial x_j} |\vec{x} - \vec{x}'|. \quad (3.4)$$

For a system with cubic symmetry it is not always possible to evaluate G analytically but in table 3.1 the Green's functions in the main symmetry directions of a cubic crystal is given.

In a first neighbour model, the springs (force or spring constants) connecting atoms at a distance $R1$ are given by:

$$f_l^{(1)} = V''(R1), \quad (3.5)$$

where l stands for longitudinal and $V''(R1)$ is the second derivative of the interaction potential $V(r)$ evaluated at the first neighbour equilibrium distance. In a second neighbour model there are two longitudinal springs $f_l^{(n)} = V''(Rn)$ and two transversal springs $f_t^{(n)} = V'(Rn)/Rn$, where t stands for transversal and $n = 1, 2$.

On the other hand, one can express the springs by the elastic data, the three first neighbour springs of the fcc lattice are:

$$f_l = \frac{a}{4}(C_{11} + C_{12} + C_{44}) \quad (3.6)$$

$$f_t = \frac{a}{4}(-C_{11} + 2 \cdot C_{44}) \quad (3.7)$$

$$f_t' = \frac{a}{4}(C_{11} - C_{12} - C_{44}) \quad (3.8)$$

Table 3.1: Numerical values of the Green's function for Pd in the main symmetry directions of the fcc lattice. The values shown are given in units $[1/f]$. Taken from [LN78].

Metal	G^0	G^{110}	G^{200}
Pd-Pd	0.421	-0.164	-0.074

 Table 3.2: Elastic data for Pd. Elastic Moduli and bulk modulus (B) for Pd. The equilibrium lattice constant is (a). Taken from [LN78, Fuk04].

Metal	C_{11} (eV/Å ³)	C_{12} (eV/Å ³)	C_{44} (eV/Å ³)	B (eV/Å ³)	a (Å)
Pd	1.41	1.1	0.45	1.22	3.89

where C_{11} , C_{12} , C_{44} are the elastic constants and a is the lattice constant (See table 3.2). For a first neighbour model the transversal springs f_t and f'_t are zero and $f = f_i$. Therefore $C_{11} = 2f/a$, $C_{12} = C_{44} = f/a$ and $\bar{C}_{11} = 12f/5a$. $\bar{C}_{11} = C_{11} - 2C_a/5$ is a Voigt's average where C_a is a measure of the anisotropy ($C_a = C_{11} - C_{12} - 2C_{44}$).

With a force pattern as shown in figure 3.2, the radial displacement of the nearest neighbours can be calculated. Let us assume that the force on the nearest neighbours is given by:

$$\vec{\kappa}(\vec{r}) = \kappa \hat{r} \quad \hat{r} = \frac{\vec{r}}{|\vec{r}|}. \quad (3.9)$$

Then, from Eq. (3.2) and Eq. (3.9) and the numerical values of G (table 3.1), it follows that the radial displacement is

$$S_r = 0.183 \frac{\kappa}{f}, \quad (3.10)$$

where κ is the Kanzaki force and f is the spring constant.

The local lattice displacement around a dilatation center can be related to the relative macroscopic volume change. The volume change due to an isotropic dipole force tensor is expressed by a surface integral

$$\Delta V = \int_S d\vec{S} \cdot \vec{S}, \quad (3.11)$$

where \vec{S} is the displacement field.

For a dilatation center $\vec{k} = -Po \cdot \partial\delta(\vec{r})$ in the middle of a sphere of isotropic material (see figure 3.3), the displacement is:

$$S_i = -P_{sk} \partial_s G_{ik}(r) = \frac{Po \cdot x_i}{4\pi C_{11} r^3} = \frac{Po \cdot \hat{r}}{4\pi C_{11} r^2} = S_r \hat{r}, \quad (3.12)$$

and from Eq. (3.11) the relative volume change ($\Delta V/V$) becomes

$$\frac{\Delta V}{V} = \frac{Po}{C_{11}} = \frac{5}{3} \cdot \frac{Po}{fa^2}, \quad (3.13)$$

where additionally it has been used that the atomic volume in a fcc lattice is given by $V = a^3/4$ and the elastic constant $\bar{C}_{11} = 12f/5a$ for a first neighbour model with spring f and lattice constant a .

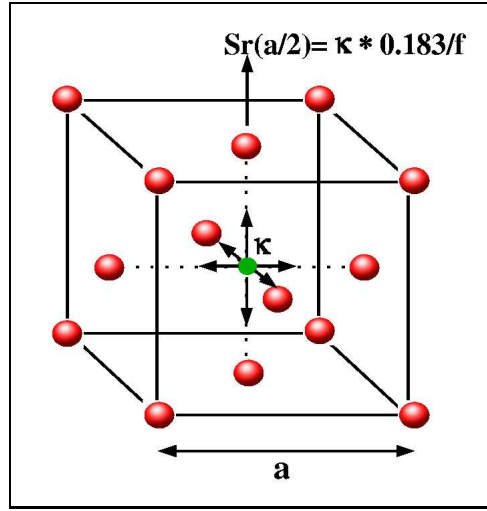


Figure 3.2: Radial displacements of the Pd nearest neighbours due to a point defect. Calculation of the radial displacement of the Pd NN using Green's function of table 3.1. It follows that $S_r = \kappa/f \cdot (0.421 + 4 \times (-0.164) - 0.074) \Rightarrow S_r = 0.183\kappa/f$, where f is the spring.

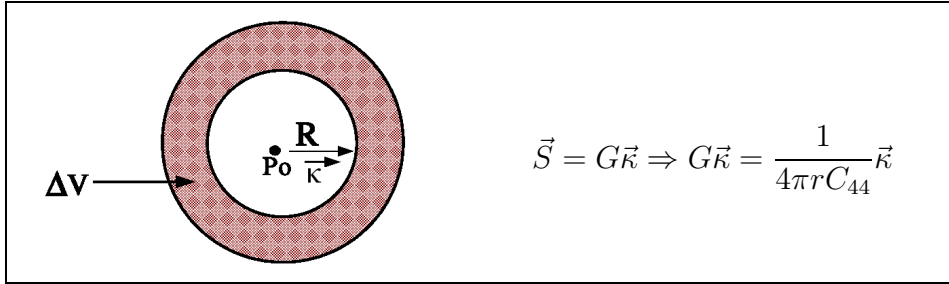


Figure 3.3: Volume change (ΔV) due to a dilatation center. Assuming a concentrated force density at the defect site in an elastically isotropic sphere, the radial displacement is $S_r = \frac{P_o}{4\pi C_{11}} \frac{\hat{r}}{r^2}$, and the volume change by this field is $\Delta V = 4\pi R^2 S_r(R)$.

With Eq. (3.13) and Eq. (3.10) it is possible to obtain a relationship between local radial displacement of the metal atoms and the relative volume change of the lattice:

$$\frac{S}{a} = 0.183 \cdot \frac{6}{10} \cdot \frac{\Delta V}{V}. \quad (3.14)$$

In the last equation, V is the atomic volume. Substituting its value ($V = d_o^3/4$) for a fcc structure, yields

$$\frac{S}{a/2} = 0.22 \cdot \frac{\Delta V}{V} \Rightarrow \frac{\Delta d}{d_o} = \frac{1}{3} \cdot \frac{\Delta V}{V_o}, \quad (3.15)$$

which is the relationship between relative lattice change and relative volume change for a cubic crystal [Pei78].

3.2 Interaction energy of two point defects

The solution of the problem of ellipsoidal inclusions in an isotropic infinite body has been given by Eshelby [Esh56]. He has determined the strain and stress fields for points inside and outside the inclusions. If the inclusion produces a dilatational strain, $\epsilon_{ij} = \delta_{ij}\epsilon_o$, the elastic strain (W) energy per unit volume V of inclusions is a

constant independent of the shape of the inclusions:

$$\frac{W}{V} = 2\mu\epsilon^2 \left(\frac{1+\nu}{1-\nu} \right). \quad (3.16)$$

The stress field is in this case

$$\sigma_{ii} = \begin{cases} -4\mu \left(\frac{1+\nu}{1-\nu} \right), & \text{inside the inclusion} \\ 0, & \text{outside the inclusion.} \end{cases} \quad (3.17)$$

Also, the strain elastic energy $W = -\frac{1}{2}\sigma_{ii}\epsilon_o V$ is zero for points outside the inclusion (no elastic interaction of the inclusions). In general, two defects in an infinite medium at sites \vec{r} and \vec{r}' have an interaction energy:

$$W(\vec{r}\vec{r}') = -P_{li} U_{i,l}(\vec{r}, \vec{r}') = P_{li} G_{ij,lk}(\vec{r} - \vec{r}') P'_{k,j}, \quad (3.18)$$

where $\vec{u}(\vec{r}, \vec{r}')$ is the displacement at \vec{r} produced by the force dipole at \vec{r}' . If in the isotropic medium one dilatation center P_o^a interacts with one general P^b , the elastic interaction energy is

$$W = \frac{P_o^a}{4\pi C_{11} r^3} [tr P^b - 3(\vec{r}, P^b \hat{r})], \quad (3.19)$$

and $\langle W \rangle_{\hat{r}} = 0$, that is the interaction of two dilation centres vanishes. Since $G \sim 1/r$, the elastic interaction between force dipoles scales as $\sim 1/r^3$.

If the medium is anisotropic with two dilatation centres of the form $P_{ij}^a = P_o^a \delta_{ij}$; $P_{mn}^b = P_o^b \delta_{mn}$, they interact according to

$$W(\vec{r}) \approx \frac{-15}{8\pi r^3} \frac{P_o^a P_o^b}{C_{11}^2} C_a \cdot A(\hat{r}), \quad (3.20)$$

where C_a is a measure of the anisotropy and $A(\hat{r})$ is a directional dependent quantity:

$$A(\hat{r}) = \frac{3}{5} - \sum_j \hat{x}_j^4 = \begin{cases} \frac{-2}{5}, & \langle 100 \rangle \\ \frac{3}{15}, & \langle 111 \rangle \\ \frac{1}{10}, & \langle 101 \rangle \end{cases} \quad (3.21)$$

which means that $C_a > 0$ for the interaction between two point defects is attractive in $\langle 100 \rangle$ and repulsive in $\langle 101 \rangle$, $\langle 111 \rangle$ directions. In this case $\epsilon_{ij} = \delta_{ij} \epsilon_o$ and the solutions of the strain fields are given by

$$\epsilon_r(r) = -\frac{2}{3} \frac{\epsilon_o a^3}{r^3} \left(\frac{1+\nu}{1-\nu} \right), \quad (3.22)$$

$$\epsilon_\theta(r) = \epsilon_\phi(r) = \frac{1}{3} \frac{\epsilon_o a^3}{r^3} \left(\frac{1+\nu}{1-\nu} \right). \quad (3.23)$$

The long range stress field within the matrix is given by:

$$\sigma_{ij} \propto \frac{B \epsilon_o a^3}{r^3} \left(\frac{1+\nu}{1-\nu} \right) \delta_{ij}, \quad (3.24)$$

where B is the bulk modulus of the medium. These long-ranged stress fields give rise to long ranged elastic interactions between the point defects.

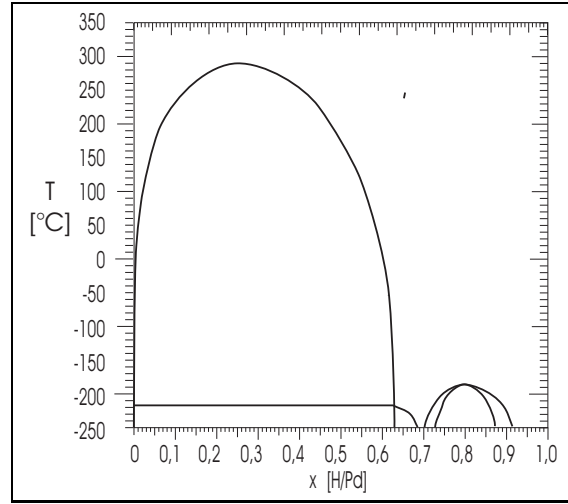


Figure 3.4: Phase Diagram of PdH bulk. At room temperature there are two solid phases with the same fcc lattice structure but different lattice constant a . At low H concentrations ($x < 0.0008$) the phase is called α . At high H concentration ($x > 0.6$) there is a pure α' phase. At concentrations in between ($0.0008 < x < 0.6$) a two phase region exist with regions α and α' that coexist in thermodynamical equilibrium. Taken from PUNDT [Pun05]

3.3 Thermodynamical properties of the H-Pd system

Under ordinary conditions ($T > 300$ K, $P < 10$ MPa), hydrogen can be described as an ideal gas. The chemical potential is given by [Fuk04]:

$$\mu^g = k_B T \ln \frac{P}{P_o(T)} - E_d, \quad (3.25)$$

$$P_o(T) = \frac{(4\pi M k_B T)^{3/2} \cdot 4\pi^2 I k_B T}{h^5}, \quad (3.26)$$

with M the mass of the hydrogen molecule and I its moment of inertia. For $T = 300$ K, $P_o(T)$ has a value for 13002 Pa.

When a Hydrogen molecule enters the surface of Pd, it dissociates. The H atoms occupy interstitial sites. Upon absorption, the lattice structure of Pd undergoes structural changes in order to accommodate a large number of H atoms. The phase diagram of Pd-H bulk is known and it is shown in figure 3.4. In the diagram, the composition is written as a ratio of the number of H atoms to the number of Pd atoms, $x = N_H/N_{Pd}$. At room temperature and at low H concentrations there is a so-called α phase which exists up to a concentration $x = 0.0008$. At higher H concentrations, there is a two- phase region $\alpha - \alpha'$ where the two phases coexist in thermodynamic equilibrium. For $x > 0.6$ there is a pure α' phase. Upon phase transformation, the system retains its fcc lattice structure but the lattice constant changes from $a = 3.89 \text{ \AA}$ to $a = 4.02 \text{ \AA}$ at 300 K.

At low H concentrations the system exhibit an ideal solution behavior. The solubility of hydrogen in the metal at a given temperature increases with increasing H pressure P_{H_2} . All isotherms have a common slope

$$x \propto \sqrt{P_{H_2}}, \quad (3.27)$$

a relationship known as Sievert's law.

At high H concentrations, the interactions between the H atoms plays a significant role. Upon H loading, the heat of solution initially decreases, followed by an increase at higher H concentrations.

The H gas at a pressure P_{H_2} in equilibrium with the α or α' phase allows to write for the chemical potential

$$\frac{1}{2}\mu^g(p, T) = \mu_H(\alpha \text{ or } \alpha', T), \quad (3.28)$$

where μ_H is the chemical potential of H in the metal. Using Eq. (3.25) and Eq. (3.28) the pressure P_{H_2} can be written as

$$P = P_o(T) \exp \left\{ \frac{2\mu_H + E_d}{k_B T} \right\} \quad (3.29)$$

which allows to determine the pressure-composition isotherms when μ_H is given.

3.3.1 Energy of a Hydrogen atom dissolved in a metal

The energy of a hydrogen atom dissolved in a metal has different contributions and can be written as

$$E = E_{\text{vib}} + E_{\text{pot}} \quad (3.30)$$

where E_{vib} can be calculated assuming that the H atoms form a harmonic oscillator system with vibrational density of states (per H atom) $\nu(\omega)$ independent of the number N_H of H atoms,

$$E_{\text{vib}} = \langle E_{\text{vib}} \rangle = N_H k_B T \int \nu_H(\omega) \ln(1 - \exp(-\hbar\omega/k_B T)) d\omega. \quad (3.31)$$

E_{pot} is the configurational potential energy. Lacher's [Lac37] treatment of the H-metal system assumed that E is given by the following expression

$$E = N_H \widetilde{E}_b + N_{HH} \chi, \quad (3.32)$$

where \widetilde{E}_b is the binding energy of 1 H in the metal, N_H is the number of hydrogen atoms in the system, χ is the interaction energy of a H atom with another H atom and N_{HH} is the number of H-H pairs. The binding energy of 1 H atom is given by

$$\widetilde{E}_b = \frac{1}{N_H} (E_{\text{pot}}(\text{H} + \text{Pd}) - E_{\text{pot}}(\text{Pd})) \quad (3.33)$$

where $E_{\text{pot}}(\text{H} + \text{Pd})$ is the potential energy of the system Pd with H and $E_{\text{pot}}(\text{Pd})$ is the potential energy of pure Pd. The enthalpy change under desorption ΔH or heat of solution is given by

$$\Delta H = -\frac{\partial H(N_H)}{\partial N_H}, \quad (3.34)$$

where

$$H(N_H) = H(\text{Pd}, N_H) - H(\text{Pd}). \quad (3.35)$$

$H(\text{Pd}, N_H)$ is the enthalpy of the Pd system with N_H H atoms and $H(\text{Pd})$ is the enthalpy of the Pd system alone. The binding energy E_b of a system with a finite number of H atoms can be obtained from the heat of solution ΔH ,

$$E_b = \Delta H + \frac{E_d}{2}. \quad (3.36)$$

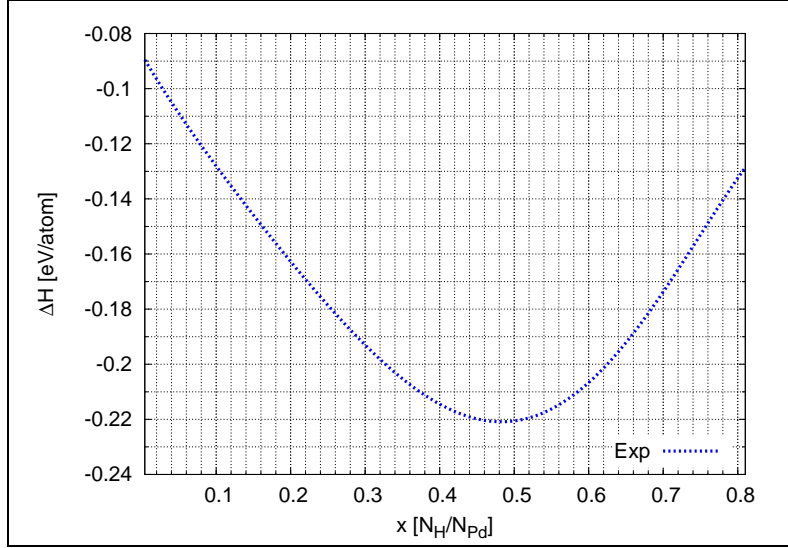


Figure 3.5: Heat of Solution of H in Pd Bulk as a function of hydrogen concentration. Experimental Results. It is shown the heat of formation of PdH as a function of the H concentration x . H is related with E_b through $E_b - E_d/2 = H$, where E_d is the H_2 dissociation energy (-4.46 eV). Taken from [Fuk04].

For Pd-H bulk

$$E_b \approx -0.2 \text{ eV} + \frac{E_d}{2} \Rightarrow E_b \approx -2.43 \text{ eV}. \quad (3.37)$$

The experimental results from OATES AND KUJI [Fuk04] (See Figure 3.5) show that the heat of solution of H in Pd is a function of the H concentration. The heat of solution turns from exothermic to endothermic at a certain H concentration.

The interaction energy χ is a quantity which can be estimated by comparing the change of lattice energy of two isolated hydrogen atoms (in the lattice, sitting far apart from each other) with the change of lattice energy of two hydrogen atoms sitting at a NN distance. That is, assuming that χn represents the H-H effective interaction, with elastic (lattice mediated, attractive) and electronic (repulsive interaction) the change in lattice energy upon H absorption is

$$\delta E_{\text{lattice}} = E_{\text{Pd}}(\text{H} + \text{Pd}) - E_{\text{Pd}}(\text{Pd}). \quad (3.38)$$

E_{Pd} is only the potential energy of the Pd atoms. Therefore

$$\chi n = (\delta E_{\text{lattice}_{\text{isol}}} - \delta E_{\text{lattice}_{\text{pair}}}) \times 6. \quad (3.39)$$

where n is the number of hydrogen atoms with which a selected H atom can interact.

3.3.2 Chemical potential of Hydrogen in a metal

For evaluating the chemical potential of Hydrogen in Palladium clusters, we have used an approach deduced from WIDOM'S [Wid63] particle insertion method. The particle insertion method is described, e.g., in the textbook by FRENKEL AND SMIT [FS05]. An application to the bulk Pd-H system has been given by SALOMONS [Sal90].

The present treatment is tailored to deal with situations where for the N-particle system well defined configurations X_α exist, characterized for example by different

distributions of the H atoms in interstitial sites of the Pd matrix, that means by different distributions of the H atoms in the cluster.

Thermodynamics then concern the competition between the various X_α and vibrational excitation of the atoms around their equilibrium positions. It is in particular assumed that the so-called transition states, where atoms are on the way between two adjacent equilibrium positions, are of negligible weight in the partition function. The main difference to Widom's [Wid63] original method lies in the fact that this method mixes entropic contribution from vibration and configuration degrees of freedom, while we use here a treatment that allows to take into account the configurational effects without their masking by vibrations.

In our application to Pd-H clusters, we assume that the Pd atoms form the backbone of the cluster, e.g., a fcc cuboctahedron with N_{Pd} Pd atoms. The number of H atoms is denoted by N_{H} . They occupy a fraction $x = N_{\text{H}}/N_\sigma$ of the octahedral sites, with N_σ the total number of available sites ².

The equilibrium thermodynamics of the system are determined by the partition function

$$Q(N, T) = \frac{1}{N!} \frac{1}{\hbar^{3N}} \cdot \int d\Lambda \exp(-H_N \beta), \quad (3.40)$$

where $\beta = 1/k_B T$ and the integration covers the whole phase space of the system. The phase space integral shall be evaluated by assumption of classical particles and classical dynamics. The prefactor takes place of quantum phenomena, that means the fact that the particles are indistinguishable and that the uncertainty principle ascribes a phase space volume \hbar^{3N} to one N-particle state in the 6N-dimensional phase space.

The treatment makes use of the concept of stationary classical configurations $X_\alpha = \{\vec{x}_1^\alpha, \dots, \vec{x}_N^\alpha\}$, where α labels the various configurations. The configurations are minima of the potential energy landscape and can be determined as fix points of the iterative mapping

$$\vec{x}_i \rightarrow \vec{x}'_i = \vec{x}_i - \frac{1}{2} \delta t^2 \nabla_i \cdot U(\vec{x}_j) \quad i \dots N, \quad (3.41)$$

where $U(\vec{x}_j)$ is the potential energy for configuration $\{\vec{x}_j\}$. To each of the fix points X_α we ascribe, e.g., via a Voronoi construction, a phase space volume Λ_α , leading to the expression

$$Q(N_{\text{H}}) = \frac{1}{N_{\text{H}}! N_{\text{Pd}}!} \sum_{\alpha} \frac{1}{\hbar^{3N}} \cdot \int_{\Lambda_\alpha} d\Lambda \exp\{[-H(r) - U_\alpha(N_{\text{H}})] \beta\} \cdot \exp\{-U_\alpha(N_{\text{H}}) \beta\}. \quad (3.42)$$

For simplicity, in the following we explicitly take into account the fact that the Pd atoms are indistinguishable. We contract into one configuration $X_{\bar{\alpha}}$ all configurations that arise from exchange between the Pd atoms. This implies that for situations where only one type of Pd cluster counts, for instance one cuboctahedral arrangement with N_{Pd} Pd-atoms, the configuration $X_{\bar{\alpha}}$ differ by the distribution of H atoms over the octahedral sites, while for all $X_{\bar{\alpha}}$ the matrix of Pd-atoms has the same topology. With this simplification Eq. (3.42) becomes

$$Q(N_{\text{H}}) = \frac{1}{N_{\text{H}}!} \sum_{\bar{\alpha}} \frac{1}{\hbar^{3N}} \cdot \int_{\Lambda_{\bar{\alpha}}} d\Lambda \exp\{[-H(r) - U_{\bar{\alpha}}(N_{\text{H}})] \beta\} \cdot \exp\{-U_{\bar{\alpha}}(N_{\text{H}}) \beta\}. \quad (3.43)$$

² $x = N_{\text{H}}/N_{\text{Pd}}$ in bulk. $x = \tilde{x} = N_{\text{H}}/N_\sigma$ in cluster. N_σ : number of available sites

The free energy

$$F(N_H) = -\frac{1}{\beta} \ln(Q(N_H)) \quad (3.44)$$

now can be written as

$$F(N_H) = F_{\text{vib}}(N_H) - \frac{1}{\beta} \ln(Q^o(N_H)), \quad (3.45)$$

with

$$Q^o(N_H) = \frac{1}{N_H!} \sum_{\bar{\alpha}} \exp\{-U_{\bar{\alpha}}(N_H)\beta\} \quad (3.46)$$

$$F_{\text{vib}}(N_H) = -\frac{1}{\beta} \ln \langle \exp\{-f_{\bar{\alpha},\text{vib}}(N_H) \cdot \beta\} \rangle_{\bar{\alpha}} \quad (3.47)$$

where

$$\langle A_{\bar{\alpha}} \rangle_{\bar{\alpha}} = \frac{\sum_{\bar{\alpha}} A_{\bar{\alpha}} \exp\{-U_{\bar{\alpha}}(N_H)\beta\}}{\sum_{\bar{\alpha}} \exp\{-U_{\bar{\alpha}}(N_H)\beta\}}, \quad (3.48)$$

$$f_{\bar{\alpha},\text{vib}}(N_H) = -\frac{1}{\beta} \ln \left[\int_{\Lambda_{\bar{\alpha}}} \frac{d\Lambda}{\hbar^{3N}} \exp\{-(H(r) - U_{\bar{\alpha}}(N_H))\beta\} \right]. \quad (3.49)$$

If in Eq. (3.49) the exploration of the phase-space volume $\Lambda_{\bar{\alpha}}$ around $X_{\bar{\alpha}}$ can be approximated by an harmonic expansion, Eq. (3.49) reduces to

$$f_{\bar{\alpha},\text{vib}}(N_H) = +\frac{1}{\beta} \sum_{j=1}^{3N-6} \ln(1 - \exp(\hbar\omega_{j,\bar{\alpha}}\beta)), \quad (3.50)$$

where $j = 1, \dots, 3N - 6$ labels the vibrational modes of the Pd-H system in configuration $\bar{\alpha}$. $F_{\text{vib}}(N_H)$ thus describes the effects of the vibrations around the $X_{\bar{\alpha}}$ in the free enthalpy, while $Q^o(N_H)$ measures the configuration part.

Evaluation of the H-atoms chemical potential $\mu_H(N_H, T)$ from Eq. (3.45) follows the idea of Widom's particle insertion method. We use

$$\mu_H(N_H, T) = F(N_H + 1) - F(N_H), \quad (3.51)$$

$$\mu_H(N_H, T) = F_{\text{vib}}(N_H + 1) - F_{\text{vib}}(N_H) - \frac{1}{\beta} \ln \left[\frac{1}{N_H + 1} \frac{Q^o(N_H + 1)}{Q^o(N_H)} \right]. \quad (3.52)$$

According to our construction we have

$$\frac{Q^o(N_H + 1)}{Q^o(N_H)} = \frac{\sum_{\bar{\alpha}'} \exp\{-U_{\bar{\alpha}'}(N_H + 1)\beta\}}{\sum_{\bar{\alpha}} \exp\{-U_{\bar{\alpha}}(N_H)\beta\}}. \quad (3.53)$$

In classical physics, insertion of one H additional atom into all unoccupied interstitial sites generates from one configuration $X_{\bar{\alpha}}(N_H)$ a set of $N_o - N_H$ configurations $X_{\bar{\alpha}'}(N_H + 1)$. Let us denote the set of these configurations by $S(\alpha, N_H)$. Further, we use $S(N_H)$ and $S(N_H + 1)$ to denote the set of all configurations of the N_H - respectively- N_{H+1} system. With this notation we have

$$\sum_{\alpha' \in S(N_H+1)} = \sum_{\alpha \in S(N_H)} \cdot \sum_{\gamma \in S(\alpha)}, \quad (3.54)$$

and

$$\frac{Q^o(N_H + 1)}{Q^o(N_H)} = \frac{\sum_{\bar{\alpha} \in \mathcal{S}(N_H)} \left(\exp \{-U_{\bar{\alpha}}(N_H)\beta\} \sum_{\gamma \in \mathcal{S}(\bar{\alpha}, N_H)} \exp \{-(U_{\gamma}(N_H + 1) - U_{\bar{\alpha}}(N_H)) \cdot \beta\} \right)}{\sum_{\bar{\alpha} \in \mathcal{S}(N_H)} \exp \{-U_{\bar{\alpha}}(N_H)\beta\}}. \quad (3.55)$$

Therefore we find

$$\mu_H(N_H) = F_{\text{vib}}(N_H + 1) - F_{\text{vib}}(N_H) + \frac{1}{\beta} \ln \frac{x + N_o^{-1}}{1 - x} - \frac{1}{\beta} \ln \langle \exp \{-\beta \Delta \epsilon_{\bar{\alpha}}(N_H)\} \rangle_{\bar{\alpha}} \quad (3.56)$$

with

$$\Delta \epsilon_{\bar{\alpha}}(N_H) = -\frac{1}{\beta} \ln \left[\frac{1}{N_o - N_H} \sum_{\gamma \in \mathcal{S}_{\bar{\alpha}, N_H}} \exp \{-\beta (U_{\gamma}(N_H + 1) - U_{\bar{\alpha}}(N_H))\} \right]. \quad (3.57)$$

For evaluation of Eq. (3.57) we generate a MC chain of states $X_{\bar{\alpha}}$, $\bar{\alpha} = 1, \dots, N_{\text{states}}$, at constant N_H . In each MC step, randomly one of the H atoms in the current configuration $X_{\bar{\alpha}}$ is removed and also randomly one H atom is transferred to one of the empty octahedral sites of $X_{\bar{\alpha}}$ (See Section 2.2.1). By a MD like steepest descent iterative mapping (Eq. (3.41)) for this geometry a tentative configuration $X_{\bar{\alpha}}^o$ is generated with potential energy $U(X_{\bar{\alpha}}^o)$. By MC using the metropolis algorithm, it is decided, whether $X_{\bar{\alpha}}^o$ is accepted or whether $X_{\bar{\alpha}}$ is retained:

$$\begin{cases} U(X_{\bar{\alpha}}^o) - U(X_{\bar{\alpha}}) < 0, & \text{accept } X_{\bar{\alpha}}^o \\ \exp \{-(U(X_{\bar{\alpha}}^o) - U(X_{\bar{\alpha}})) \cdot \beta\} > \varsigma_c, & \text{accept } X_{\bar{\alpha}}^o \\ \text{otherwise,} & \text{retain and count again } X_{\bar{\alpha}}^o \end{cases} \quad (3.58)$$

where ς_c is a random number. Afterwards, a representative group of $X_{\alpha} \in X_{\bar{\alpha}}$ is chosen (See Section 2.2.1). Additional states X_{γ} are generated by introducing 1 H atom at $N_o - N_H$ sites and $\Delta E = U_{\gamma}(N_H + 1) - U_{\alpha}(N_H)$ is calculated.

Chapter 4

Interaction Potentials

An important issue in any molecular-dynamics simulation is the selection of a suitable approach to the forces. Much work has been directed along these lines, i.e., to construct empirical and ab initio sets of two-body potentials for pure Pd and for the system Pd-H [FS86, MDB84, Gil86, TSL91, RGL89]. However there is no model capable of describing all desired physical properties of the Pd-H system. In this work, we choose as important properties to be reproduced by the model the following quantities: the equilibrium lattice constant (a), the cohesion energy (E_{coh}) and the bulk modulus (B) of pure Pd, also the relative volume change ($\Delta V/V$) upon H loading and the binding energy (E_b) of H in Pd as a function of H concentration. Also it is considered how much time the model needs to perform a MD simulation. This last factor is important regarding implementation in the MD-MC hybrid calculation, which requires at least 1000×5000 MD integration steps.

In this chapter we describe different interaction potentials used in this work. In section 4.1, three different Pd-Pd interaction potentials are proposed: The EAM potential from BASKES et. al. [FS86] and two new Pd-Pd interaction potentials which have the advantage of taking into account less neighbours than the EAM potential. In section 4.2 it is explained how the H-Pd interaction is constructed to account for the relative volume change upon H loading. A set of parameters is given for each Pd-Pd interaction potential. Finally in section 4.3 the H-H interaction potential is constructed to reproduce not only qualitatively the shape of the solubility isotherms of H in bulk-Pd but also Sievert's law at low H concentrations.

4.1 Pd-Pd Interaction Potential

4.1.1 Embedded Atom Method potential (EAM)

The EAM model [FS86, MDB84] is a third neighbour model (see Appendix B). In this model the energy of a system of N atoms is

$$V(r) = \frac{1}{2} \cdot \sum_i \sum_{j \neq i} V_P(r) + \sum_i F(\rho_i) \quad (4.1)$$

where V_P is the pair potential describing the interaction between atoms i and j . r is the separation distance between the atoms and $F(\rho)$ is the embedding function or many body function. The embedding function is evaluated for each atom i and

accounts for the local variation of electron density, ρ_i is the contribution of neighbouring atoms j at the position of the atom i

$$\rho_i = \sum_{j \neq i} \phi_j(r), \quad (4.2)$$

where ϕ_j , a function of the distance r between atoms i and j , is interpreted as the contribution of atom j to the electron density at the position of atom i . The function $\phi_j(r)$ is a sum of the atomic s- and d- like spherically averaged electronic densities.

The embedding function and the pair potential are fitted to reproduce as closely as possible the following equilibrium properties of Pd: Equilibrium lattice parameters, cohesive energy, elastic moduli and vacancy formation energy which are shown in table 4.1. The embedding function is given numerically (in the form of a Table) in the MD program and it is shown together with the pair potential in figure 4.1

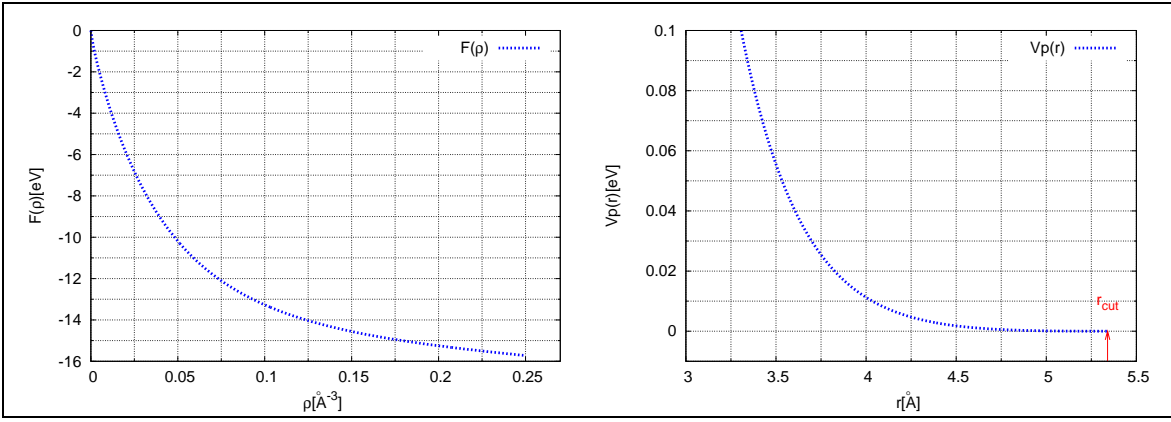


Figure 4.1: Pd-Pd EAM Interaction Potential. *Left:* The embedding function $F(\rho)$ approaches zero when the density ρ becomes small. The bonding strength decreases as the particles separate. When the density becomes large the cohesion increases. This part of the energy is attractive. *Right:* The pair potential part of the EAM interaction is repulsive. For atomic distances $r \geq r_{\text{cut}} = 5.34 \text{ \AA}$, the interaction is set to zero.

4.1.2 Pair potential I (ppI)

Here our so called pair potential I (ppI) will be described. ppI is a first neighbour model. The following function is proposed to model the first neighbour Pd-Pd interaction:

$$V(r) = -\alpha(r - r_o)^3 + \gamma(r - r_o) + \delta. \quad (4.3)$$

The parameters α , γ , δ and r_o are chosen to reproduce the experimental quantities for an acceptable description of Bulk Pd, which are shown in table 4.1. Additionally the analytical form of equation (4.3) possess some properties which makes the fitting straightforward. These properties are:

- $V(r)=0$ for:

$$r = r_{\text{cut}} = \sqrt{\gamma/3\alpha} + r_o, \quad (4.4)$$

$$r = r_1 = -2\sqrt{\gamma/3\alpha} + r_o, \quad (4.5)$$

- $V'(r)=0$ for:

$$r = r_{\text{min}} = -\sqrt{\gamma/3\alpha} + r_o, \quad (4.6)$$

Table 4.1: Experimental Quantities for Bulk Pd. The observed experimental quantities are to be reproduced by the interaction potentials. ppI was fitted to reproduce the equilibrium lattice constant (a) and the bulk modulus (B). ppII was fitted to reproduce the lattice constant (a), the bulk modulus (B), the vacancy formation energy (E_v^f) and the cohesion energy (E_{coh}). EAM potential was fitted to reproduce a , E_{coh} , E_v^f and also the elastic constants C_{11} , C_{12} and C_{44} . Taken from [LN78, Fuk04].

a (Å)	B (eV/Å ³)	E_v^f (eV)	E_{coh} (eV)	C_{11} (eV/Å ³)	C_{12} (eV/Å ³)	C_{44} (eV/Å ³)
3.89	1.22	1.4	3.94	1.41	1.1	0.45

Table 4.2: Pd-Pd ppI Interaction Potential parameters. ppI is a first neighbour model. The parameters were fitted to reproduce the lattice constant (a) and the bulk modulus (B)

Interaction	α (eV/Å ³)	γ (eV/Å)	δ (eV)	r_o (Å)	r_{cut} (Å)
Pd-Pd	1.32	0.7998	-0.2396	3.20	3.65

where r_{cut} is the cutoff radius, that is, the separation distance between two atoms, at which the interaction energy goes to zero. r_1 is the distance at which a Pd atom feels the restoring force far from the equilibrium position r_{min} .

The Bulk modulus is related to the second derivative of the interaction potential. It is basically the curvature at the minimum. For a first neighbour model one obtains (see Appendix B):

$$B = \frac{4}{3} \cdot \frac{V''(r_{\text{min}} - r_o)}{a}. \quad (4.7)$$

With the experimental Bulk modulus value and using equation (4.7) the value of α is obtained. Using equations (4.4) and (4.6) the two parameters left, γ and δ can be calculated. The parameters are shown in table 4.2 and the interaction potential is plotted in figure 4.2.

Basic properties of bulk Pd described by the ppI potential

MD simulations in pure bulk Pd with 864 atoms (box size = 23.34 Å) are performed using the ppI model. These simulations use periodic boundary conditions, an integration step $\Delta t = 2.0 \text{ fs}$ and a temperature of 300 K. The system was allowed to relax and after 20 ps statistical averages over the last 5000 integration steps were taken. Using the ppI potential, a first approximation in describing pure Pd is obtained.

As shown in Table 4.3 this pair potential is suited for describing the equilibrium lattice parameter a and the Bulk modulus B but it does underestimate the cohesion energy E_{coh} by approximately 1 eV when compared to the experimental value for pure Pd. In order to overcome this difficulty an electron gas term (See Appendix C) was introduced to provide the difference which, in this work, is delivered through the energy of the s electrons in the system. MD simulations were also carried out with this electron gas term and the results are shown in Table 4.3. The lattice parameter a and the bulk modulus B remain almost unchanged. Besides from the fact that

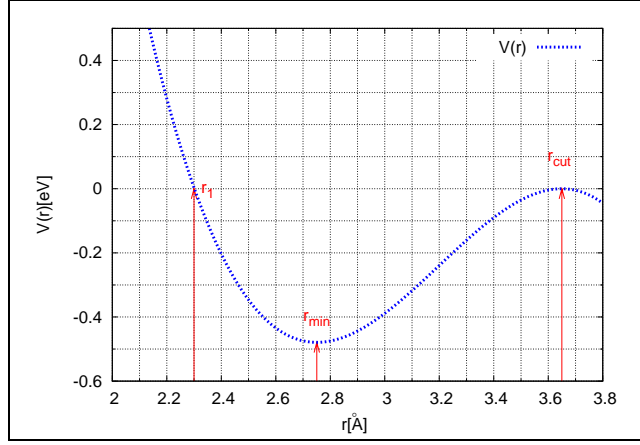


Figure 4.2: Pd-Pd pair potential I (ppI). The interaction potential has a minimum at $r = r_{\min} = 2.7506 \text{ \AA}$ which is the nearest neighbour (NN) equilibrium distance in Bulk Pd. Each Pd atom interacts with 12 NN. The contribution per atom to the total potential energy is $6 \times V(r_{\min})$. That is $E_{\text{coh}} = -0.4792 \text{ eV} \times 6 = -2.88 \text{ eV}$. r_{cut} is a value between the first and second shell of neighbours. For atomic distances $r \geq r_{\text{cut}}$ the interaction is set to zero.

Table 4.3: Basic Properties of Pd Bulk described by the ppI potential. The ppI was fitted to reproduce the equilibrium lattice constant (a) and the bulk modulus (B) which are given in Table 4.1. Values of the cohesion energy (E_{coh}) also with changes in a and B with and without the contribution of the electron gas term are given. (For the experimental values see Table 4.1).

	a (\AA)	B ($\text{eV}/\text{\AA}^3$)	E_{coh} (eV)
without E_{gas}	3.89	1.4 (-0.01)	-2.88
with E_{gas}	3.88	1.2	-3.90

this is a first neighbour model the potential ppI is a good choice for describing basic properties of Pd bulk.

4.1.3 Pair potential II (ppII)

For many metallic systems, a two body core-core interaction generally fails. The reason for this is that two-body potentials imply Cauchy relation for the elastic constants ($C_{12}=C_{44}$) which is not true for transition metals. A model that avoids this problem was proposed by FINNIS AND SINCLAIR [FS84]. The potential energy is constructed from two terms; a two body core-core repulsive interaction (V_P), and a N-body potential (V_N), which describes the energy changes due to variation of atomic configurations at constant average *density* ϕ . V_N incorporates the essential character of metallic cohesion through an *embedding function* $f(\phi)$ similar to the one used in the embedded atom method. The parameterization of the Pd-Pd potential used here, has the same form as the one proposed by FINNIS AND SINCLAIR [FS84]. However, the potential parameters used here, were adjusted to reproduce cohesion energy, lattice parameter, bulk modulus, vacancy formation energy and the stability conditions at the potential minima. In order to improve the Pd-Pd ppI interaction model we considered an analytical fit to include the second shell of neighbours. We proceeded to write the N-body term U_N in an empirical way. The contribution of atom i to the

total energy is:

$$U_{\text{TOT}}(i) = U_{\text{N}} + \sum_{j \neq i} U_{\text{P}}. \quad (4.8)$$

U_{N} is given by

$$U_{\text{N}}(i) = -AA \cdot f(\phi_i), \quad (4.9)$$

where the form $f(\phi_i)$ is taken similar to the tight-binding calculation [RGL89] of the energy within the second moment approximation of the density of states. $f(\phi_i)$ is analytic and equal the negative square root of ϕ_i . The physical meaning of ϕ_i is that it represents the sum of the squares of the bond integrals between atomic sites i and j . We follow FINNIS AND SINCLAIR [FS84] and use for the function ϕ the form:

$$\phi = (r - d)^2, \quad (4.10)$$

and

$$f(\phi_i) = -AA \cdot \sqrt{\sum_{\substack{j \neq i \\ j}} (r - d)^2}. \quad (4.11)$$

The many body term $f(\phi_i)$ is a nonlinear function of the distance r between atoms i and j . d is a unknown parameter to be determined.

U_{P} is given by

$$U_{\text{P}} = V = (r - r_{\text{cut}})^2 \cdot (a + b * r + c * r^2), \quad (4.12)$$

r is the distance between atoms i and j and r_{cut} , a , b and c are parameters to be fitted.

The bulk modulus (B), the cohesion energy (E_{coh}), the vacancy formation energy (E_{v}^f) and the stability conditions at the potential minima allows us to parameterize Eq. (4.11) and (4.12). For a second neighbour interaction model we obtain (see Appendix B):

$$\begin{aligned} B = & \frac{4}{3 \cdot a^2} \cdot \left[a \cdot V_1'' + a \cdot V_2'' - 2 \cdot \sqrt{2} \cdot V_1' - 2 \cdot V_2' \right] \\ & - \frac{8 \cdot AA}{3 \cdot a^2} \cdot \left[6 \cdot a \cdot f'' \cdot (\sqrt{2} \cdot \phi_1' + \phi_2')^2 \right. \\ & \left. + a \cdot (\phi_1'' + \phi_2'') - 2 \cdot (\sqrt{2} \cdot \phi_1' + \phi_2') \right], \end{aligned} \quad (4.13)$$

$$\begin{aligned} E_{\text{v}}^f = & -AA \cdot (12 \cdot \sqrt{11 \cdot \phi_1 + 6 \cdot \phi_2} + 6 \cdot \sqrt{12 \cdot \phi_1 + 5 \cdot \phi_2} \\ & - 18 \cdot AA \cdot \sqrt{12 \cdot \phi_1 + 6 \cdot \phi_2}) - (6 \cdot V_1 + 3 \cdot V_2), \end{aligned} \quad (4.14)$$

$$E_{\text{coh}} = 6 \cdot V_1 + 3 \cdot V_2 - AA \cdot \sqrt{12 \cdot \phi_1 + 6 \cdot \phi_2}, \quad (4.15)$$

$$6 \cdot V_1' + 3 \cdot V_2' - AA \cdot \frac{12 \cdot \phi_1 + 6 \cdot \phi_2}{\sqrt{12 \cdot \phi_1 + 6 \cdot \phi_2}} = 0. \quad (4.16)$$

where V_1 , V_2 are the values of Eq. (4.12) evaluated at r the distance of the first nearest neighbors R_1 , and the distance of the second nearest neighbors R_2 , respectively. V_1' , V_2' , V_1'' and V_2'' are the first derivatives of Eq. (4.12) and the second derivatives of Eq. (4.12) evaluated at $r=R_1$ and at $r=R_2$ respectively. ϕ_1 , ϕ_2 , ϕ_1' , ϕ_2' , ϕ_1'' , ϕ_2'' are the values of Eq. (4.10), the first derivative of Eq. (4.10), and the second derivative of Eq. (4.10) evaluated at $r=R_1$ and at $r=R_2$ respectively.

Conditions (4.13), (4.14), (4.15) and (4.16) together with the experimental quantities (shown in table 4.1) allows to give the set of parameters given in table 4.4. The fitting was done by using the program Maple [Map05] (see Appendix B.2). The ppII interaction potential is plotted in figure 4.3. The interaction potential goes smoothly to zero after r_{cut} , that is, atoms that would be at a separation distance $r=r_{\text{cut}}$ experience some forces. However, in PdH atoms would experience a maximum displacement to $R_2=4.025 \text{ \AA}$ being this distance much smaller than r_{cut} .

Table 4.4: Pd-Pd ppII Interaction Potential parameters. ppII is a second neighbour model. The parameters were fitted to reproduce the lattice constant (a), the bulk modulus (B), the cohesion energy (E_{coh}), the vacancy formation energy (E_v^f) and the stability conditions at the minima. The choice of parameters is not unique, but with this choice the value of E_{coh} is comparable with the experiment

Interaction	a (eV/Å ²)	b (eV/Å ³)	c (eV/Å ⁴)	d (Å)	r_{cut} (Å)	AA (eV/Å)
Pd-Pd	5.786536	-3.985932	0.644633	4.4	4.2	0.023760

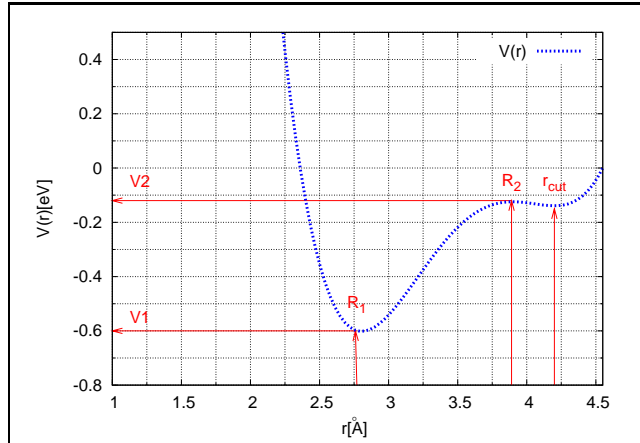


Figure 4.3: Pd-Pd pair potential II (ppII). This potential has two minima. The first NN neighbours are at a separation distance of $R_1=2.7506 \text{ \AA}$. The second NN are at a separation distance $R_2=3.89 \text{ \AA}$. The contribution to the E_{coh} from each shell of neighbours is $E_{\text{coh}} = 6 \times V_1 + 3 \times V_2 = 3.91 \text{ eV}$. r_{cut} lies between the second and third shell of neighbours.

4.2 H-Pd interaction potential

As already mentioned in Section 3.1, the H atom causes a local displacement of the neighbouring Pd atoms. This displacement can be represented by effective forces that produce the actual displacements in the crystal. These forces are restricted to a small region of space and can be characterized by the force dipole tensor (or double force tensor) P_{ij} . If the medium is isotropic then $P_{ij}=\text{Pd}\delta_{ij}$. The trace of the force dipole for H in Pd has been experimentally determined (see table 4.5) and can be used to fit the H-Pd interaction potential. Using Eq. (3.1) the force constant κ can be calculated: $\kappa=\text{Tr}P/a \sim =0.9 \text{ eV/\AA}$. The first neighbour model Eq. (4.3) was used to make an analytical fit of the H-Pd interaction. The force exerted to a Pd atom is

Table 4.5: Experimental bulk H-Pd Quantities. It was required that the H-Pd Interaction should be able to reproduce the binding energy of H in Pd (E_b), the relative volume change of the Pd lattice under H loading ($\Delta V/V$) and the force dipole (P) [Pei78]

E_b (eV)	$\Delta V/V$ $x = 0.008$	P_{ii} (eV)
-2.43	0.19	3.30

Table 4.6: H-Pd Interaction Parameters. It is shown a set of parameters corresponding to each Pd-Pd interaction. With this choice of parameters the required Pd displacement $S=0.04 \text{ \AA}$ is assured. The value shown in parenthesis is obtained without the requirement to reproduce E_b .

Interaction Model	α (eV/ \AA^3)	γ (eV/ \AA)	δ (eV)	r_o (\AA)	r_{cut} (\AA)
EAM	0.3560	0.3	-0.3	2.77	3.3
PPI	0.4527	0.3	-0.4395 (-0.094)	2.83	3.3
PPII	0.4938	0.3	-0.48	2.85	3.3

equal to the force constant but with opposite sign, that is:

$$V'(r_1) = -0.9 \text{ eV}/\text{\AA} \quad (4.17)$$

where r_1 is the distance between a H and a Pd atom. Using equations (4.3) and (4.17), parameter γ can be calculated. Then using conditions (4.4), (4.6) and (4.5) the other parameters were determined.

The next question that arises is, whether this set of parameters supplies the correct displacement S of the Pd atoms. From condition (3.14) S must be 0.04 \AA in order to have the correct relative volume change. It was also required that the H-Pd interaction gives the experimental H binding energy (see table 4.5). Regarding this, an additional adjustment on the parameters was carried on. A final set of parameters is given in table 4.6. Also in figure 4.4 the H-Pd interaction potentials are plotted. As can be seen, a further adjustment of the potential was made for $r > 3 \text{ \AA}$, in order to assure that it goes smoothly to zero beyond r_{cut} . In any case, the distance r between a H atom and its neighboring Pd atoms is never $> 2.03 \text{ \AA}$.

Testing the H-Pd interaction

In order to test the H-Pd interaction, MD simulations using one hydrogen atom at an octahedral site in bulk Pd were carried out. The first fitting of the interaction potential was made to guarantee the theoretical local displacement S of the next nearest Pd neighbours when a point defect is introduced in the lattice. The displacement S is related to the relative lattice volume change through Eq. 3.14. A second adjustment was made to obtain the correct value of the binding energy E_b . The simulations were performed using a relaxed Pd lattice, placing a hydrogen atom randomly at an octahedral site. The system was allowed to further relax using an integration step $\delta t = 0.25 \text{ fs}$ for 5000 integration steps and a temperature of 0.05 K. Statistical averages over the last 1000 integration steps were taken and the results are shown in Table 4.7.

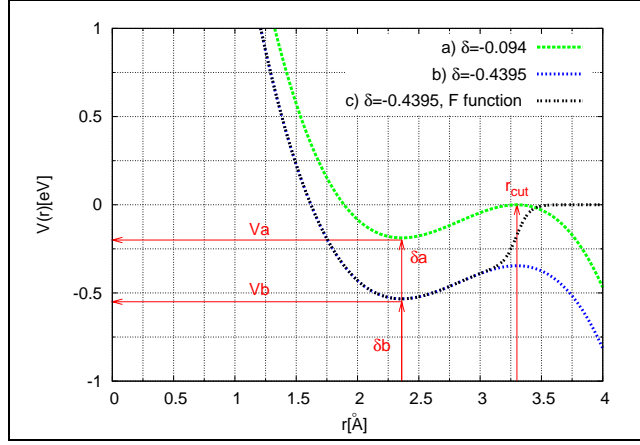


Figure 4.4: H-Pd (HPd) Interaction Potential. In this figure it is shown as an example the H-Pd interaction potential corresponding to the ppI Pd-Pd interaction potential. Curve **a** corresponds to the original fitting of Eq. (4.3). A H atom has 6 NN Pd atoms. The contribution to the H-Pd interaction energy is $-0.046 \text{ eV} \times 6 = -0.27 \text{ eV}$. Curve **a** corresponds to the set of parameters obtained when the system is required to give the correct value of S . The contribution to the H-Pd interaction energy is $-0.3912 \text{ eV} \times 6 = -2.35 \text{ eV}$. Curve **c** is the same as curve **b**, but multiplied by the Fermi function $(\exp((x - 3.3)/0.05) + 1)^{-1}$. This assures that the potential goes smoothly to zero beyond r_{cut} . In this case δ was adjusted within a MD simulation in order to obtain the correct value of E_b .

Table 4.7: Basic Properties described by the HPd potential. The HPd interaction potential was fitted to reproduce the relative lattice volume change $\Delta V/V$ through the displacement S of the Pd nearest neighbours generated by the Kanzaki forces. This model also reproduces the binding energy of H in Pd E_b . Values obtained in the simulation are the following:

S (Å)	E_b (eV)
0.04	-2.43

At room temperature, experimentally the monohydride PdH has fcc structure with HPd-distance r of 2.013 \AA [WB78]. In the solid solution, PdH_x at high H concentrations ($x > 0.1$), the Kanzaki force, produce a r comparable with these results. This change is accompanied by a significant change of the contribution of the HPd interaction energy, as shown in figures 4.6 and 4.7. As described later, in Section 5.2 (See Fig. 5.6) this effect must be corrected in order to be able to reproduce qualitative the binding energy curve of bulk Pd with high H concentrations. This is achieved through a modified HPd interaction potential (HPd_{mod}) which is given by:

$$V(r) = \begin{cases} -\alpha(r - r_o)^3 + \gamma(r - r_o) + \delta, & r_{\text{HPd}} < 2 \text{ \AA} \\ -\alpha'(r - r_o)^3 + \gamma'(r - r_o) + \delta', & r_{\text{HPd}} \geq 2 \text{ \AA} \end{cases} \quad (4.18)$$

The parameters for the HPd_{mod} are given in Table 4.8. A sketch of the HPd_{mod} interaction potential is shown in figures 4.5 and 4.6 and its effect on the average distance a H atom and its neighboring Pd atoms is shown in figure 4.7.

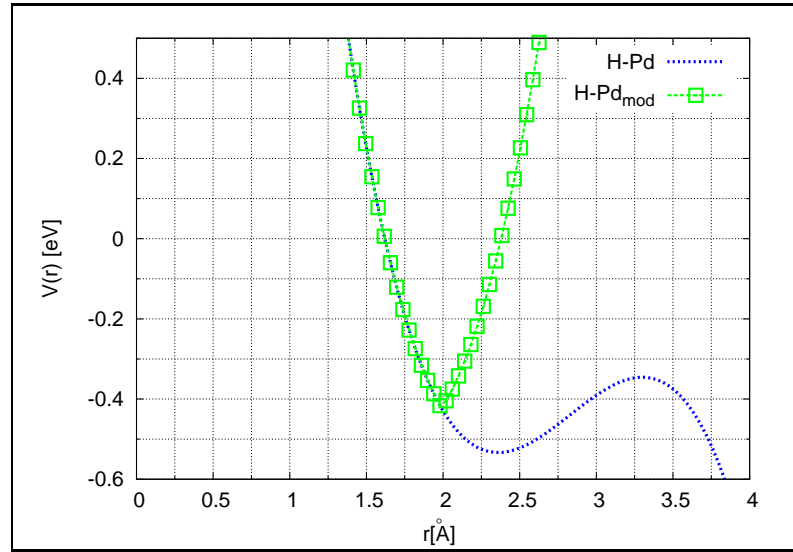


Figure 4.5: H-Pd modified (HPd_{mod}) Interaction Potential. It is shown the H-Pd and the H-Pd modified interaction potential.

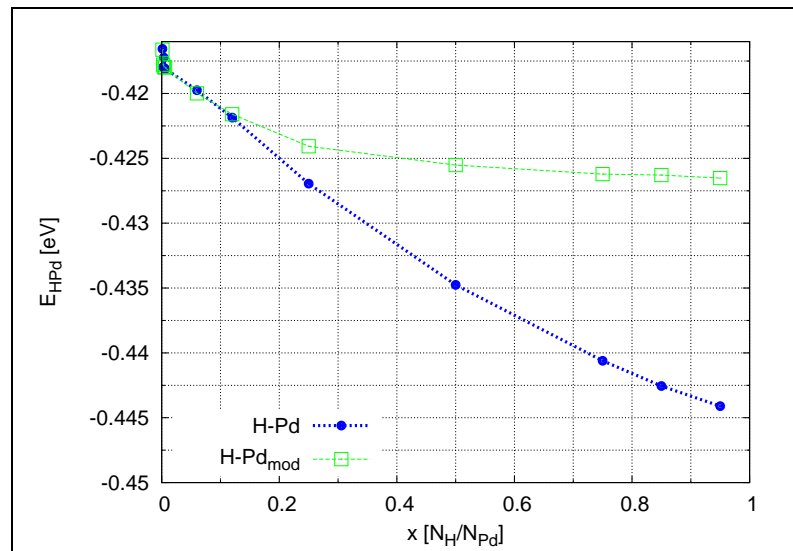


Figure 4.6: Effect of the HPd_{mod} modified Interaction Potential on the energy contribution per H atom. It is shown the H-Pd interaction as a function of the H concentration in bulk Pd per pair for the interaction potential described in Section 4.2 and the interaction per pair of a modified H-Pd interaction (H-Pd_{mod}) as a function of the H concentration in bulk Pd. The contribution of the H-Pd interaction per H atom increases from -2.49 eV (-0.42×6) at low H concentrations to -2.65 eV (-0.44×6) at high H concentrations. The modified H-Pd_{mod} changes slowly with the H concentration.

Table 4.8: HPd modified Interaction Parameters for the ppl interaction model. With this choice of parameters the required Pd displacement $S=0.04\text{\AA}$ is assured at low H concentrations. For H concentrations $x \geq 0.1$ the interaction energy changes not so drastically.

α (eV/ \AA^3)	α' (eV/ \AA^3)	γ (eV/ \AA)	γ' (eV/ \AA)	δ (eV)	δ' (eV)	r_o (\AA)	r_{cut} (\AA)	r'_{cut} (\AA)
0.4527	-0.1999	0.3	-1.7821	-0.4395	1.54696	2.83	3.3	2.4

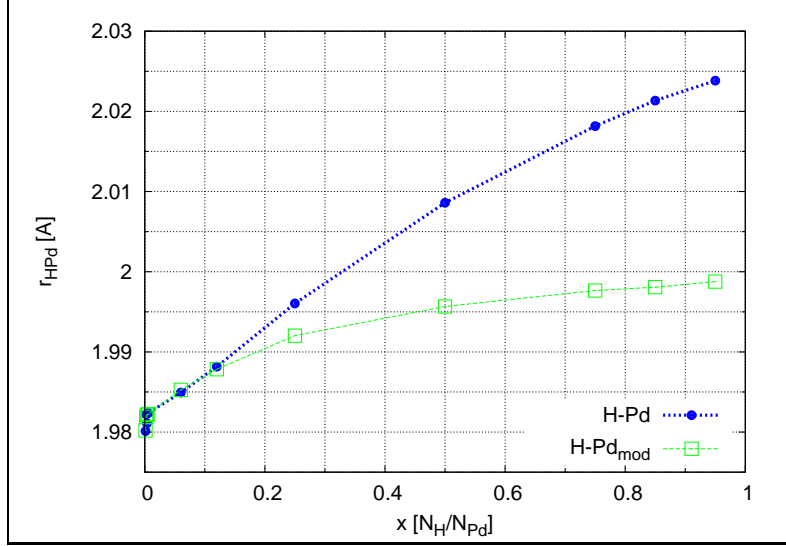


Figure 4.7: Effect of the HPd modified Interaction Potential on the average distance between H and nearest neighbour Pd atoms. It is shown the average distance between the H atoms and the NN Pd atoms as a function of the concentration x . It was calculated using the HPd and the HPd modified interaction potential. With the modified HPd interaction at low H concentrations the distance r_{HPd} changes fast with the H concentration in contrast at higher concentrations.

4.3 H-H interaction potential

As already mentioned in Section 3.2, the effective H-H interaction in metal has two contributions: an attractive long range contribution mediated by the lattice which is a result of the interaction of one point defect with the stress field of another point defect and a repulsive short range interaction arising from the interaction with the metallic electrons. While the attractive contribution is already implicit in the H-Pd interaction, we need explicitly to account for the repulsive contribution. According to the effective medium theory [CDJ⁺89] the H-H interaction in Pd is more repulsive than in the gas phase. Also it is known from experiments [Swi79, RJ85] that in the metal two H atoms do not come closer than 2\AA . Taking this into account it is proposed the following first neighbour model (HH*) for the H-H interaction in Pd:

$$V(r) = C1 \cdot \exp(-r/c3) \quad (4.19)$$

where $C1$ is a scaling factor which essentially determines the strength of the H-H interaction per pair of H atoms. $C3$ delivers the range of the interaction. The parameters were adjusted to assure that at high H concentrations, the H atoms do not come closer than 2\AA . The adjustment was done with the help of the MC-MD procedure described in Section 2.2. In figure 4.8 the H-H interaction potential is plotted that corresponds to the Pd-Pd ppl interaction potential. In table 4.9 a set of parame-

ters is given. As described later in Section 5.2 this H-H interaction potential does not reproduce the expected binding energy curve of bulk at high H concentrations. In order to try overcome this problem this potential was made more repulsive (HH^*_{mod}) and its is shown in figure 4.8. To reproduce qualitative the solubility of H in bulk Pd

Table 4.9: H-H Interaction Parameters for the ppl interaction model. It is shown a set of parameters corresponding to the repulsive H-H interaction (HH^*). This is a first neighbour model.

$C1$ (eV)	$C3$ (Å)	r_{cut} (Å)
0.045	0.4	3.0

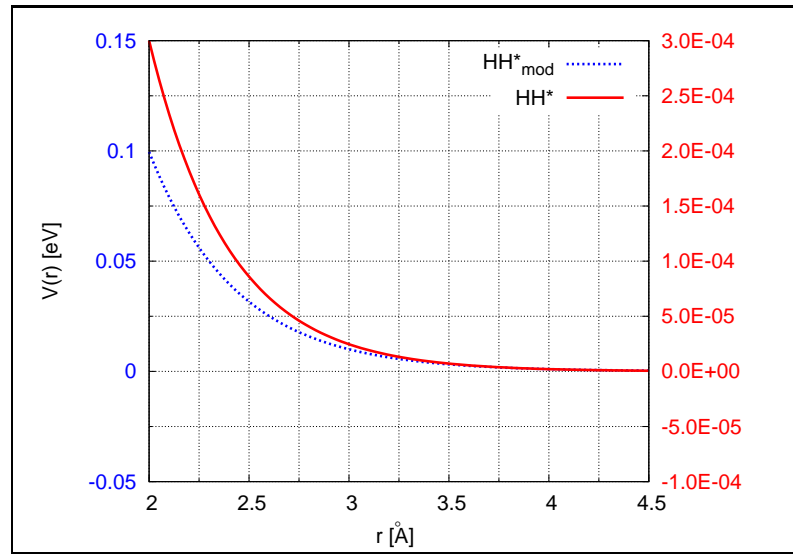


Figure 4.8: H-H (HH^* and HH^*_{mod}) Interaction Potentials. It is shown the H-H interaction potential HH^* and an interaction potential that is more repulsive HH^*_{mod} . $V(r) \text{HH}^*_{\text{mod}} = 9.82 \cdot \exp(-2.3 \cdot r)$. At an equilibrium H-H distance $r \approx 2.75 \text{ \AA}$, $V(r) \approx 0.00004 \text{ eV}$ (HH^*) in contrast with $V(r) \approx 0.02$ (HH^*_{mod}).

and clusters known from experiments it is necessary to take also into account H-H interaction contributions arising from the next nearest neighbours so that at high H concentrations the mean H-H contribution per atom is reduced. Such a model can be written as:

$$\begin{aligned}
 V(r) = & 0.75 \cdot \left[\frac{1}{(0.398 \cdot r)^2} - 1 \right] \cdot \exp \left[\frac{1}{0.398 \cdot r - 1.99} \right] \\
 & + 0.75 \cdot 0.105 \cdot \exp \left[-3.25 \cdot (r - 3.21)^2 \right] + 0.05
 \end{aligned} \tag{4.20}$$

It is shown in Figure 4.9.

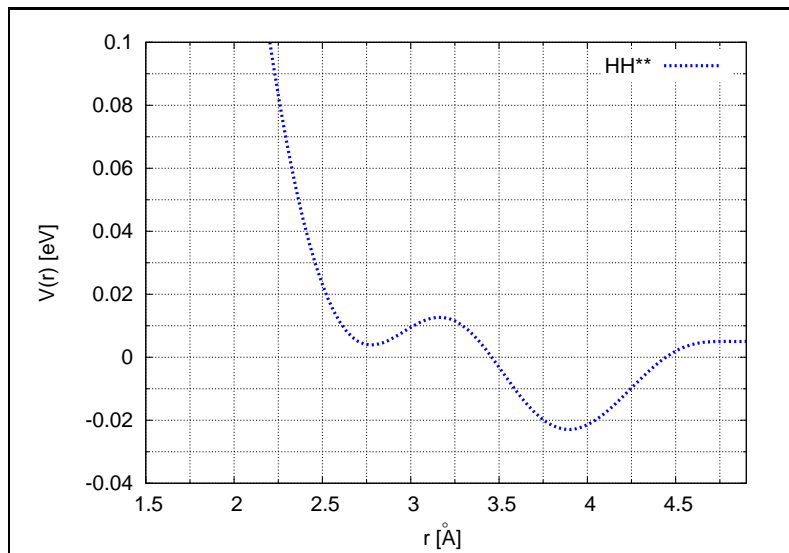


Figure 4.9: H-H (HH**) Interaction Potential. It is shown a modified H-H interaction potential which takes into account contributions from the N and NN neighbours. At low H concentrations the hydrogen atoms would have an interaction of -0.023 eV pro pair. At high H concentrations the hydrogen atoms would have an interaction of $-0.023 \times 3 + 0.004 \times 6$ eV.

Chapter 5

Simulations of Hydrogen Loaded Pd

In this chapter the results of the simulations of hydrogen loaded bulk Pd and cluster are presented and discussed. In order to test the simulation models, calculations for bulk Pd are first done. Then, using the same set of interaction potentials, calculations for Pd clusters are performed. We mainly focused on describing correctly the equilibrium lattice constant a of pure Pd, the binding energy of hydrogen E_b in Pd, the cohesion energy E_{coh} of Pd and PdH, the relative volume change $\Delta V/V$ under hydrogen loading. Afterwards, the chemical potential and solubility isotherms in dependence on the hydrogen concentration are calculated. Comparison between experimental and simulation results are made. Also comparison between the results from bulk and cluster simulations are discussed.

5.1 Relative Volume Change in Bulk Pd under H Loading

The relative lattice volume change ($\Delta V/V$) was calculated with the H-Pd interaction model of Section 4.2 (See Table 4.6). The relative lattice volume change under hydrogen loading is comparable at low H concentrations with the experimental results presented in Section 3.3. As seen in Figure 5.1, although the displacement S was chosen to follow the Kanzaki forces, only at low H concentrations the simulation results are comparable with the experimental results. At higher H concentrations, the difference is about 2.4%. This deviation can be attributed to interaction effects between hydrogen atoms, making that the linear response model is no longer valid, which is assumed in the Green's function approach.

The cohesion energy of a metal consists of a volume energy, which is structure dependent, and a pair interaction energy. In our case, the volume energy is taken as the contribution E_{eg} of an homogeneous electron gas provided through the s and p electrons in the system. As described in Appendix C, the relative number of s electrons was taken to be $n_{\text{Pd}} = 0.4$ and $n_{\text{H}} = 1$ for Pd and H respectively. According to Figure 5.1, the electron gas contribution has nearly no effect on the H induced expansion in the lattice.

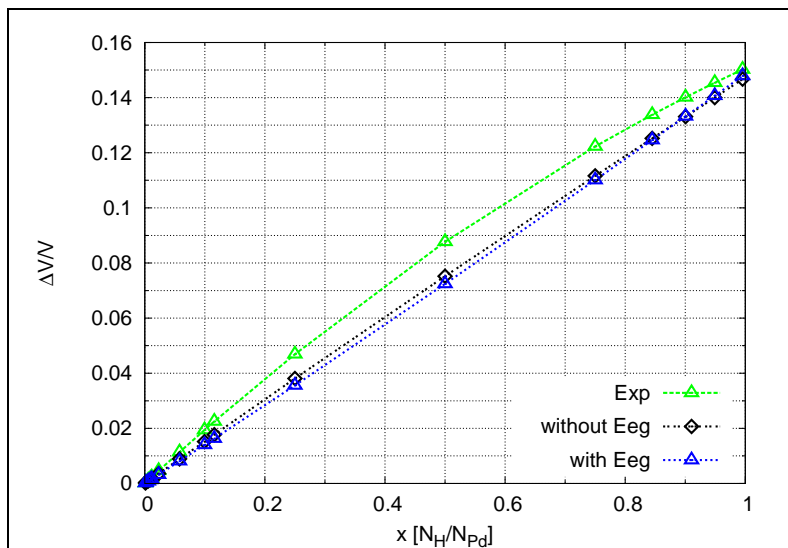


Figure 5.1: Relative volume change $\Delta V/V$ of PdH as a function of hydrogen concentration. It is shown the lattice expansion under hydrogen loading due to different contributions. Only at low H concentrations the results are comparable with the experimental results [FGG86]. The electron gas term taking into account the s electron contributions provided by the H and Pd atoms, has nearly no effect on the lattice expansion.

5.2 Binding Energy Calculations

As described in Section 1, experimentally there is a shift of the lower solubility limit to higher H concentrations when comparing the solubility isotherms of bulk Pd and clusters. This shift is ascribed to an increase of absorption sites in clusters compared to bulk. The absorption sites are interpreted as surface sites. It is known that in a small cluster there are more surface-like atoms than bulk-like atoms. In order to test this assumption, calculations of the binding energy E_b of 1 H atom in Pd as a function of surface and subsurface sites were made. It was calculated following Eq. 3.33. A fcc system with 792 Pd atoms was used. In order to simulate surface effects, periodic boundary conditions for the Z axis were removed, yielding a Pd (100) surface. The system was allowed to relax (200 ps) and then one H atom was placed at an octahedral site. The system was allowed to equilibrate (80 ps). In order to calculate E_b at this site, statistical averages over the last 1000 integration steps (2.6 ps), were taken.

Calculations were carried out with the potential models ppI, ppII, and EAM described in Chapter 4, together with their corresponding H-Pd interaction potentials. Different sites were tested corresponding to surface (5s), subsurface (6s, 6ss, 6sss) and bulk (6i) sites (See Fig. 5.2). The indexes s, ss, sss and i denotes surface, subsurface, subsurface, and inner sites, respectively (when going from the surface to the inner sites). The number 5 or 6, denotes the number of Pd nearest neighbours a H atom has. The results are presented in Table 5.1. For comparison, the experimental results are also displayed. The results corresponding to the 3 different Pd-Pd interaction potentials follow the same tendency. In each case, we observed surface, subsurface and bulk like places, which are distinguished by different E_b values. As observed experimentally by OKUYAMA ET AL [OST⁺98], the H binding energy, E_b , at subsurface sites is larger than in bulk. OKUYAMA additionally found a dissociative chemisorption state on the surface, which corresponds to a four-fold hollow site composed of the outermost Pd atoms. In the present work this surface site is labelled as

Table 5.1: Binding Energy E_b calculations of H in Pd at a Pd (100) Surface. E_b was estimated by using the different interaction potentials for Pd with their corresponding H-Pd interaction potentials described in Chapter 4. The simulation results follow the same tendency than the experimental results from OKUYAMA. There are surface, subsurface and bulk-like sites. The numbers 5 and 6 means that the hydrogen atom at this sites has 5 or 6 nearest neighbours. The indexes s, ss, sss and i corresponds to surface, subsurface, subsurface and inner (See Fig. 5.2).

NN-Site	E_b (eV)			
	Exp	EAM	PPI	PPII
5-s	-2.28	-2.137	-2.135	-2.278
6-s	-2.38	-2.361	-2.418	-2.413
6-ss		-2.393	-2.412	-2.505
6-sss		-2.389	-2.411	-2.399
6-sss		-2.385	-2.411	-2.399
6-i	-2.33	-2.391	-2.411	-2.399
Δ_{6s-6i}	-0.05	0.03	-0.007	-0.014

5s. The H atom sits at a four-fold hollow site and has 5 Pd nearest neighbors (4 Pd atoms at the same layer and 1 Pd atom from the layer below). The value of E_b for H at this site agrees qualitative with the results from OKUYAMA. It is smaller than the subsurface and bulk E_b values. The E_b values calculated in our work correspond to single atom adsorption experiments and those values from OKUYAMA to more than 1 L coverage. With increasing H concentration, the binding energy E_b decreases, explaining the difference in the values of E_b between experiment and the present calculations. However, the tendency between surface, subsurface and bulk values is in agreement with the experiments. The value of E_b for H on a Pd (100) surface was calculated in previous studies by WILKE ET AL [WHL94] and by BASKES [MDB84]. WILKE ET AL made ab initio calculations and found a surface and a subsurface site at a coverage 1. In contradiction to OKUYAMA, they found that the subsurface site has a larger energy than the surface site and also that there are small differences between a subsurface site and bulk sites. BASKES made calculations with the embedded atom potential (EAM) and found surface states on the Pd (100) and Pd (111) surface both with the same E_b value (-2.91 eV). They found also top and bridge sites, which were not found in the present work.

Although our results for the EAM, ppI and ppII models display the same tendency in the energy of surface, subsurface and bulk E_b values, the relative difference between sites is different. This is due to relaxation effects of the different Pd atomic layers provided by the interaction models.

For pure Pd surfaces, the top atomic layer and the inner atomic layers relax differently [WFG⁺99]. It is known from experiments at the (100) Pd surface [QLT⁺90] that there is an outward relaxation (3%) for the last Pd atomic layer while the second layer exhibit an inward relaxation (-1%). At the (111) Pd surface there is an inward relaxation for the first two atomic layers.

Although simple pair potentials do not predict correctly surface relaxations, with the ppI and ppII models the top layer undergoes an outward expansion opposed to the predictions of our EAM calculations and in agreement with the experimental results (See table 5.2). As can also be observed for the ppI and ppII models, there is a slight difference in the distance between the first (d_{12}) and second (d_{23}) layer.

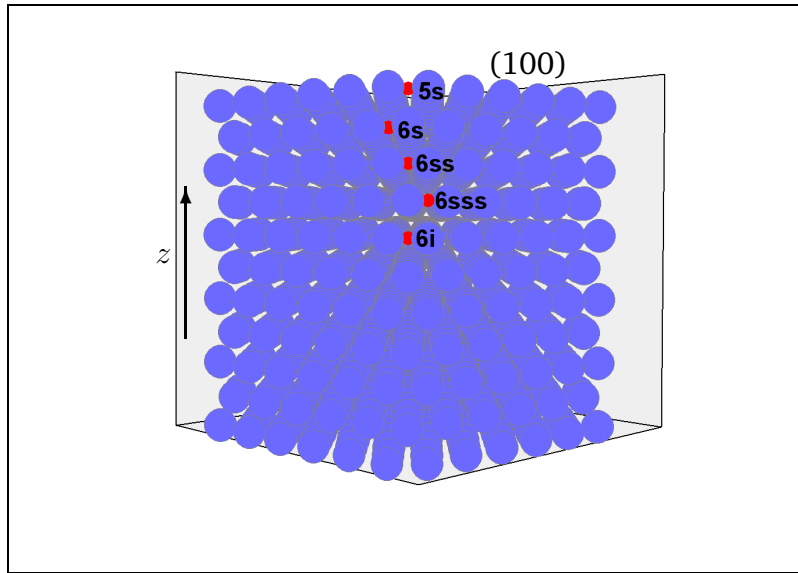


Figure 5.2: Testing sites at a Pd (100) surface. Periodic boundary conditions along the z direction were removed in order to yield a Pd (100) surface. The atoms in red correspond to H atoms sitting at different octahedral sites, which are labelled as **s**: surface, **ss**: subsurface, **sss**: subsurface and **i**: inner sites. 6 or 5 denotes the number of Pd nearest neighbours a H atom has.

Table 5.2: Pd (100) Surface Relaxation. It is shown the difference in % between the first (d_{12}) and second d_{23} Pd layer as calculated with the 3 different interaction models for Pd: ppI, ppII and EAM. The difference was taken comparing the values in the relaxed surface and the values for relaxed bulk.

	Pd (100) surface			
	ppI	ppII	EAM	Exp
d_{12} (Å)	0.31	1.1	-3.1	3.0
d_{23} (Å)	0.57	0.8	0.34	-1.0

Therefore, for these two models the difference in E_b values is mostly due to the coordination number of the H atoms at surface and subsurface sites. The three Pd-Pd interaction models do not describe properly the surface relaxation. However, when a H atom is introduced it displaces the nearest Pd atoms by the same amount independent of the original distance between neighboring Pd atoms. This is a direct consequence of the way the H-Pd interaction was constructed. Therefore the E_b values follow the experimental observed tendency.

The interaction potentials are also used in calculations for clusters. Calculations were performed on a 923-Pd cuboctahedral cluster (See Figure 5.4). In order to simulate free surfaces, boundary conditions corresponding to the X- Y- and Z- axes are removed.

As seen in Section 4.1.2, the model ppI can be used to describe basic Pd properties, like the lattice constant a and the bulk modulus B . If the model is completed by an electron gas term, the cohesion energy E_{coh} can also be described. It is established [Sul03] from experiments that in a cluster there is a change in the lattice constant in comparison to bulk. Also, between different atomic layers, the lattice constant can decrease when going from inner to outer layers. The lattice constant in clusters is also a function of the cluster size as determined experimentally [SA01b]

Table 5.3: Basic Properties of Pd Cluster described by the ppI potential. It is shown the average lattice constant (a_{avg}), the bulk modulus (B) and values of the cohesion energy (E_{coh}) with and without the contribution of the electron gas term. a varies inside the cluster (See Fig. 5.3)

	a per Layer (Å)	a_{avg} (Å)	B (eV/Å ³)	E_{coh} (eV)
without E_{gas}	3.8938 3.8903 3.8895	3.89	1.2	-2.48
with E_{gas}	3.8952 3.8889 3.8889	3.89	0.9	-3.68

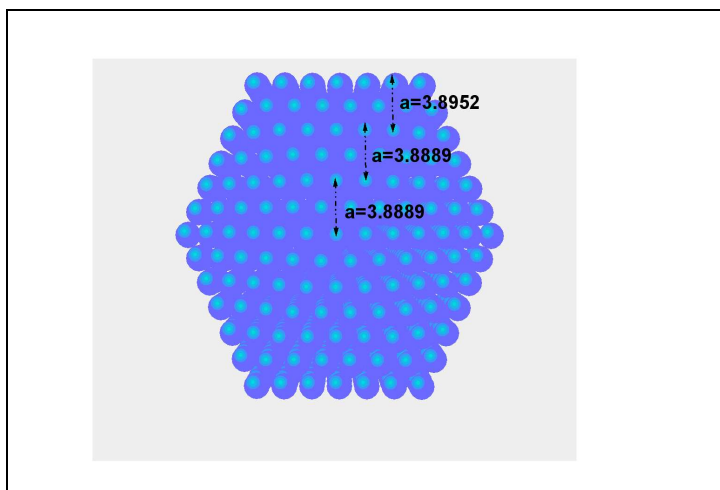


Figure 5.3: Lattice constant variation in the 923-Pd cuboctahedral cluster. Calculated using the electron gas term. The lattice constant is not uniform inside the cluster. There are small variations.

and also proved by computer simulations [SA96]. Table 5.3 shows the predictions for a , B and E_{coh} from ppI. Obviously, there is a difference in the lattice constant inside the cluster when going from the inner to the outer layers. When including the electron gas term in the calculations, the lattice constant decreases as observed experimentally. The electron gas term provides a pressure contribution which yields a positive (tensile) stress at the surfaces, favouring smaller lattice constants. Also in comparison with bulk, the cohesion energy is smaller. Each Pd atom at the surface has a contribution to the potential energy given by 5 nearest neighbour Pd atoms, making this contribution smaller than the contribution of the Pd atoms in the inner. As a consequence the total potential energy per atom is smaller.

In small clusters, there is a larger number of surface atoms than of volume atoms. For cuboctahedral clusters, the following equation relates the number of atoms n_i to the number i of the shell:

$$n_i = 10 * i^2 + 2. \quad (5.1)$$

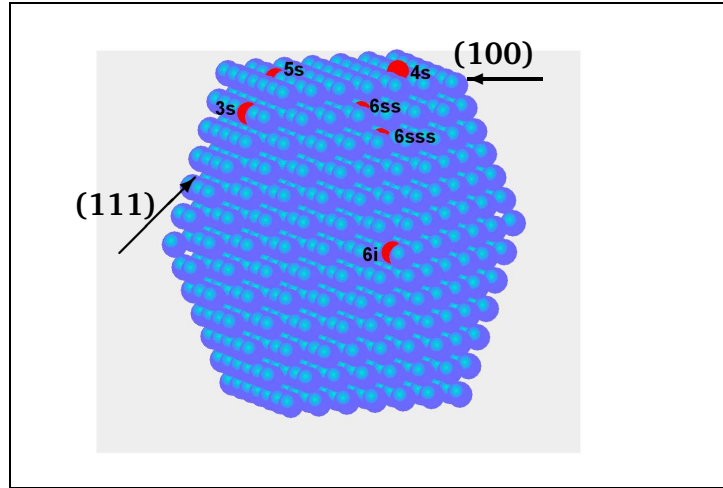


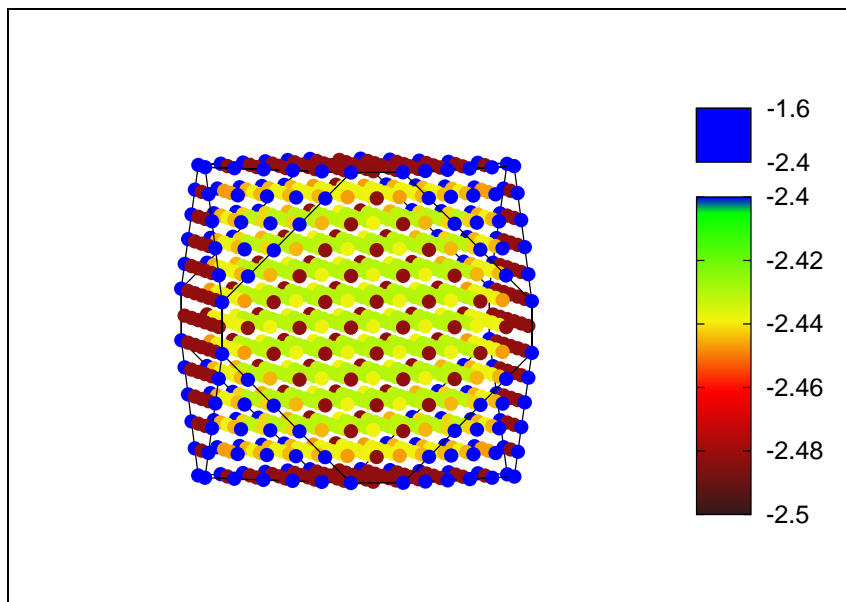
Figure 5.4: Testing sites in the Pd cluster. It is shown a Pd surface and the different sites that can occur. The atoms in red correspond to H atoms sitting at octahedral sites, which are labelled as **s**: surface, **ss**: subsurface, **sss**: subsurface and **i**: inner sites. 3, 4, 5 or 6 denotes the number of nearest neighbours a H atom has.

The total number of atoms, N , belonging to a cluster with i shells is:

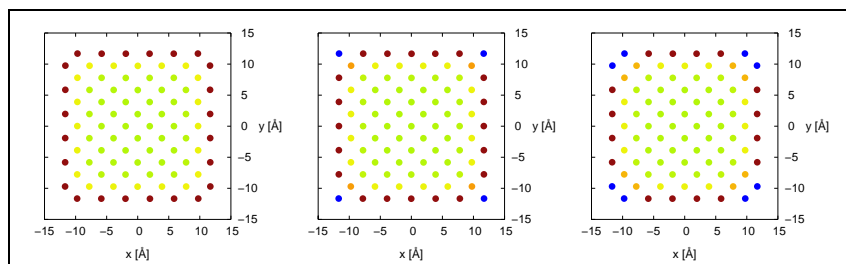
$$N = 1 + \sum_{j=1}^i (10 * j^2 + 2). \quad (5.2)$$

A cuboctahedral cluster with 923 atoms has $i = 6$ shells. Pd surface atoms belong to the last shell. Therefore, in this case the number of surface atoms is $N_s=362$ [Sac98]. It is of interest to calculate the dependence of the binding energy E_b for the various sites in a cluster. An already relaxed pure Pd cluster was used and E_b was calculated (with Eq. 3.33) by setting 1 H atom into an octahedral site. Different octahedral sites were tested along the $\langle 111 \rangle$ and $\langle 100 \rangle$ directions. The results are shown in Table 5.4. It is found that surface sites, subsurface sites and bulk-like sites have different E_b values. Also edge sites exist, but because of their low E_b values, they do not contribute to the solubility of H in the Pd cluster. The simulation results for the cluster follow the same tendency as the results at the surface. A directional dependence was not found, instead the E_b value turned out to depend on the number of nearest neighbours, indicating that the relaxations at the (100) and (111) surfaces are similar. As seen in Table 5.4, our EAM calculations done in this work do not predict energetic preference of 5s or 6ss sites in the cluster in contradiction with the experimental results of PUNDT, SACHS AND SULEIMAN [PSW⁺99, SA01a, Sul03]. PII predicts preference of the 6ss site but not of the 5s, while the model ppI predict energetic preference of both surface states. Therefore it was decided to use the model ppI for further chemical potential calculations. For the 923 Pd cuboctahedral cluster, we found 994 sites for H occupation. All site energies (E_b at that site) were calculated and the values are shown in Figure 5.5.

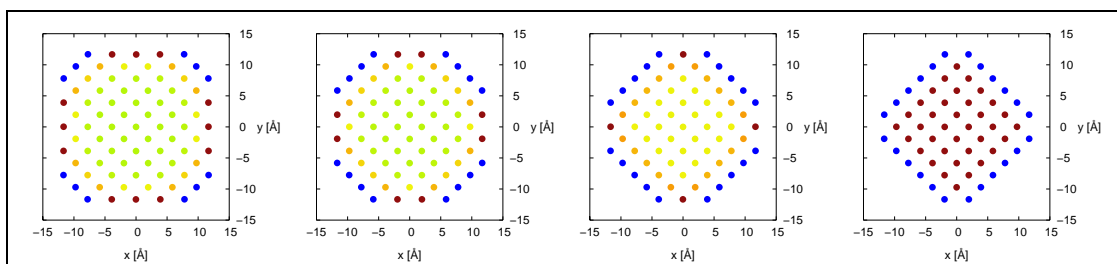
As function of the H concentration, the binding energy E_b was calculated using the model ppI for the Pd-Pd interaction (without electron gas term) and using the two different H-H interaction models (HH*, HH**) described in Section 4.3. In order to compare E_b with the experimental heat of solution values, it was calculated following Eq. 3.34 and Eq. 3.36. The results are shown in Figure 5.6 (more details about the H-H interaction potentials will be discussed later). As can be seen, if the HH* nearest neighbour is used, the absolute value of E_b increases drastically (at $x >$



(a) *Left*: Distribution of the different values of binding energies in the cluster. *Right*: Energy scale in eV.



(b) *Left*: Innermost layer at $z=0$. *Middle*: Layer I at $z=a/2$. *Middle*: Layer II at $z=a$.



(c) *Leftmost*: Layer III at $z=3a/2$. *Rightmost*: Layer VI at $z=3a$.

Figure 5.5: Site energies in the 923-Pd cuboctahedral cluster. It is shown how E_b is distributed in the cluster. Different cross sections corresponding to layers along the positive z direction are also shown. The negative z direction is similar.

Table 5.4: Binding Energy E_b in a 923-Pd Cuboctahedral Cluster. A hydrogen atom has different values of E_b depending on surface or bulk-like sites. The numbers 3, 4, 5 or 6 means that the hydrogen atom at this sites has 3, 4, 5 or 6 NN. The indexes e, s, ss, sss and i corresponds to edge, surface, subsurface, subsurface or inner sites (See Fig. 5.4).

NN-Site	E_b (eV)		
	EAM	PPI	PPII
3-s	-1.678	-1.601	-1.710
4-s	-2.16	-2.1	-2.296
5-s	-2.23	-2.447	-2.34
6-ss	-2.432	-2.439	-2.43
6-sss	-2.468	-2.432	-2.411
6-i	-2.473	-2.430	-2.416
Δ_{5s-6i}	0.243	-0.016	0.076
Δ_{6ss-6i}	0.041	-0.009	-0.014

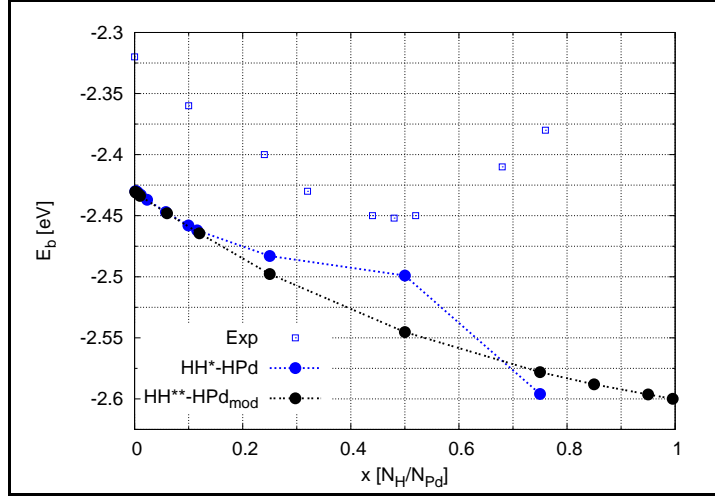


Figure 5.6: Binding energy E_b for H in Bulk Pd as function of hydrogen concentration. The models HH* with HPd (which takes into account only the nearest neighbours) and HH** with HPd_{mod} (which takes into account the nearest and next nearest neighbours) were used and are described in Section 4.3. Exp is the experimental data taken from Fig. 3.5.

0.5) with increasing H concentration in contradiction with the experimental results. If the HH** interaction model with nearest and next nearest neighbours is used one finds the expected behavior, that is, for all H concentrations there is a mild increase of the absolute value of E_b with increasing x . This is due, to the HPd interaction used in this case. With HH** the HPd interaction (HPd_{mod}), was fitted so that the change in total potential energy is milder than when using the HPd. The interaction between the H atoms is for all x concentrations attractive. Therefore, the repulsive effect of the H atoms will not cause a decrease of the absolute value of E_b . Experimentally the absorption heat turns from exothermic to endothermic at $x \approx 0.5$ (See Figure 3.5). This is not reproduced by the present simulation. One may take this as an indication that either band structure effects play an essential role, which are not included here, or that there are rather strong repulsive effects between the H atoms at higher concentrations.

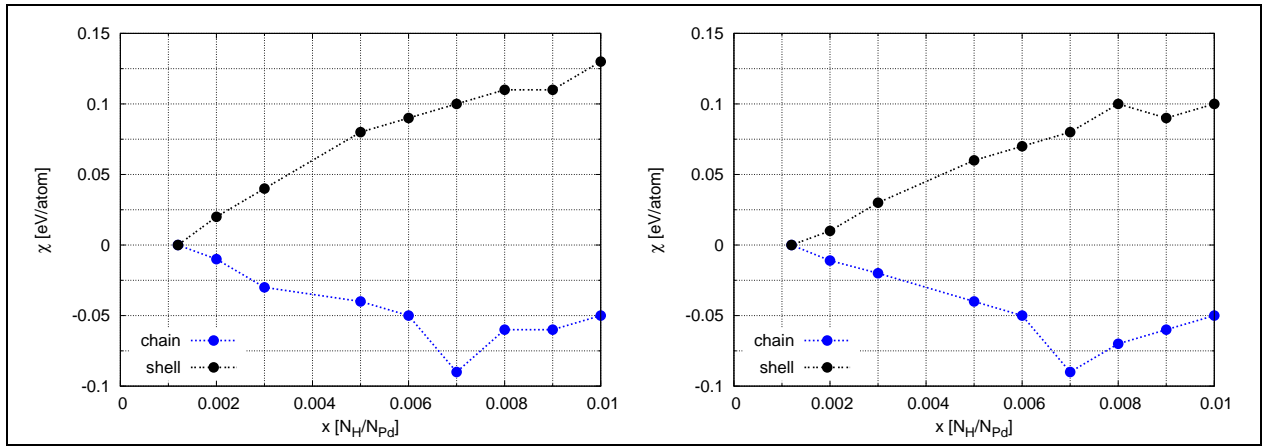


Figure 5.7: H-H elastic interaction in bulk at low H concentrations. *Left*: Calculations made using ppI without the direct H-H interaction, that is, the lattice mediated elastic part is estimated. At low x , the chain configuration along a $\langle 100 \rangle$ direction is energetically more favourable than the closed shell configuration along the $\langle 110 \rangle$ direction. *Right*: Using ppI with the direct H-H interaction, that means the effective H-H is estimated.

5.3 H-H Effective Interaction in Pd

As already mentioned in Section 4.3, the effective H-H interaction is composed of two contributions: the long-range lattice mediated attractive interaction and the short range repulsive interaction from local electronic effects. Following Section 3.3.1, the effective H-H interaction can be estimated. Using the ppI and neglecting any direct H-H interaction, the magnitude and behavior of the elastic lattice mediated interaction energy was calculated, as function of the H concentration. Results are shown in Figure 5.7. In the cubic Pd structure, the elastic H-H interaction is different along the $\langle 110 \rangle$ and $\langle 100 \rangle$ directions (see Section 3.2). Although ppI is a first neighbour model, the direction dependency arises from the fact that the transversal springs are zero, therefore $C_a = -f/a$ (see Section 3.1). The H-H effective interaction χ was estimated following Eq. 3.39. As seen in Figure 5.7, a second hydrogen atom in the structure prefers a next nearest neighbour (NN) site rather than a nearest neighbour (N) site. Also, at low H concentrations, chain like H configurations in $\langle 100 \rangle$ directions are energetically more favourable than closed shell like configurations.

Also, as can be deduced by comparing the data in Figure 5.7 at low H concentrations, the direct H-H interaction is irrelevant. SALOMONS [Sal90] performed molecular dynamics simulations of the Bulk PdH system. Using a first neighbour H-H interaction model he obtained that the repulsion between two H-H atoms is $V_{H-H} = 0.005$ eV at a H-H separation $r_{HH} = 2.8284$ Å. In our work $V_{H-H} = 0.00004$ eV at a H-H separation $r_{HH} = 2.75$ Å when using HH^* , or $V_{H-H} = (0.004 \cdot r_{HHN} - 0.0227 \cdot r_{HHNN})$ when using HH^{**} .

The H-H elastic lattice mediated interaction is calculated in the the cluster at low H concentrations along the $\langle 100 \rangle$ (a chain of H atoms starting from a central site) and $\langle 110 \rangle$ directions (considered is a shell around a central atom). The results are shown in Fig 5.8. As in bulk, due to the anisotropy present in the lattice, chain like configurations are energetically more favourable than the closed shell like configurations. However, the H-H elastic interaction is weaker in clusters (See Table 5.5). It is found that the direct HH^* interaction (first neighbour model, See Section 4.3) influences mainly H atoms sitting at nearest neighbour positions, while its influence is negligible in cluster. A direct HH^{**} interaction (second neighbour model, See Sec-

Table 5.5: H-H interaction in Pd clusters. It is shown the H-H interaction per pair along the $\langle 100 \rangle$ and $\langle 110 \rangle$ directions (as origin the center of the cluster was taken). The elastic interaction was calculated through Eq. 3.39. The effective interaction is also calculated through Eq. 3.39 but additionally with the direct H-H (HH* or HH**) interaction potential. HH* takes into account a first neighbour interaction and HH** takes into account a first and second neighbour interaction.

	bulk		cluster	
	$\langle 100 \rangle$	$\langle 110 \rangle$	$\langle 100 \rangle$	$\langle 110 \rangle$
HH _{elastic} (eV)	-0.012	0.018	-0.0107	0.0105
HH* _{effective} (eV)	-0.010	0.011	-0.0107	0.0105
HH** _{effective} (eV)	-0.011	0.011	-0.0114	0.0103

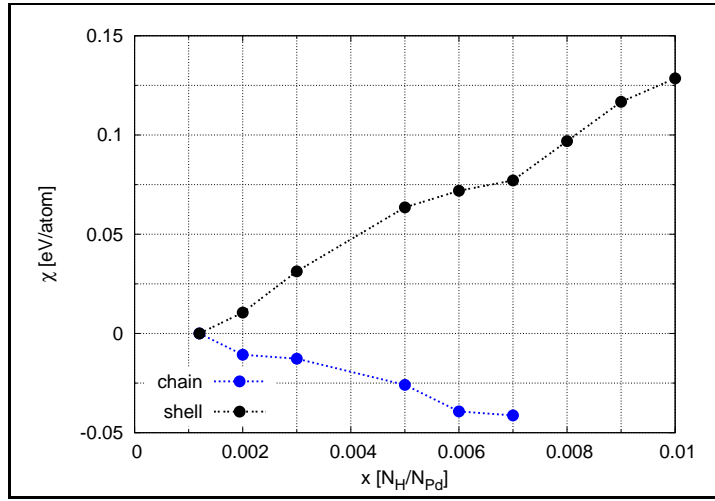


Figure 5.8: H-H elastic interaction in cluster at low H concentrations. The chain configuration is energetically more favourable than the shell configuration. However, in the cluster it is weaker than in bulk Pd.

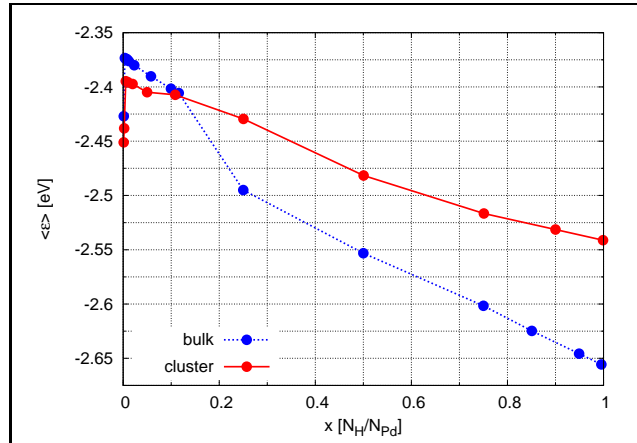
tion 4.3) has a small influence in the cluster, while it is not noticeable in bulk, due to the strong elastic interaction.

5.4 Chemical Potential Calculations of H in Pd

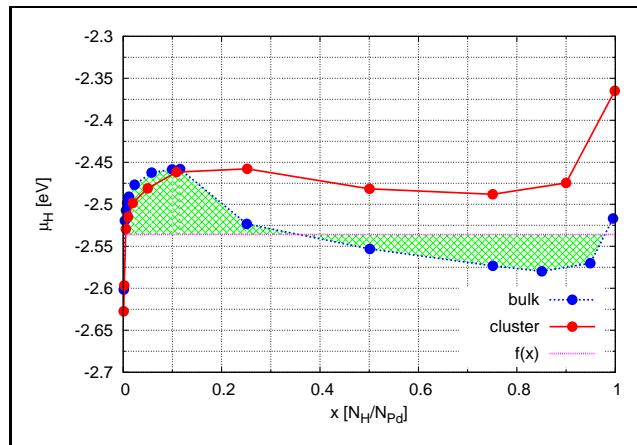
The chemical potential μ_H in bulk Pd and in cluster was calculated following the method described in Section 2.2. Calculations were carried out at T=300K using at first the ppI interaction potential for Pd-Pd and the HH* model for the H-H interaction. Also, calculations were done for ppI with the HH*_{mod} interaction model. The results are shown in Section 5.4.1. Later on, these curves are discussed and it is shown that it is necessary to introduce a HPd_{mod} and a HH** interaction models in order to obtain results that are comparable with the experiments.

5.4.1 Testing of the interaction potentials

Figure 5.9 shows the results for $\langle \epsilon(x) \rangle$ (Eq. 2.26) and μ_H (Eq. 2.28) from bulk and in cluster using the interaction models ppI-HH*-HPd. For both bulk and cluster the energy gain $\langle \epsilon(x) \rangle$ decreases with increasing H concentration.



(a) Energy gain of the system $\langle \epsilon(x) \rangle$ calculated with Eq. 2.26.



(b) Chemical potential and Maxwell construction for bulk. The areas of the shaded regions above and below $f(x)$ are approximately equal. $f(x) = -2.536$ eV, indicates that for the applied ppl-HH*-HPd model the upper limit of the α phase in the applied model lies around $x=0.003$.

Figure 5.9: Chemical Potential of H in Pd bulk and cluster - I. Using the HH* interaction model for the H atoms, only the α phase appears at low H concentrations. For the cluster, the limit is displaced to higher H concentrations in comparison to bulk.

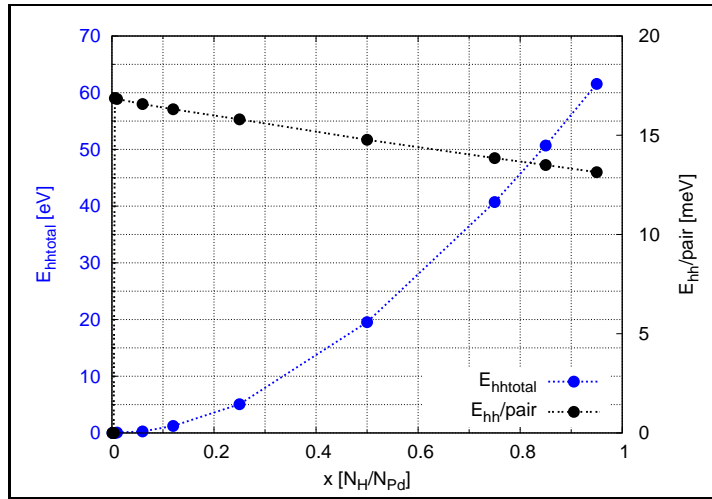


Figure 5.10: HH direct interaction (using HH^*_{mod}) as function of hydrogen concentration. It is shown the direct H-H interaction (total and per pair). At low H concentrations the interaction is zero (as expected) and increases as the H concentration increases, in order to deliver a more repulsive interaction at higher concentrations.

As can be seen, the shape of the isotherms in bulk and in cluster indicates the existence of an α phase at low H concentrations. According to the experimental observations, for clusters the α phase is displaced to higher H concentrations compared to bulk.

The instability of the system against the formation of a two-phases structure is modelled in Figure 5.9 by means of the Maxwell construction corresponding to bulk Pd. With help of this construction, in the ppI-model with HH^* interaction, the upper limit of the α phase is found at approximately $x = 0.003$, in contradiction to the experimental results, where one has $x = 0.015$ (see Figure 5.20). Further modifications were therefore performed for the H-H and H-Pd interaction potentials in order to obtain the expected behavior for μ_H , that is, at least a reasonable value for the α phase solubility limit. In what follows, these modifications are described.

About the H-H interaction model

The chemical potential shown in Figure 5.9 is calculated with the HH^* interaction model described in Section 4.3. For testing effects of the H-H interaction, we made this interaction potential more repulsive (HH^*_{mod}) (See Figure 4.8). In HH^* the interaction between two H atoms is modelled by $V(r) = 9.82 * \exp(-2.3 * r)$. The contribution $E_{hhtotal}$ to the total potential energy of the system is given by summing $V(r)$ over all H pairs in the system. In Figure 5.10, this contribution is shown and also the contribution per pair, $E_{hh/pair}$.

Figure 5.11 shows the chemical potential curve for H in bulk Pd, when using the models ppI-HPd- HH^*_{mod} . As can be seen, at higher H concentrations the chemical potential still decreases. According to the Maxwell construction, the upper limit of the α phase lies far beyond $x=0.015$. A two phase region can be observed with α' above $x \approx 0.98$. Although the H-H interaction HH^*_{mod} is more repulsive, than in the HH^* model, the chemical potential μ_H still shows the beginning of the α' at $x > 0.6$.

Modifying this first neighbour H-H interaction model to account for a more repulsive interaction still delivers a similar behavior for the chemical potential shown in Figure 5.9.

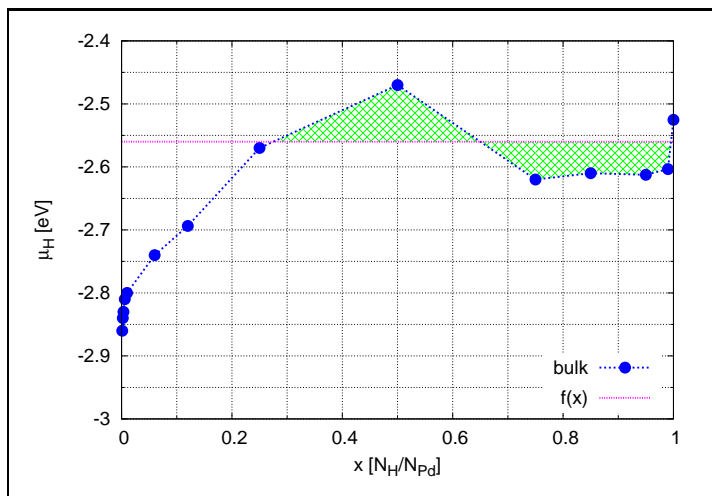


Figure 5.11: Chemical potential of H in bulk Pd - II. Calculations made using an HH^*_{mod} interaction potential (See Section 4.3). With help of the Maxwell construction, $x \approx 0.25$. $f(x) = -2.56$ eV.

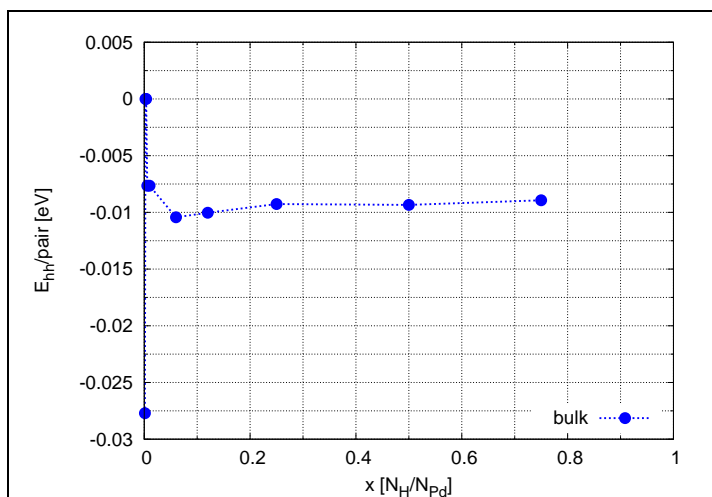


Figure 5.12: HH direct interaction (using HH^{**}) as function of hydrogen concentration. Calculation made using an HH^{**} interaction potential (See Section 4.3). It is shown the direct H-H interaction per pair obtained using this interaction potential. As expected for $N_{\text{H}}=2$ or $N_{\text{H}}=3$ the H atoms prefer to be at NN neighbour positions with ≈ -0.02 eV, at higher H concentrations they receive contributions from the N and NN atoms.

As already shown in Figure 5.7, the lattice mediated H-H interaction receive contributions from the first and second neighbours. At diluted H concentrations, the NN neighbour positions are preferred because they are energetically favourable (the interaction is attractive) compared to the N neighbour positions (repulsive interaction). At higher H concentrations, and without the H-H direct interaction potential, the H-H elastic interaction would have contributions arising from $-a \times NN/2 + b \times N/2$ (with NN the number of next nearest neighbours and N the number of nearest neighbours). Because of the elastic contributions arising from nearest and next nearest neighbours, a direct H-H interaction potential is chosen so that $-a \times 3 + b \times 6$ delivers an attractive interaction. As seen in Figure 5.12, at low H concentrations still the NN configurations are preferred and at high H concentrations $-a \times 3 + b \times 6$ delivers a mean attractive interaction. Therefore, a second neighbour interaction model (HH**) is appropriate. This model is described in Section 4.3. Figure 5.12 shows the contribution per pair $E_{hh/pair}$ of the HH** interaction potential. If $N_H=2$ or $N_H=3$, the H atoms prefer to sit either at next nearest (NN) neighbour positions (due to the elastic interaction) or they prefer to be far apart. Therefore, their contribution is ≈ -0.02 eV. For $x > 0.1$, the H atoms have contributions from N and NN positions, thus this contribution is ≈ -0.01 eV per pair.

About the H-Pd interaction model

The chemical potential shown in Figure 5.9 is calculated using the H-Pd interaction model (HPd) described in Section 4.2. According to its construction, this potential reproduces well the Kanzaki forces at low H concentrations. However, at high H concentrations, the resulting lattice expansion is accompanied by a significant change of the H-Pd interaction energy. That is, the contribution of the H-Pd interaction per H atom increases from -2.49 eV at low H concentrations to -2.65 eV at high H concentrations (See Figure 4.6). The distance between the H and the nearest neighbour Pd atoms changes from 1.98 Å to 2.02 Å (See Figure 4.7). This significant contribution is the cause of the change in binding energy of 0.18 eV from low to high H concentrations (See Figure 5.6).

A slightly modified HPd (HPd_{mod}) was developed to overcome this problem (See Figure 4.5). The modified HPd potential still reproduces the change in next neighbour distance $S = 0.04$ at low H concentrations and at high H concentrations, the distances r_{HPd} between H and the N neighboring Pd atoms remains nearly constant with the increasing H concentration allowing that the change in the H-Pd interaction remains very weak. Figure 5.13 shows the effect of this modification on the binding energy E_b in bulk. At lower x concentrations ($x < 0.1$), the E_b values calculated with HPd_{mod}, tend to increase with increasing x concentration, more than the E_b calculated with the HPd.

With increasing H concentration, the contribution $E_{hh/pair}$ (Figure 5.14), allows to overcome the effect arising from the H-Pd interaction per H atom to the total potential energy. As can be deduced from Figure 5.15, with the use of a H-H interaction potential (HH**), which includes contributions from the N and NN neighbours and with the modified H-Pd interaction (HPd_{mod}), the existence of the transition region (miscibility gap) is also obtained. In comparison to Figures 5.9 and 5.11 the beginning of the α' phase is displaced to lower x concentrations. Also at concentrations $x \leq 0.1$ the same μ_H is obtained using the two different potential combinations (HH**-HPd, HH**-HPd_{mod}). HPd_{mod} is essentially the same HPd for $x \leq 0.1$.

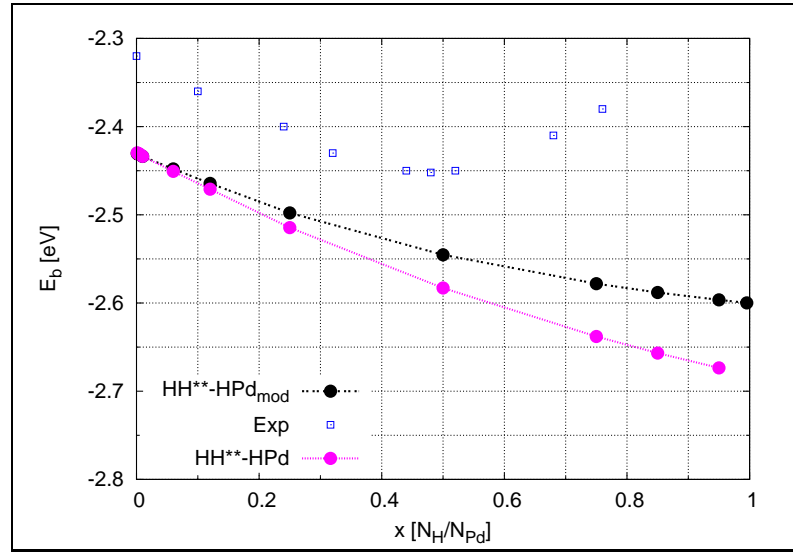


Figure 5.13: Effect of the modified Interaction Potential HPd_{mod} on E_b in bulk. It is shown the E_b dependence on x using a second neighbour model for the H-H interaction and the modified H-Pd interaction model. **HPd**: Original HPd interaction, **HPd_{mod}**: similar to HPd, but modified at higher x concentrations ($x > 0.1$), **HH****: second neighbour interaction model.

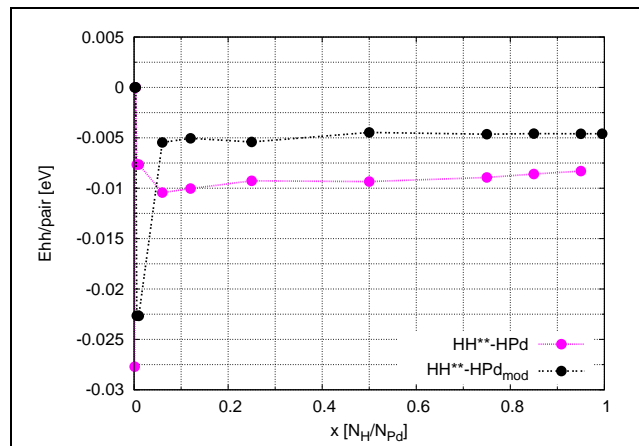


Figure 5.14: Effect of the HPd modified Interaction Potential on the Direct H-H Interaction in bulk. It is shown the direct H-H interaction per pair obtained using the modified H-Pd potential and a second neighbour model for the H-H interaction. As expected for 2 or 3 H atoms they prefer to be at NN neighbour positions at higher H concentrations they receive contributions from the NN and NNN.

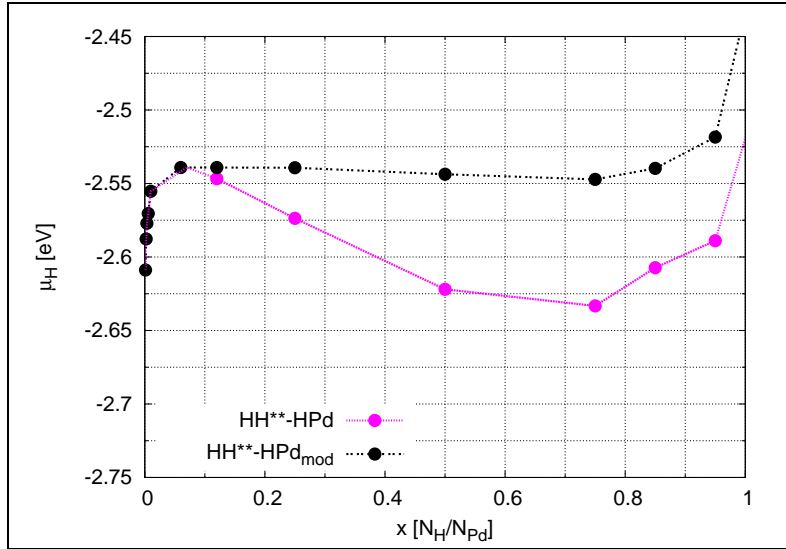
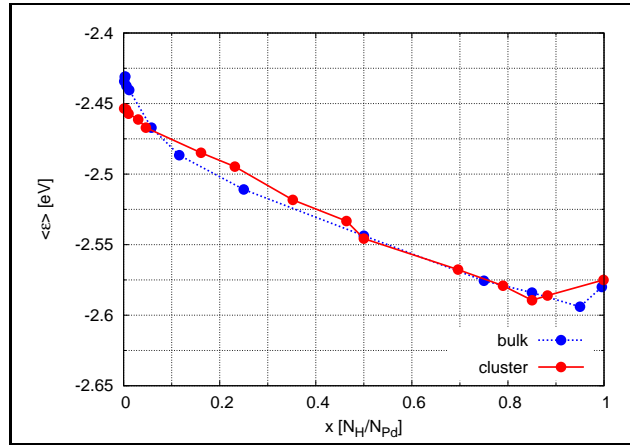
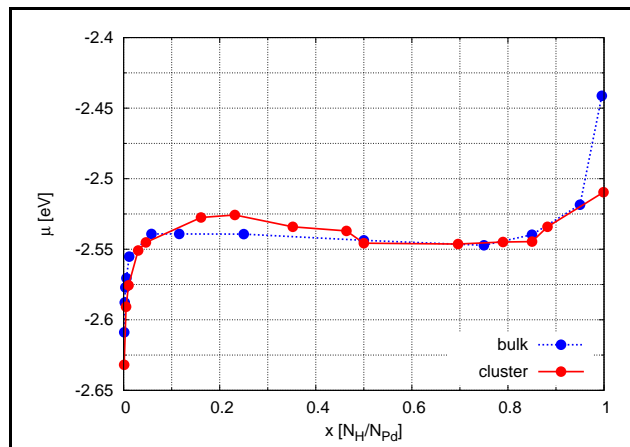


Figure 5.15: Effect of the HPd modified Interaction Potential on μ_{H} in bulk. It is shown the μ_{H} dependence on x using a second neighbour model for the H-H interaction and a modified H-Pd interaction model. **HPd**: Original HPd interaction, **HPd_{mod}**: same HPd, but modified at higher x concentrations ($x > 0.1$), **HH****: second neighbour interaction model.

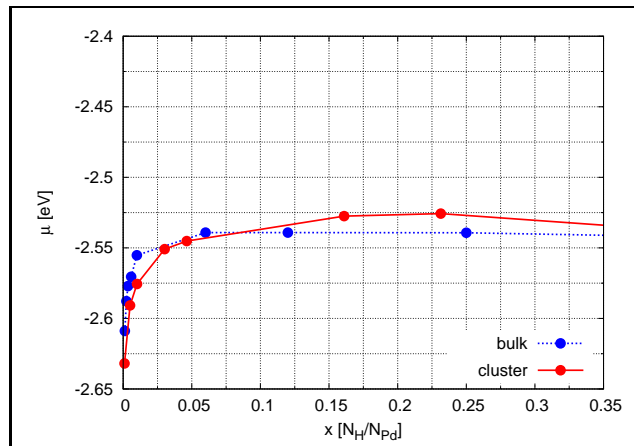
As pointed out by BRODOWSKY [WB78], μ_{H} in the metal is composed of a protonic contribution and an electronic contribution. The protonic contribution refers to the H-H lattice mediated interaction and the screened electrostatic repulsive interaction between the H atoms at high x concentrations. In addition, there is an electronic contribution (μ_e) from the ascent of the Fermi energy by the electrons of the dissolved hydrogen. The x -dependence of μ_e [WB78] provides a strong rise of μ_{H} in the α' phase due to the rise of the Fermi energy of the 4d band. At $x > 0.5$, there is a sharp rise coming from the filling of the 5s band density of states in Pd. This rise is not observed in our work because only the protonic contribution was taken into account in our present study. Besides the absence of the sharp rise for $x > 0.8$, the curve corresponding to the HH****-HPd_{mod}** combination qualitatively reproduce the behaviour of μ_{H} in bulk Pd at 300 K.

For the cuboctahedral cluster the chemical potential μ_{H} was calculated using the HPd_{mod}-HH****-ppI** potential models. The curve is shown in Figure 5.16 together with the bulk μ_{H} curve. It indicates that the lower solubility limit is shifted to higher concentrations in comparison to bulk, in agreement with the experimental observations. At higher x concentrations the sharp rise, ascribed in some studies [WB78, FGG86] to the electronic contribution, is missing.

From the E_{b} calculations using a single H atom in the Pd cluster (with Eq. 3.33), different surface- and bulk-like sites were identified by comparing the E_{b} values obtained in the cluster with the E_{b} values obtained for the Pd surface (See Tables 5.1 and 5.4). Surface-like sites have E_{b} values between -2.5 eV and -2.44 eV. Bulk-like sites have E_{b} values between -2.430 eV and -2.435 eV. Edge sites have E_{b} values of approximately -1.6 eV. For a 923 Pd cuboctahedral cluster the total number of surface- and bulk-like sites is 504 and 490 respectively. The average $\Delta\bar{E}_i$, over all configurations $\bar{X}_{N_{\text{H}+1}}^\gamma$, of the energy difference ($E_{N_{\text{H}+1}} - E_{N_{\text{H}}}$) is defined in this work as the site energy. For $N_{\text{H}}=1$, $\Delta\bar{E}_i$ is the same E_{b} . For $N_{\text{H}} > 1$, $\Delta\bar{E}_i$ changes with x , as observed in Fig. 5.17. In our work it was found at all x concentrations, the number of surface-like available sites that can be occupied in the $\bar{X}_{N_{\text{H}+1}}^\gamma$ configurations, is slightly larger than the number of bulk-like sites. The former sites have an average


 (a) Energy gain $\langle \epsilon(x) \rangle$.


(b) At high H concentrations the strong rise of the chemical potential is missing.



(c) At low H concentrations the curves follow qualitatively the experimental results.

Figure 5.16: Chemical Potential in bulk and cluster - III. Calculations were done using the $\text{ppI-HH}^{**}\text{-HPd}_{\text{mod}}$ potentials. It is shown $\langle \epsilon(x) \rangle$ and μ_H as a function of x in bulk and cluster. At low H concentrations the curves follow qualitatively the experimental results. At high H concentrations the strong rise of the chemical potential is missing. The uppermost x value in the left figure is $x=0.99$. The logarithmic increase of μ_H apparently takes place at higher x values.

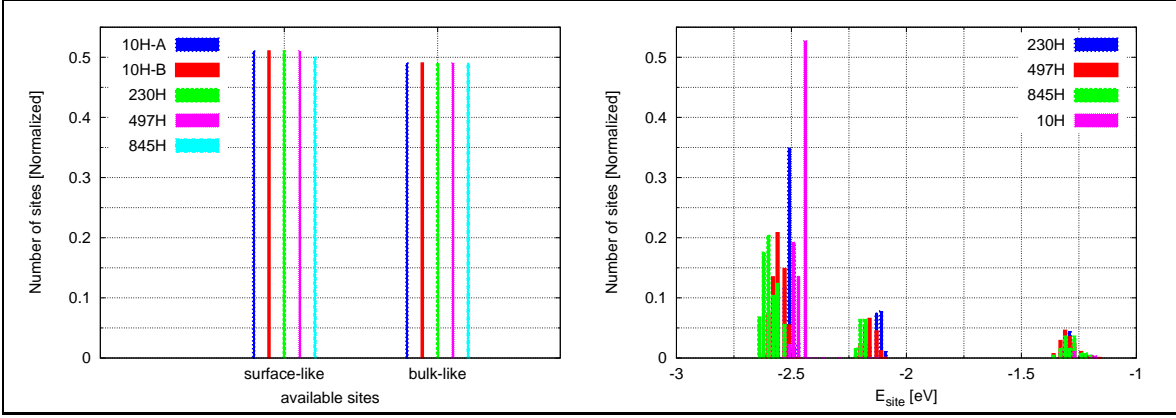


Figure 5.17: Fraction of empty bulk- and surface-like sites and site energies in the cuboctahedral cluster as a function of the H concentration. *Left*: It is shown the number of available sites that can be occupied (in the configurations $\bar{X}_{N_{H+1}}^\gamma$). *Right*: It is shown a normalized histogram of the site energies for a cluster with 10, 230, 497 and 845 H atoms. In general, the site energy decreases, with increasing x concentration.

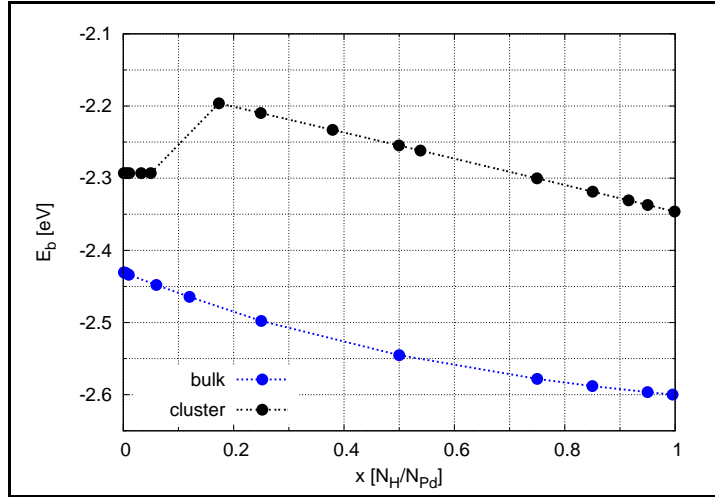


Figure 5.18: Binding Energy of H in Pd bulk and cluster using the HPd modified interaction potential. It is shown E_b as a function of x in Bulk and Cluster.

energy $\bar{\Delta E}_{\text{surface}} \approx -2.45$ eV, whereas bulk-like sites have an average energy $\bar{\Delta E}_{\text{bulk}} \approx -2.43$ eV at $x < 0.3$ concentrations. There are also surface states 4s, belonging to the (111) surface, with $\bar{\Delta E}_{\text{surface}} \approx -2.1$ eV. These states were observed for $x > 0.25$. Accordingly, the chemical potential slope in Fig. 5.16(b) ($0.1 < x < 0.25$) arises from the surface-like sites (surface, subsurface and subsurface) contributions.

At higher x , a nearly identical number of surface- and bulk-like places can be occupied. At these x concentrations, the surface sites have an average energy $\bar{\Delta E}_{\text{surface}} \approx -2.5$ eV, whereas bulk-like sites have an average energy $\bar{\Delta E}_{\text{bulk}} \approx -2.6$ eV. This slightly reduces μ_H to lower values. As observed in Fig. 5.17, with increasing number of H atoms, all site energies (besides the corresponding to edge sites) tend to follow the behavior of E_b seen in Fig. 5.18. That is, E_b decreases with increasing x concentration. This contributes also to the behavior of the μ_H curve for $x > 0.3$.

The binding energy E_b , which is the mean desorption energy as a function of the hydrogen concentration x , decreases with increasing x concentration, for both systems bulk and cluster. Particularly, in cluster, there is observed a constant value of the binding energy up to $x \approx 0.1$. This is due to occupation of one type of sites

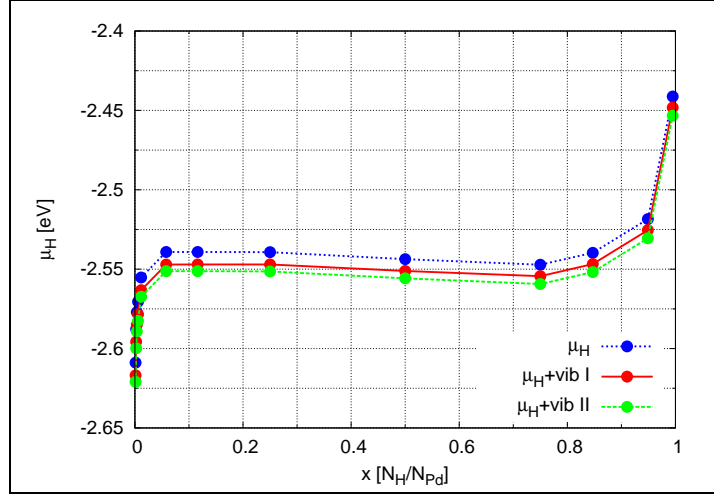


Figure 5.19: Vibrational Contribution of the Chemical Potential μ_H in bulk. Using the ppI-HH**^{*}-HPdmod, μ_{vib} is calculated for two different dependencies of $\hbar\omega(x)$. The vibrational contribution of μ_H as a function of the hydrogen concentration x displaces the μ_H to lower energy values.

(the surface-like sites). For higher concentrations the E_b behaviour is similar as in bulk. Like in bulk Pd, there was not observed in the cluster the change in the heat of formation from exothermic to endothermic [Pei78]. This may be due to the neglect of the band structure electronic effects.

About the vibrational contribution

The vibrational energy ($\hbar\omega$) of a hydrogen atom is a function of the hydrogen concentration as established experimentally [NT83, SN67, BG60]. In the literature there were found two different dependencies $\hbar\omega(x)$ as function of concentration x . These can be written as:

$$\hbar\omega(x)_I = (3.5x + 60) \text{ meV}, \quad (5.3)$$

$$\hbar\omega(x)_{II} = (-16.3934x + 66.3279) \text{ meV}, \quad (5.4)$$

where Eq. 5.3 was deduced for vibrations of H in Pd surface sites, and Eq. 5.4 interpolates the data in bulk Pd. The vibrational contribution of the chemical potential can be written as

$$\mu_{\text{vib}} = 3k_B \ln(1 - \exp(-\hbar\omega/k_B T)). \quad (5.5)$$

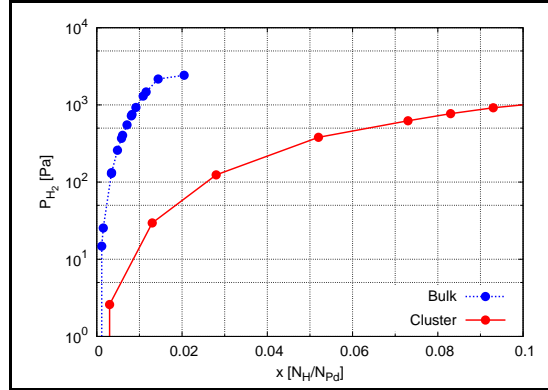
Using equations 5.3, 5.4 and 5.5, μ_{vib} calculated for the bulk system as a function of the H concentration is shown in Fig. 5.19. Although $\hbar\omega(x)_I$ and $\hbar\omega(x)_{II}$ have an opposite x dependence, μ_H is displaced to lower energy values for both expressions.

5.4.2 Solubility isotherms and determination of the solubility limit

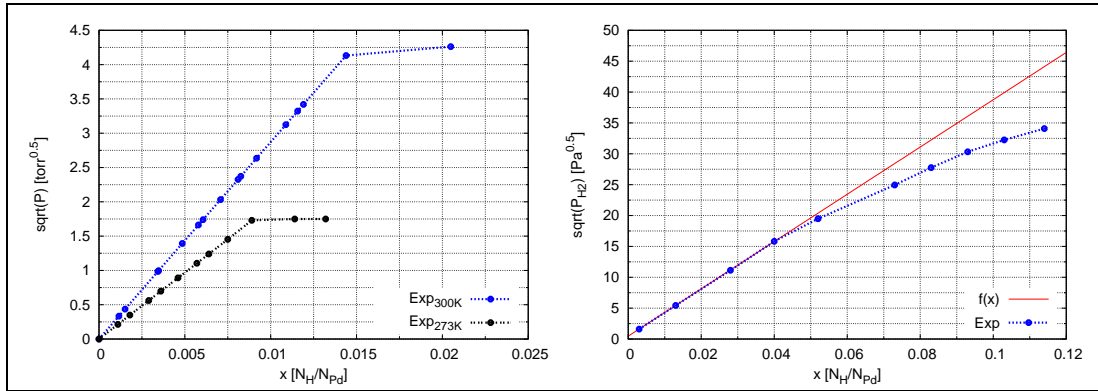
As demonstrated by Figure 5.9 at low x concentrations it is possible to identify the existence of an α phase. Sievert's law establishes a proportionality at low x concentrations between the square root of the H_2 pressure and the x concentration in the metal, given by Eq. 3.27. In bulk Pd at 300 K, Sievert's law holds in the entire α phase regime, up to $x \approx 0.015$. In the cluster, Sievert's law is fulfilled for $x \approx 0.04$, while in the α phase with higher x , $\sqrt{P_{H_2}}$ lies below Sievert's line. It is possible to determine the limit of Sievert's law by calculating the x concentration at which the

proportionality no longer holds. In Figure 5.20, an analytical fit was made to the curves and Sievert's law limits, that means deviation from proportionality between $\sqrt{P_{H_2}}$ and x , were determined for both systems, bulk and cluster.

In Figure 5.21 the solubility isotherms at low H concentrations obtained in this work, are shown corresponding to bulk and cluster. The H_2 calculated gas pressure was calculated using μ_H , through Eq. 3.29.



(a) Experimental values at 300 K in bulk and cluster. Taken from PUNDT ET AL [PSW⁺99, SB01].

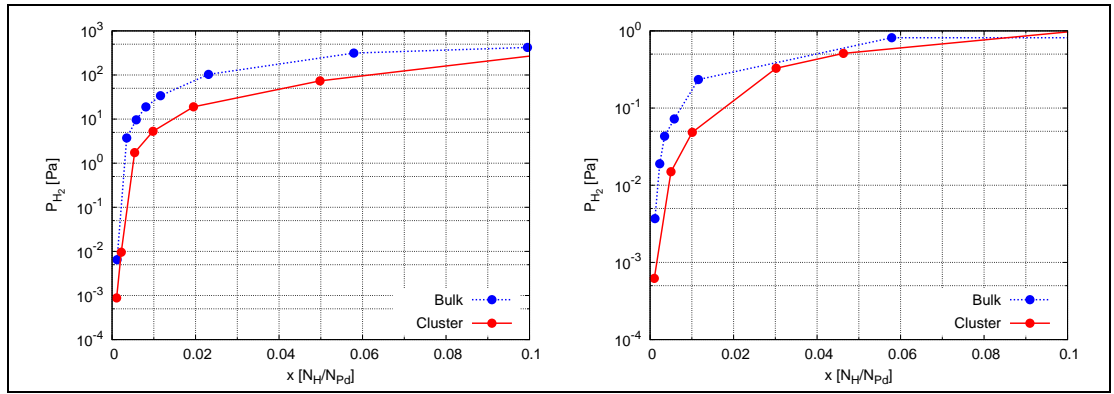


(b) Left: At 273 K Sievert's law limit is $x \approx 0.008$ and at 300 K is $x \approx 0.015$. Right: At 300 K Sievert's law limit is $x \approx 0.04$ as determined by fitting the data, where $f(x) = 383 \cdot x + 0.461$.

Figure 5.20: Solubility Isotherm of H in Pd in bulk and cluster at low H concentrations at 300 K - Experiment. It is shown the experimental P_{H_2} curve as function of x at low H concentrations in bulk and cluster. The curves $\sqrt{P_{H_2}}$ are also shown to demonstrate the validity of Sievert's law.

As can be appreciated, at low H concentrations, the cluster curve is shifted to higher H concentrations in comparison to bulk for both HH^* -HPd and HH^{**} -HPd_{mod} models. Our results describe qualitative the behavior of both solubility curves when compared to the experimental curves seen in Figure 5.20. The pressure ranges are different from the experimental values. The small difference (≈ 0.1 eV) between the calculated E_b values and the experimental E_b values results in larger differences in the H_2 pressure.

Figure 5.22 shows the simulation results at 300 K, for to the square root of the H pressure for bulk and cluster as a function of x . An analytical fit was made to the curves and it was found that in both systems cluster and bulk, Sievert's law is satisfied for both HH^* -HPd and HH^{**} -HPd_{mod} models. As can be observed the upper limit of Sievert's law for cluster are shifted to higher x concentrations in comparison to bulk. The H-H interaction affects these limits. When HH^* is used, the limits lies

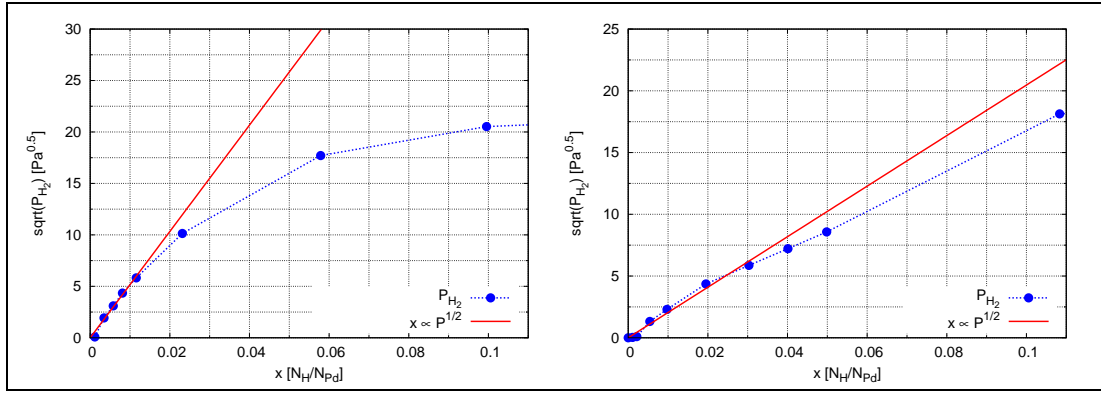


(a) *Left*: Solubility isotherms using the pI-HH*-HPd interaction models. *Right*: Solubility isotherms using the pI-HH**-HPd_{mod} interaction models

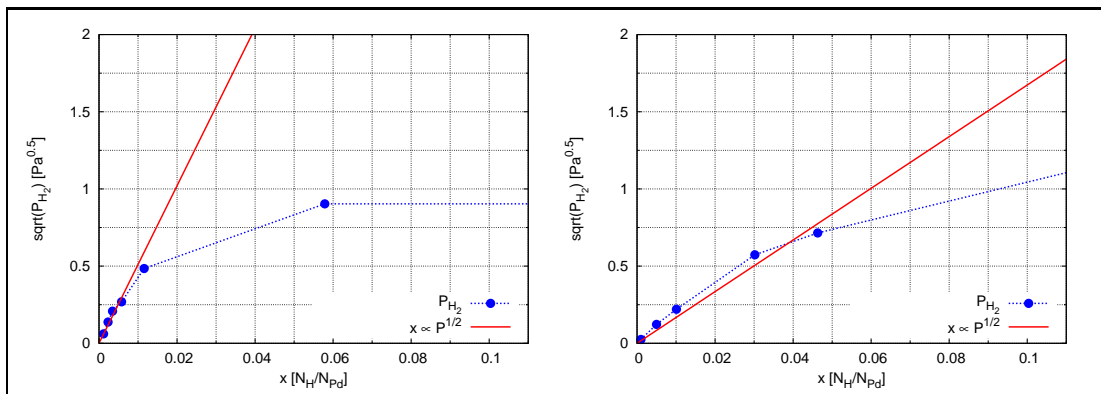
Figure 5.21: Solubility Isotherm of H in Pd in bulk and cluster at low H concentrations at 300 K. The cluster curve is shifted to higher x concentrations in comparison with bulk.

at $x \approx 0.012$ and at $x \approx 0.03$ for bulk and cluster respectively, and are in reasonable agreement with the experimental results (see Figure 5.20). The H-H interaction per pair is weaker for the HH* model as for the HH** model.

Determining the *solubility limit* requires the Maxwell construction, since the crossover between increasing μ_H and Maxwell plateau means the *upper solubility limit in the α -phase*. The Maxwell construction was calculated for the model pI-HH**-HPd_{mod} for both bulk and cluster and it is shown in Figure 5.23. As observed, the lower limit of the two phase region in cluster is shifted to higher x concentrations in comparison to bulk ($x_{\text{bulk}} \approx 0.06$ and $x_{\text{cluster}} \approx 0.09$). The upper limit of the two phase region is similar for both bulk and cluster. At higher x concentrations there is missing the electronic contribution, therefore the determination of the limits is not exact. It is not really possible to determine the *solubility limits*, however, the presence of an $\alpha - \alpha'$ two phase region is observed.



(a) Using the pPI-HH*-HPd model. *Left*: bulk: The proportionality constant is $516.535 \text{ Pa}^{0.5}$. The upper limit of Sievert's law lies at $x \approx 0.012$. *Right*: cluster: The proportionality constant is $204.67 \text{ Pa}^{0.5}$. The upper limit of the Sievert's law lies at $x \approx 0.03$.



(b) Using the pPI-HH*-HPd_{mod} model. *Left*: bulk: The proportionality constant is $51.0344 \text{ Pa}^{0.5}$. The upper limit of Sievert's law lies at $x \approx 0.005$. *Right*: cluster: The proportionality constant is $16.7296 \text{ Pa}^{0.5}$. The upper limit of the Sievert's law lies at $x \approx 0.04$.

Figure 5.22: Sievert's law in bulk and cluster at 300 K. The calculated Sievert's law limit of the cluster is displaced to higher H concentrations when compared to bulk.

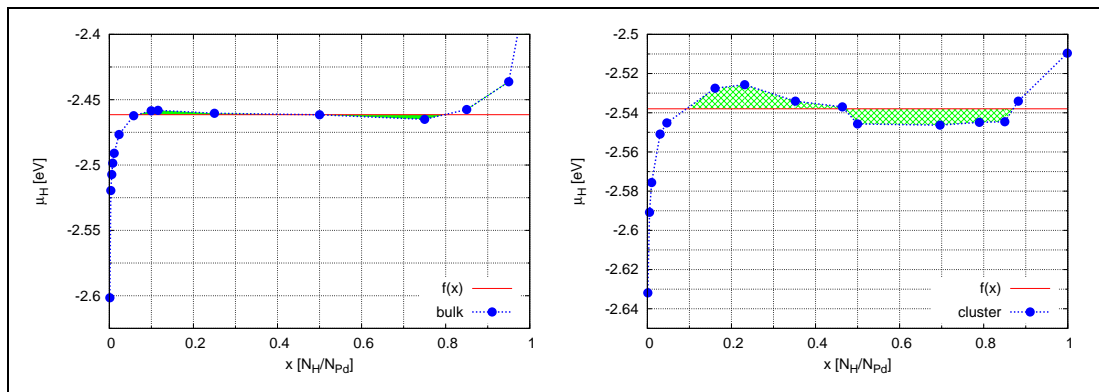


Figure 5.23: Chemical Potential of H in Pd bulk and cluster IV. Maxwell Construction. *Left*: The areas above and below $f(x)$ (shaded region) are \approx equal. $f(x) = -2.4615$. The lower and upper limit of the two phase region is at $x = 0.06$ and $x = 0.8$ respectively. *Right*: The area above and below $f(x)$ (shaded region) is \approx equal. $f(x) = -2.538$. The lower and upper limit of the two phase region is at $x = 0.09$ and $x = 0.87$ respectively.

5.4.3 About the distribution of H atoms in the cluster

With the use of the MC-MD procedure, for a fixed number N_H of H atoms, different possible states (accepted configurations) ($\bar{X}_{N_H}^\alpha$) were found in the MC-chain (See Figure 5.24).

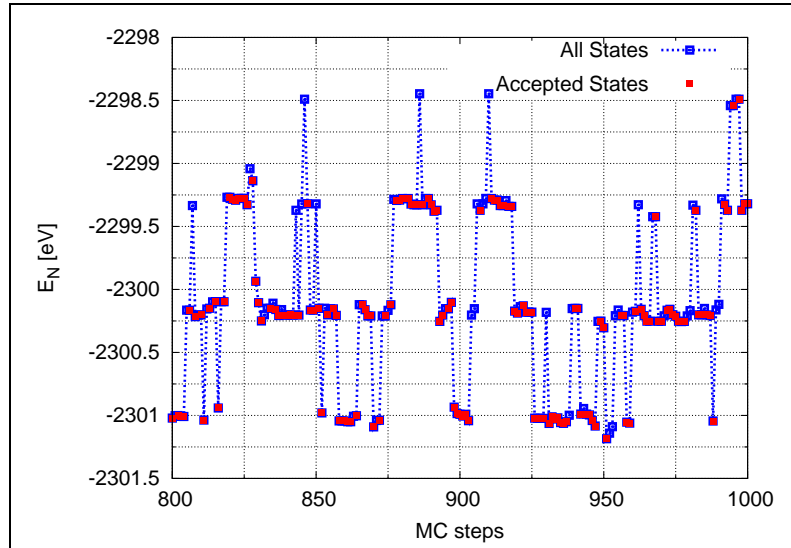


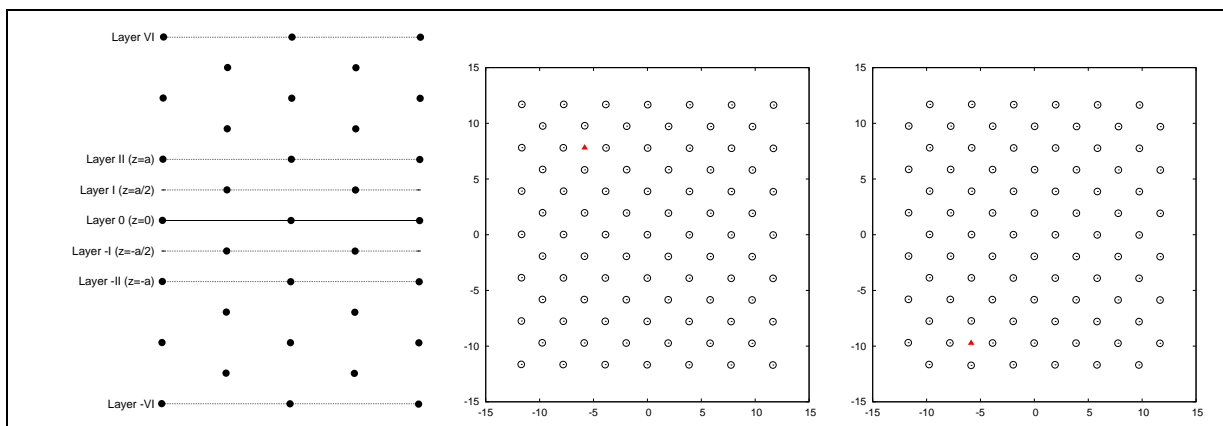
Figure 5.24: State energies for the Cluster with $N_H=5$. The accepted steps are those taken into account in the MC chain.

At these low x concentrations, the H atoms prefer to be far away from each other. They can also occupy next nearest (NN) neighboring positions or they occupy nearest (N) neighboring positions. In Figures 5.25(a), 5.25(b) and 5.25(c), there are shown, as an example, some configurations corresponding to $N_H=5$. Configurations I and II correspond to a lower energy state with $E=-2301$ eV and configuration III corresponds to a higher energy state with $E=-2298.5$ eV. This last configuration was chosen as accepted (although its high energy value) according to the Metropolis algorithm.

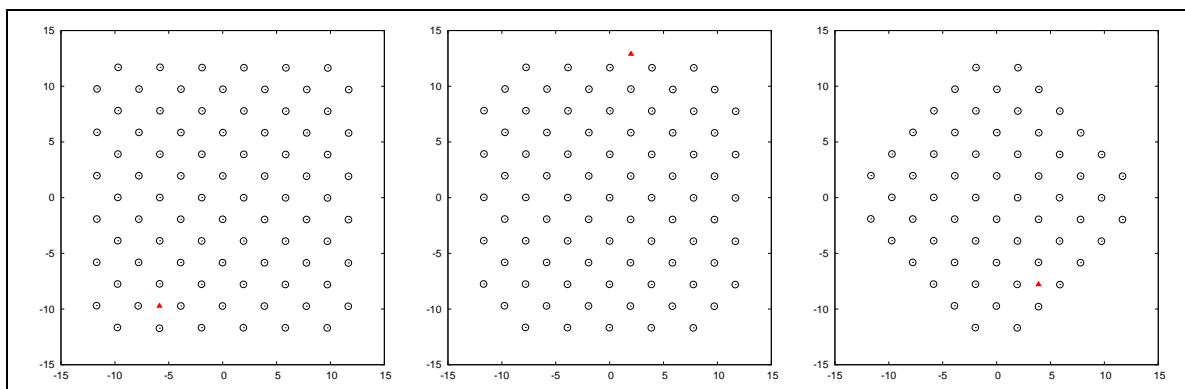
In Figure 5.25(c) a nearest neighbour H atom (*shell-like*) and a next nearest neighbour H atom (*chain-like*) configurations are shown. It was shown in Section 5.3 that the chain-like configuration is energetically favourable in comparison with the shell-like configuration. In the present simulation, however, the shell like configurations belongs to a lowerer energy state than the chain configurations. The combination shell like with atoms sitting at surface-like sites, are configurations which have a lower energy than the chain like with atoms sitting at surface-like sites. As displayed in Figure 5.26, at higher x concentrations, half of the occupied sites corresponds to surface-like sites and half of the occupied sites corresponds to bulk-like sites. There is no preference in occupying surface- or bulk-like sites. For different configurations ($\bar{X}_{N_H}^\alpha$), the number of N and NN neighboring atoms per H atom were calculated. Results are shown in Table 5.6. As can be observed it is found more NN neighbours per H atom, than N neighbours, as the concentration x increases. That is, there is a certain preference to allow the formation of chain-like H distributions. As an example, in Figures 5.27(a)-5.27(d) it is shown the H distribution in the cluster when $H=230$ atoms ($x = 0.25$).

In bulk Pd at this concentration, there is a observed, sharp interfaces between regions of α phase and α' phase [Pei78] (this corresponds to the two phase region). In this work, we found for the small cluster, no sharp interfaces but appreciable strong spatial concentration fluctuations. Experimental results in clusters [Sul03] have not shown α or α' regions coexisting at these concentrations. The experimental results show clusters with a defined α or α' regions, depending on the hydrogen concentration. The formation of surfaces already costs an amount of energy. Additionally, formation of interfaces costs energy. The cluster, would not be a energetically stable system with surfaces and interfaces.

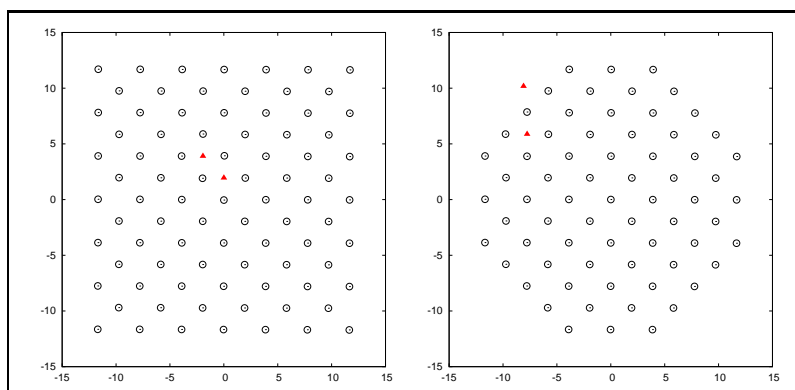
In this work, it was observed in the cluster a *curve* which increases with increasing x , until $x \approx 0.25$ (see Fig 5.16(b)). However, its form cannot be compared to the *beginning* of the *slope* in the experimental results of SULEIMAN [Sul03]. His results show that the *slope* appears when the system is already in the two phase region. In this work, it was determined that the form of the *curve* (observed until $x \approx 0.25$) is an indicator of the amount of surface sites involved and arises from the contribution of the site energies that corresponds to surface-like sites. It does not extend to higher x concentrations, due to the limited number of absorption sites that corresponds to surface-like sites (compared to the amount of bulk-like sites), and/or, the behavior of $\langle \epsilon(x) \rangle$ at higher x (see Fig 5.16(a)). GRIESSEN [Gri83] studied an amorphous metal hydride system. He assumed that as a consequence of configurational disorder, the site energy varies from site to site. He calculated μ_{H} and obtained a *slope* in the region that corresponds to the two phase region. Our explanation for the *curve* agrees with the explanation of GRIESSEN which relates the existence of different sites and the form of the curve. However, GRIESSEN assumes that the H-H interaction would not contribute in a significantly way. Meaning, that a two phase region could not be obtained. SULEIMAN finds a two phase region and also a slope. Which means that the different site existence explanation of GRIESSEN, cannot explain the *slope* existence.



(a) *Left*: The different layers from the Pd cluster where separated along the z direction. Configuration I with $E=-2301$ eV. *Middle*: Layer -III. *Right*: Layer 0.



(b) Configuration I. *Left*: Layer I. *Middle*: Layer II. *Right*: Layer V.



(c) *Left*: Configuration II Layer 0. This configuration has an $E=-2301$ eV. *Right*: Configuration III Layer IV. This configuration has an $E=-2298.5$ eV.

Figure 5.25: H distributions in cluster. Possible configurations with $N_H=5$. The positions of the palladium atoms correspond to (\circ) and N_H hydrogen atoms to (\blacktriangle) .

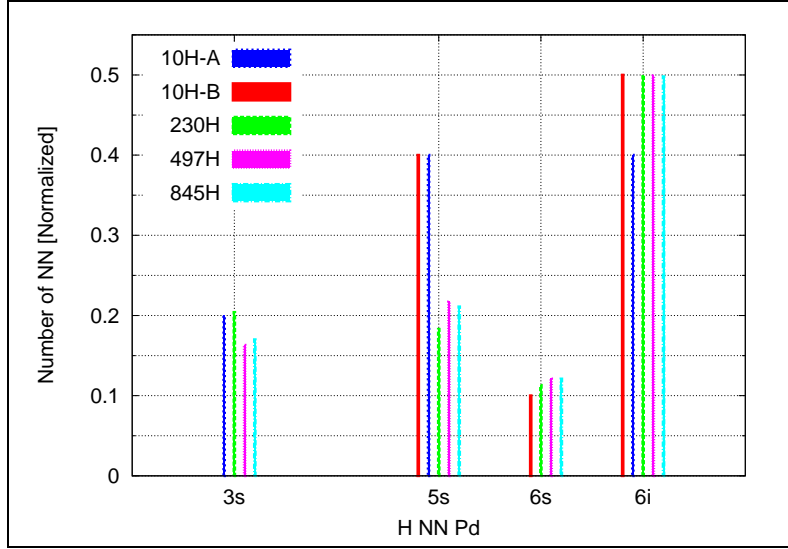
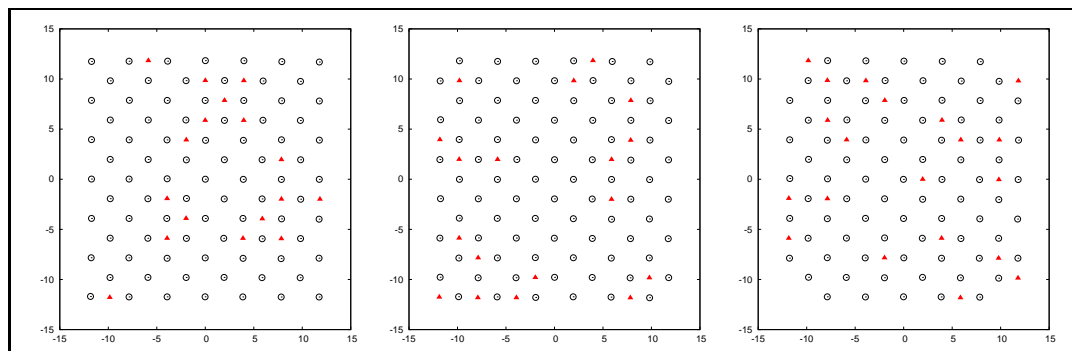


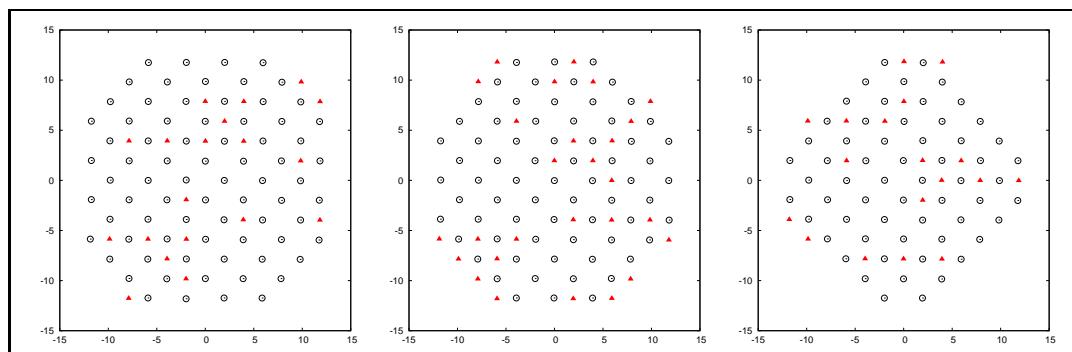
Figure 5.26: Fraction of occupied bulk- and surface-like sites in cluster for different configurations $\bar{X}_{N_H}^\alpha$. In general, surface like sites (3s, 5s, 6s) are equally occupied as bulk like sites (6s).

Table 5.6: Chain and shell like H distributions in cluster. It is shown the number of nearest (N) neighbours and next nearest (NN) neighbours per H atom.

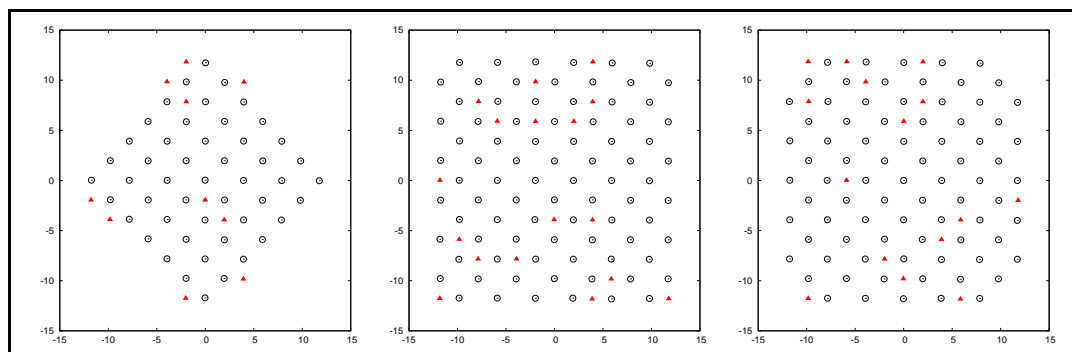
H	NN/atom $\langle 100 \rangle$	N/atom $\langle 110 \rangle$
10 _A	0	0
10 _B	1	1
30	1	1
46	1.33	1
160	1.75	1.24
230	1.98	1.37
497	3.16	1.95
845	4.94	2.69



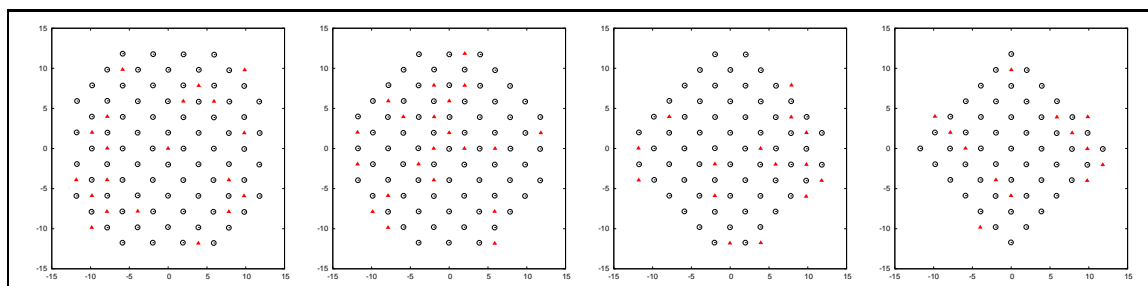
(a) Configuration I. *Left: Layer 0. Middle: Layer I. Right: Layer II.*



(b) Configuration I. *Left: Layer III. Middle: Layer IV. Right: Layer V.*



(c) Configuration I. *Left: Layer VI. Middle: Layer -I. Right: Layer -II.*



(d) Configuration I. *From Left to Right: Layer -III to Layer -VI.*

Figure 5.27: H distributions in cluster. Possible configurations with $N_H=230$. The positions of the palladium atoms correspond to (O) and N_H hydrogen atoms to (▲).

Chapter 6

Conclusions

From the preceding results some conclusions can be drawn, which seems valid on general reasons beyond the particular values from the special models considered here.

First, there is the verification of Sievert's law in the low H concentration limit. Like in the phenomenological ideal solution models, validity of Sievert's law is based on the fact that in the chemical potential there is a $k_B T \ln(x/1-x)$ contribution which gives the dominant x -dependence of μ_H in the dilute limit. In the present treatment, its validity thus is based on the observation that a separation of μ_H in a $k_B T \ln(x/1-x)$ term and $\langle \epsilon(x) \rangle$ in a strict way is possible, with $\langle \epsilon(x) \rangle$ weakly dependent on x or $\langle \epsilon(x) \rangle$ varying proportional to $\ln x$.

In particular, in the dilute concentration regime, $\langle \epsilon(x) \rangle$ in bulk Pd has a similar slope like the phenomenological desorption energy, which means that the range of applicability of Sievert's law from the present modelling shall be similar to experimental bulk Pd. Experimentally Sievert's law is limited by the solubility limit of the α phase, which is, however, determined by the effects of the competing α' and hence reflects properties of the concentrated H-system. In the cluster, the here and in the experiments [Sul03] observed deviation from Sievert's law with increasing x seems to be an effect of the x -dependence of $\langle \epsilon(x) \rangle$, since the $k_B T \ln(x/1-x)$ contribution would give a raise of $\sqrt{P_{H_2}}$ above Sievert's line.

Secondly, at intermediate concentrations where the miscibility gap between α and α' phase is found, the present simulations do not show a separation of the concentration profile in the cluster, that means coexistence of α and α' within one cluster. Nevertheless, there are marked concentration fluctuations visible, e.g. in Figures 5.27(a)-5.27(d) for the 230 H-atoms cluster. One may speculate that the missing long-range deformation field around a hypothetical α' particle and the structural flexibility of the cluster reduce the probability for forming α' regions. According to our present results, the two phase regime in the p - x isotherm reflects a mixture of clusters, each either in the α or in the α' configuration, in agreement with recent experimental studies [Sul03]. There shall be, however, marked fluctuations among the individual clusters, as each cluster presents a small, finite system, where the thermodynamic limit means consideration of an infinite set of clusters.

Thirdly, in agreement with the prediction from the lattice-Green's function formalism, our results demonstrates that two hydrogen atoms in next nearest (NN) neighbour (100) configuration show a rather strong attractive lattice mediated interaction, while the nearest (N) neighbour pairs (110) have a repulsive lattice mediated coupling. This predicts that in the α -phase regime at moderate temperatures (100)

chain-like H distributions shall be preferred in the structure.

Fourth, from the here used formalism, which is exact up to the neglect of saddle-point configurations to the equilibrium partition function, the asymmetry in the Pd-H phase diagram, visible as a shift of the miscibility gap towards the lower H-concentrations, is fully encoded in the quantity $\langle \epsilon(x) \rangle$. The asymmetry may be either caused by strong repulsive interactions at larger x , as considered for the statistical treatment of H surface layers on Pd by BINDER ET AL [BL81], or it may be due to, e.g., the electron band structure effects. Although the treatment of the asymmetry was outside the present study it is quite clear that the present formalism leaves space for both interpretations.

Chapter 7

Summary

In this work, a new expression for the chemical potential μ_{H} of H in Pd is used, which relies on an extension of Widom's particle insertion method. Being an exact expression, this μ_{H} contains a term that agrees with the configurational entropy of the ideal solution model, and a term which describes the energy gain in the system when adding an extra H atom. This latter term is due to direct hydrogen-hydrogen interactions, deformations of the lattice by the absorbed hydrogen atoms, the energy gain from lattice relaxation and the binding energy E_{b} of H in Pd. The calculation of μ_{H} is carried out in bulk Pd and in a 923 Pd-atoms cuboctahedral cluster within a hybrid monte carlo - molecular dynamics (MC-MD) procedure. Also E_{b} is determined as function of the hydrogen concentration x in bulk and in cluster. In order to perform the calculations a set of interaction potentials are applied to describe the Pd-Pd, H-Pd and the H-H interactions. For the Pd-Pd interaction several models were tested, which include a first, second or third shell of neighbours. The H-Pd interaction is a first neighbour model. For the H-H interaction a next neighbour model and next nearest neighbour model are used. The chosen Pd-Pd interaction describes the equilibrium lattice constant of pure Pd. The H-Pd interaction model was constructed to reproduce the elastic properties of the H atoms in the metal and its relationship to the relative volume change under H loading, and also the binding energy E_{b} at dilute concentrations. The H-H interaction potential describes the appearance of the two phase region in PdH bulk.

Binding energy E_{b} calculations are carried out with 1 H atom to test sites at the surface and in the cluster. Energies are found for different surface-like and bulk-like sites, in agreement with experimental results. E_{b} calculation in cluster shows no directional dependence, but one that follows the geometry of the system. Also E_{b} as function of x , at low x concentrations, is in qualitative good agreement with experimental results. The discrepancy at higher x concentrations is due to the missing electronic band structure effects or due to very strong H-H repulsive interactions that were not taken into account. Also at low x concentrations, the relative volume change $\Delta V/V$ reproduces the experimental results. It is found that, with the interaction potential set ppI-HH**-HPd_{mod}, it is possible to describe μ_{H} in bulk at 300 K. The presence of a α - α' phase transition was established. In cluster, μ_{H} at 300 K, was also calculated. It was possible to identify an α - α' phase transition. Sievert's law limit was estimated in good agreement with the experiment, for both bulk and cluster. In cluster it is shifted to higher x concentrations when compared to bulk in agreement with the experiments. Using the Maxwell construction, the phase solubility limits were determined both in cluster and bulk. It was not possible to calculate them properly,

due to a neglect of the empirical electronic contribution to μ_{H} at higher x in bulk Pd and in the cluster. Experimentally, in a cluster system, μ_{H} displays a finite slope in the α - α' two phase regime [Sul03]. For amorphous systems, such a behaviour was related by GRIESSEN [Gri83] to the fluctuating site energies. Although there is a wide spread of site energies in the present clusters with surface, subsurface, and bulk sites, the shape of $\langle \epsilon(x) \rangle$ at higher x , presented e.g. in Fig. 5.16(a)), leaves no space for a linear increase in μ_{H} . Accordingly, the form of the μ_{H} curve until $x \approx 0.25$ should not be interpreted as the beginning of the experimentally found slope. However, the present results leave space to relate the slope to fluctuations in the cluster distribution or couplings between the clusters.

Bibliography

- [AT87] M.P. Allen and D.J Tildesly. *Computer Simulation of Liquids*. Oxford Science Publications, 1987.
- [BDH96] C.B. Barber, D.P. Dobkin, and H.T. Huhdanpaa. The Quickhull algorithm for convex hulls. <http://www.qhull.org>, 1996.
- [BG60] J. Bergsma and Z.A. Goedkoop. . *Physica*, 26:744, 1960.
- [BL81] K. Binder and D. Landau. Square lattice gases with two- and three-body interactions:A model for the adsorption of hydrogen on Pd(100). *Surface Science*, 108:503–525, 1981.
- [BPvG⁺84] H.J.C. Berendsen, J.P.M. Postma, W.F. van Gunsteren, A. DiNola, and J.R. Haak. Molecular dynamics with coupling to an external bath. *J. Chem. Phys.*, 81:3684–3690, 1984.
- [CC06] F. Calvo and A. Carre. Structural transitions and stabilization of palladium nanoparticles upon hydrogenation. *Nanotechnology*, 17:1292–1299, 2006.
- [CDJ⁺89] O. Christensen, P. Ditlevsen, K. Jacobsen, P. Stoltze, O. Nielsen, and J. Nørskov. H-H interactions in Pd. *Phys. Rev. B*, 40(3):1993–1996, 1989.
- [CXWB92] H. Cheng, X. Xi, R. Whetten, and S. Berry. Complete statistical thermodynamics of the cluster solid-liquid transition. *Phys. Rev. A.*, 46(2):791–800, 1992.
- [Esh56] J.D. Eshelby. *The Continuum Theory of Lattice Defect*. Solid State Physics, Vol. 3, 1956.
- [FGG86] R. Feenstra, R. Griessen, and D. Groot. Hydrogen induced lattice expansion and effective H-H interaction in single phase PdH_c. *J. Phys. F.*, 16:1933–1952, 1986.
- [FL75] T. Flanagan and J. Lynch. Thermodynamics of a Gas in Equilibrium with Two Nonstoichiometric Condensed Phases. Application to Metal/Hydrogen Systems. *J. Phys. Chem.*, 79(5):444–448, 1975.
- [FS84] M. W. Finnis and J. E. Sinclair. A simple empirical N-body potential for transition metals. *Phi. Mag. A*, 50:45–55, 1984.
- [FS86] Baskes M. I. Foiles and Daw M. S. Embedded atom method functions for the fcc metals Cu, Ag, Au, Ni, Pd, Pt, and their alloys. *Phys. Rev. B*, 33(12):7983–7991, 1986.

- [FS05] D. Frenkel and B. Smit. *Understanding Molecular Simulations*. Academic Press, 2005.
- [Fuk04] Y. Fukai. *The Metal-Hydrogen System*. Springer Verlag, 2004.
- [GD84] R. Griessen and A. Driessen. Heat of formation and band structure of binary and ternary metal hydrides. *Phys. Rev. B.*, 30(8):4372–4381, 1984.
- [Gil86] M. J. Gillan. A simulation model for hydrogen in Palladium:I. Single particle dynamics. *J. Phys. C*, 19:6169–6184, 1986.
- [Gri83] R. Griessen. Phase separation in amorphous metal hydrides: A Stoner-type criterion. *Phys. Rev. B.*, 27(12):7575–7582, 1983.
- [Haf87] J. Hafner. *From Hamiltonians to Phase Diagrams*. Springer Verlag, 1987.
- [Lac37] J.R. Lacher. A Theoretical Formula for the Solubility of Hydrogen in Palladium. *Proc. Roy. Soc.*, 161A(907):525–545, 1937.
- [LN78] G. Leibfried and Breuer N. *Point Defects in Metals I*. Springer Verlag, 1978.
- [Map05] Maple. *Computer software for mathematical solutions*. Maplesoft, 2005.
- [MDB84] S. Murray Daw and M.I. Baskes. Embedded atom method: Derivation and application to impurities, surfaces, and other defects in metals. *Phys. Rev. B*, 29(12):6443–6452, 1984.
- [NT83] C. Nyberg and C. Tengstael. Vibrational Interaction between Hydrogen Atoms Adsorbed on Pd(100). *Phys. Rev. Lett.*, 50(21):1680–1683, 1983.
- [OST⁺98] H. Okuyama, W. Siga, N. Takagi, M. Nishijima, and T. Aruga. Path and mechanism of hydrogen absorption at Pd(100). *Surface Science*, 401:344–354, 1998.
- [Pei78] H. Peisl. *Lattice Strains due to Hydrogen in Metals*. Springer Verlag, Hydrogen in Metals I, 1978.
- [PNM81] M.J. Puska, R.M. Nieminen, and Manninen M. Atoms embedded in an electron gas: Immersion energies. *Phys. Rev. B.*, 24(6):3037–3047, 1981.
- [PSW⁺99] A. Pundt, C. Sachs, M. Winter, M.T. Reetz, D. Fritsch, and R. Kirchheim. Hydrogen sorption in elastically soft stabilized Pd-clusters. *J. Alloys and Compounds*, 480:293–295, 1999.
- [Pun05] A. Pundt. *Nanoskalige Metall-Wasserstoff-Systeme*. Universitätsverlag Göttingen, <http://resolver.sub.uni-goettingen.de/purl/?webdoc-150>, 2005. Habilitation Thesis.
- [QLT⁺90] J. Quinn, Y. Li, D. Tian, H. Li, and F. Jona. Anomalous multilayer relaxation of Pd100. *Phys. Rev. B.*, 42(17):11348–11351, 1990.

- [Rap04] D.C. Rapaport. *The Art of Molecular Dynamics Simulation*. Cambridge University Press, 2004.
- [RGGR⁺93] C. Rey, L.J. Gallego, J. Garcia-Rodeja, J.A. Alonso, and M.P.XS Iniguez. Molecular-dynamics study of the binding energy and melting of transition-metal clusters. *Phys. Rev. B*, 48(11):8253–8262, 1993.
- [RGL89] V. Rosato, M. Guillope, and B. Legrand. Thermodynamical and structural properties of f.c.c. transition metals using a simple tight-binding model. *Phi. Mag. A*, pages 321–336, 1989.
- [RJ85] B.K. Rao and P. Jena. Switendick criterion for stable hydrides. *Phys. Rev. B*, 10(117):6726–6730, 1985.
- [SA96] E. Silva and A. Antonelli. Size dependence of the lattice parameter for Pd clusters: A molecular-dynamics study. *Phys. Rev. B*, 54(23):17057–17060, 1996.
- [SA01a] C. Sachs and et. Al. Solubility of Hydrogen in single-sized Clusters of Palladium. *Phys. Rev. B*, 64:75408, 2001.
- [SA01b] M. Suleiman and et. Al. Hydrogen loading of Pd-clusters, lattice expansion, phase transition and size dependence. *Hamburger Synchrotron Labor Annual Report*, pages 209–210, 2001.
- [Sac98] C. Sachs. *Zur Loeslichkeit von Wasserstoff in Palladiumclustern*. PhD thesis, Goettigen, 1998.
- [Sal90] E. Salomons. Elastic interaction of hydrogen in palladium studied by molecular-dynamics simulation. *Phys. Rev. B*, 42(2):1183–1188, 1990.
- [SB01] V. Srivastava and R. Balasubramaniam. Theoretical modeling of metal-hydrogen interactions in Pd clusters. *Mat. Sci. Eng.*, a(304-306):897–900, 2001.
- [Sch88] L. Schlapbach. *Hydrogen in intermetallic compounds*. Springer Verlag, Berlin, 1988.
- [SG02] D. Sun and X. Gong. A new constant-pressure molecular dynamics method for finite systems. *J. Phys. Condens. Matter*, 14:L487–L493, 2002.
- [SN67] K. Skoeld and G. Nelin. . *J. Phys. Chem. Solids*, 28:2369, 1967.
- [Sul03] M. Suleiman. *Size-selective synthesis of nanometersized Palladium clusters and their hydrogen solvation behaviour*. PhD thesis, Goettigen, 2003.
- [Swi79] A.C. Switendick. Band structure calculations for metal hydrogen systems. *Z. Phys. Chem.*, 117:89–112, 1979.
- [Tei96] H. Teichler. *Simulationstechniken in der Materialwissenschaft*. P. Klimanek and W. Pantleon, 1996.

- [TSL91] D. Tománek, Z. Sun, and S. Louie. Ab initio calculation of chemisorption systems: H on Pd(001) and Pd(110). *Phys. Rev. B*, 43(6):4699–4713, 1991.
- [Wal72] D. Wallace. *Thermodynamics of Crystals*. Dover Publications Inc., 1972.
- [WB78] E. Wicke and H. Brodowsky. *Hydrogen in Palladium and Palladium Alloys*. Springer Verlag, Hydrogen in Metals II, 1978.
- [WFG⁺99] J. Wan, Y. Fan, D. Gong, S. Shen, and X. Fan. Surface relaxation and stress of fcc metals: Cu, Ag, Au, Ni, Pd, Pt, Al and Pb. *Modelling Simul. Mater. Sci. Eng.*, 7:189–206, 1999.
- [WH83] J. Willis and W. Harrison. Interionic interactions in transition metals. *Phys. Rev. B*, 28(8):4363–4373, 1983.
- [WHL94] S. Wilke, D. Hennig, and R. Løber. Ab initio calculations of hydrogen adsorption on (100) surfaces of palladium and rhodium. *Phys. Rev. B*, 50(4):2548–2557, 1994.
- [Wid63] B. Widom. Some Topics in the Theory of Fluids. *J. Chem. Phys.*, 39(11):2808–2812, 1963.
- [WN64] E. Wicke and G. Nernst. Phase diagram and thermodynamic behaviour of the systems Pd/H₂ and Pd/D₂ at normal temperatures: H/D separation effects. *Ber. Bunsenges. Phys. Chem.*, 68(3):224–235, 1964.

Appendix A

Output of the simulation of bulk Pd with H=2. Example

***** number of total atoms n=nh+npd 866 *****

Energy of Initial Structure : -2486.7305 eV

Average Values for the last 1000 out of 1000 Dynamics Steps

Simulation Time 260.0000 Picosecond

Tot real Time 4.0154 Second

Ekin 0.02847609 eV (+/- 0.01446185)
Tot Energy -2489.10843856 eV (+/- 0.01885515)
Ehpd -5.00958628 eV (+/- 0.06525077)
Epd -2484.12732836 eV (+/- 0.06282376)
Epot -2489.13691464 eV (+/- 0.01607635)
Eb -2.40641650 eV (+/- 0.01607635)
Ehh 0.00000000 eV (+/- 0.00000000)
box 23.34130217 A (+/- 0.00021270)
Temp 0.25461241 K (+/- 0.12929634)
Press 0.00015991 eV/A3 (+/- 0.00003555)

Average Values for the last 1000 out of 2000 Dynamics Steps

Simulation Time 520.0000 Picosecond

Tot real Time 7.9678 Second

Ekin 0.01113447 eV (+/- 0.00242025)
Tot Energy -2489.14319906 eV (+/- 0.00458235)
Ehpd -5.01073250 eV (+/- 0.01681043)
Epd -2484.14360103 eV (+/- 0.01653460)
Epot -2489.15433353 eV (+/- 0.00279359)
Eb -2.42383539 eV (+/- 0.00279359)
Ehh 0.00000000 eV (+/- 0.00000000)

box 23.34182476 A (+/- 0.00010108)
Temp 0.09951497 K (+/- 0.02164835)
Press 0.00007565 eV/A3 (+/- 0.00001630)

Average Values for the last 1000 out of 3000 Dynamics Steps

Simulation Time 780.0000 Picosecond

Tot real Time 11.9272 Second

Ekin 0.00684281 eV (+/- 0.00086841)
Tot Energy -2489.15199162 eV (+/- 0.00116887)
Ehpd -5.01086511 eV (+/- 0.00840088)
Epd -2484.14796933 eV (+/- 0.00813914)
Epot -2489.15883443 eV (+/- 0.00069445)
Eb -2.42833629 eV (+/- 0.00069445)
Ehh 0.00000000 eV (+/- 0.00000000)
box 23.34207348 A (+/- 0.00004825)
Temp 0.06115817 K (+/- 0.00775750)
Press 0.00003617 eV/A3 (+/- 0.00000781)

Average Values for the last 1000 out of 4000 Dynamics Steps

Simulation Time 1040.0000 Picosecond

Tot real Time 15.8836 Second

Ekin 0.00583417 eV (+/- 0.00055249)
Tot Energy -2489.15422022 eV (+/- 0.00034658)
Ehpd -5.01080381 eV (+/- 0.00410511)
Epd -2484.14925058 eV (+/- 0.00427867)
Epot -2489.16005439 eV (+/- 0.00057237)
Eb -2.42955625 eV (+/- 0.00057237)
Ehh 0.00000000 eV (+/- 0.00000000)
box 23.34219240 A (+/- 0.00002317)
Temp 0.05216357 K (+/- 0.00493980)
Press 0.00001732 eV/A3 (+/- 0.00000369)

Average Values for the last 1000 out of 5000 Dynamics Steps

Simulation Time 1300.0000 Picosecond

Tot real Time 19.8400 Second

Ekin 0.00539407 eV (+/- 0.00063207)
Tot Energy -2489.15478742 eV (+/- 0.00010629)
Ehpd -5.01135991 eV (+/- 0.00773876)
Epd -2484.14882157 eV (+/- 0.00779479)
Epot -2489.16018148 eV (+/- 0.00065532)

APPENDIX A. OUTPUT OF THE SIMULATION OF BULK PD WITH H=2. EXAMPLE

Eb -2.42968334 eV (+/- 0.00065532)
Ehh 0.00000000 eV (+/- 0.00000000)
box 23.34224943 A (+/- 0.00001109)
Temp 0.04822826 K (+/- 0.00565120)
Press 0.00000836 eV/A³ (+/- 0.00000177)
Step: 1 Accept: 1.000 Current: -2489.1602 Global: -2489.1602

Appendix B

Fitting of the Interaction Potentials

In the fcc lattice structure, an atom N has different number of neighbours, with which it interacts, depending on how many shells of atoms are considered in the interaction model. In Table B.1 it is shown how many neighbours the atom N has per shell and also the distance (r_{NS}) between N and the other atoms belonging to the same shell [Wal72]. This knowledge becomes important when fitting the interaction potentials.

Table B.1: Number of Neighbours per shell in the fcc lattice. It is shown the number of atoms per shell in the fcc lattice, also the distance (r_{NS}) between an atom N and the other atoms belonging to the shell. As a reference it is given the cutoff distances r_{cut} for Pd used in different interaction models.

Shell	Number of atoms	Distance (r_{NS}) (\AA)	r_{cut} (\AA)
1	12	$\frac{a\sqrt{2}}{2}$	3.65
2	6	a	4.2
3	24	$\frac{a\sqrt{6}}{2}$	5.4
4	12	\sqrt{a}	6.0
5	24	$\frac{a\sqrt{10}}{2}$	7.4

B.1 Fitting of the Pd-Pd 1st neighbour interaction model.

In Figure B.1 it is shown a sketch on the interaction potential between two metal atoms as a function of their separation distance r . The cohesion energy E_{coh} of the metal is given through the contribution of the interaction potential at the equilibrium separation distance r_{min} multiplied by half the number of nearest neighbours, that is, $E_{\text{coh}} = 6 \cdot V(r_{\text{min}})$. In the case of Pd, the pair potential contribution must be supplemented with an additional contribution delivered through an electron gas term, in order to reproduce the experimental cohesion energy, therefore:

$$E_{\text{coh}} = 6 \cdot V(r_{\text{min}}) + E_{\text{eg}}/\text{atom} \quad (\text{B.1})$$

To describe the pair potential contribution of the Pd-Pd interaction, a third order polynomial was chosen:

$$V(r) = -\alpha(r - r_o)^3 + \gamma(r - r_o) + \delta \quad (\text{B.2})$$

where the parameters α , γ , δ and r_o are to be fitted. The pressure P of the system

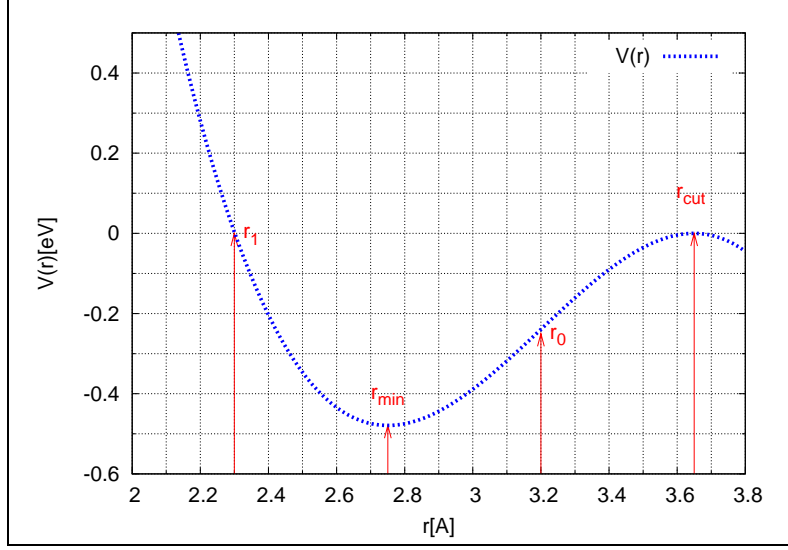


Figure B.1: Sketch of the pair potential between two metal atoms. The cohesion energy is given by $E_{\text{coh}} = 6 \cdot V(r_{\text{min}}) + E_{\text{eg}}$

can be derived from the potential energy U and the atomic volume Ω :

$$P = -\frac{dU}{d\Omega} \quad (\text{B.3})$$

For a fcc structure Ω is given by $a^3/4$. For a 1st neighbour model, $U = 6 \cdot V_1$, where V_1 is the interaction potential (B.2) evaluated at the nearest neighbour distance $R_1 = \frac{a\sqrt{2}}{2}$. Therefore,

$$P = -4 \cdot \sqrt{2} V_1' \quad (\text{B.4})$$

The Bulk Modulus B is determined using the pressure:

$$B = -\Omega \frac{dP}{d\Omega} \quad (\text{B.5})$$

Using Eq.(B.4) it is possible to write B as a function of V_1 :

$$B = \frac{4V_1''}{3a} \quad (\text{B.6})$$

that is, the bulk modulus B is proportional to the curvature of the potential at the equilibrium separation distance. a is the lattice constant. With Eq. (B.2), (B.6) and the experimental value of the bulk modulus B , the parameter α can be written as:

$$\alpha = -\frac{aB}{8 \cdot (r_{\text{min}} - r_o)} \quad (\text{B.7})$$

Eq. (B.2), has the following properties:

$$V(r) = 0 \begin{cases} \sqrt{\gamma/3\alpha} + r_o & = r = r_{\text{cut}} \\ -2\sqrt{\gamma/3\alpha} + r_o & = r = r_1 \end{cases} \quad (\text{B.8})$$

$$V'(r) = 0 \begin{cases} -\sqrt{\gamma/3\alpha} + r_o & = r = r_{\text{min}} \end{cases} \quad (\text{B.9})$$

For Pd, $r_{\text{min}} = 2.7506 \text{ \AA}$. Choosing r_{cut} at 3.65 \AA and r_o at 3.2 \AA , parameters γ and δ are determined.

B.2 Fitting of the Pd-Pd 2nd neighbour interaction model.

For an interaction potential with a N-body term U_N and a pair potential term U_P ($=V(r)$) of the form:

$$U_{\text{TOT}}(i) = U_N + \sum_{j \neq i} U_P \quad (\text{B.10})$$

U_N is given by

$$U_N(i) = -AA \cdot f(\phi_i) \quad (\text{B.11})$$

where $f(\phi)$ and U_P are a function of the separation r between the Pd atoms, using Eq. (B.3) the pressure can be written as:

$$P = -\frac{4}{a^2} \left[\sqrt{2}V_1' + V_2' \right] + \frac{8AAf'}{a^2} \left[\sqrt{2}\phi_1' + \phi_2' \right] \quad (\text{B.12})$$

where it has been taken into account that the potential energy U_P and ϕ have contributions arising from the first and second shell of neighbours, that is:

$$U_P = 6 \cdot V_1 + 3 \cdot V_2 \quad (\text{B.13})$$

$$\phi = 12 \cdot \phi_1 + 6 \cdot \phi_2 \quad (\text{B.14})$$

The bulk modulus can be determined through Eq. (B.5) and (B.12) and it is given by

$$\begin{aligned} B = & \frac{4}{3a^2} \left[aV_1'' + aV_2'' - 2\sqrt{2}V_1' - 2V_2' \right] \\ & - \frac{8 \cdot AA}{3 \cdot a^2} \cdot \left[6 \cdot a \cdot f'' \cdot (\sqrt{2} \cdot \phi_1' + \phi_2')^2 \right. \\ & \left. + a \cdot (\phi_1'' + \phi_2'') - 2 \cdot (\sqrt{2} \cdot \phi_1' + \phi_2') \right] \end{aligned} \quad (\text{B.15})$$

Taking into account Eq. (B.13) and (B.14), the cohesion energy E_{coh} is:

$$E_{\text{coh}} = 6 \cdot V_1 + 3 \cdot V_2 - AA \cdot f(12 \cdot \phi_1 + 6 \cdot \phi_2) \quad (\text{B.16})$$

The stability condition at the potential minima is $dU_{\text{TOT}}/dr = 0$, therefore:

$$6 \cdot V_1' + 3 \cdot V_2' - AA \cdot \frac{12 \cdot \phi_1' + 6 \cdot \phi_2'}{\sqrt{12 \cdot \phi_1 + 6 \cdot \phi_2}} = 0 \quad (\text{B.17})$$

Additionally, the vacancy formation energy can be written as:

$$\begin{aligned} E_v^f = & -AA \cdot (12 \cdot \sqrt{11 \cdot \phi_1 + 6 \cdot \phi_2} + 6 \cdot \sqrt{12 \cdot \phi_1 + 5 \cdot \phi_2} \\ & - 18 \cdot AA \cdot \sqrt{12 \cdot \phi_1 + 6 \cdot \phi_2}) - (6 \cdot V_1 + 3 \cdot V_2) \end{aligned} \quad (\text{B.18})$$

Assuming the following analytical forms for U_P and U_N

$$U_P = V = (r - r_{\text{cut}})^2 \cdot (a + b * r + c * r^2) \quad (\text{B.19})$$

$$U_N = -AA \cdot \sqrt{(r - d)^2} \quad (\text{B.20})$$

and choosing some appropriate values for r_{cut} and d , the unknown parameters a , b , c and AA can be determined through conditions (B.15), (B.16), (B.17) and (B.18).

Appendix C

Electron Gas Term

The cohesion energy of a transition metal may be decomposed into contributions from the s and d electrons:

$$E = E_s + E_d \quad (\text{C.1})$$

In this work it was assumed that the s-electron contribution corresponds to the energy of an electron gas which can be taken into account in terms of a volume energy. The energy of the electron gas pro atom is taken as [Haf87]:

$$E_{eg} = Z_s \cdot Ryd \cdot [0.982 \cdot a_o^2/r_s^2 - 0.712 \cdot a_o/r_s + 0.031 \cdot \ln(r_s/a_o) - 0.110] \quad (\text{C.2})$$

where Z_s is the number of free s electrons pro ion, a_o is the Bohr radius ($a_o=0.5291777 \text{ \AA}$), Ryd is the rydberg constant ($Ryd=13.6058 \text{ eV}$), r_s is the radius of a sphere containing one electron on average (in this case, r_s is the mean electron density in the alloy) and it is related to the Wigner-Seitz radius r_{ws} ($r_s = r_{ws} \cdot Z_s^{1/3}$). The volume of the Wigner-Seitz sphere is equal to the atomic volume Ω . Therefore:

$$r_s = \left[\frac{3\Omega}{4 \cdot \pi} \right]^{1/3} \cdot Z_s^{-1/3} \quad (\text{C.3})$$

In this work, Ω was taken as

$$\Omega = \frac{a_o^3}{4} + \frac{a_o^3}{4} \cdot \frac{\Delta V}{V} \cdot x \quad (\text{C.4})$$

where a_o is the lattice constant of pure palladium and $\Delta V/V$ is the relative volume change under H loading.

Z_s is taken as:

$$Z_s = n_H \cdot x + n_{Pd} \cdot (1 - x) \quad (\text{C.5})$$

n_H and n_{Pd} are the electronic contributions provided by the H and Pd atoms respectively and x is the H concentration.

WILLIS ET AL [WH83] made a calculation of the total energy of a transition metal by extending the nearly free electron theory to include the effect of the d band to the cohesion energy for the pure crystal metal and obtained $n_{Pd}=1.5$. In this work in order to reproduce the experimental value of E_{coh} it was established that the number of s electrons n_{Pd} from Pd should be 0.4. With this value the experimental value of the cohesion energy of Pd can be reproduced. In order to reproduce the cohesion energy of the system PdH and the relative volume change at higher concentrations it is necessary to know the relative number of s electrons n_H for H, that is how many s

electrons participates in the bonding with the Pd atoms. Two different values for n_H were assumed. From an ab initio calculation [PNM81] it was established that $n_H = 0.2$, that is, the bonding between H and Pd is more of a covalent character. However, we used in the calculations involving the electron gas term the value $n_H = 1$ because as seen in Figure C.1 this value would deliver the expected energy contribution to the cohesion energy (See Figure C.2).

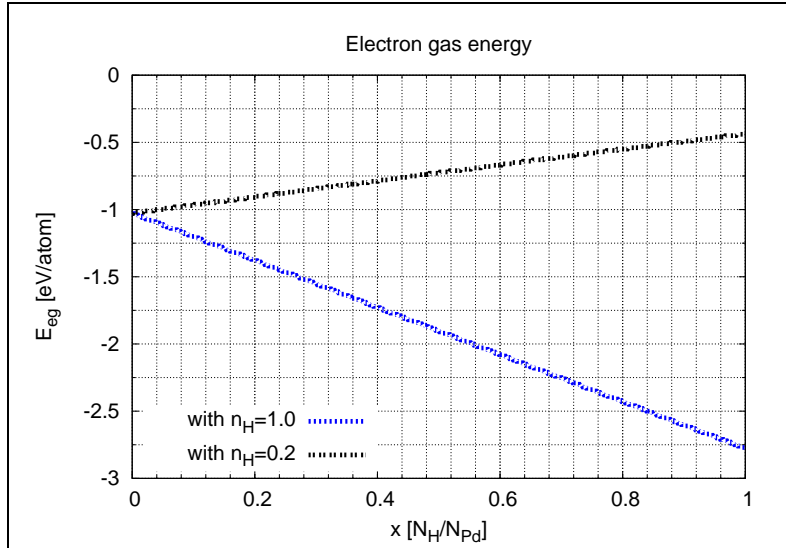


Figure C.1: Contribution to the total cohesion energy of PdH provided through the electron gas term as a function of hydrogen concentration. Two values for the relative number of s electron n_H were tested. With the value $n_H = 1$ an decreasing energy contribution is obtained. This energy decrease would give the right cohesion energy tendency under H loading (See figure below).

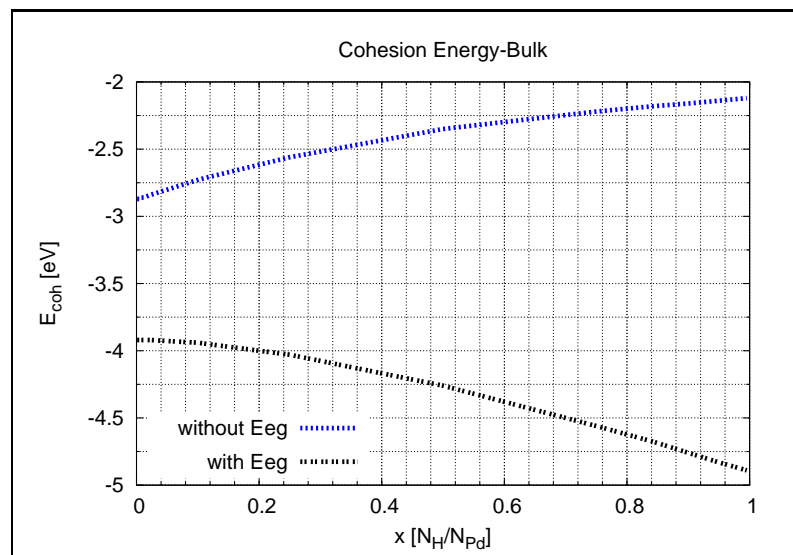


Figure C.2: Cohesion energy of PdH bulk as a function of hydrogen concentration. It is shown the tendency for the cohesion energy of PdH. Using ppI alone does not give the expected experimental tendency for the cohesion energy. Therefore the contribution of the electron gas term is used, and in this case the expected tendency can be reproduced. In this calculation was not taken into account the H-H interaction.

Acknowledgments

I would like to express my gratitude for the opportunity that I had in beginning this challenging work and also for the opportunity that I had in finishing it. To my supervisor, Prof. Dr. H. Teichler, whose expertise added considerably to my graduate experience. I would also like to thank PD. Dr. A. Pundt for the vast knowledge and for assistance provided at all levels of the research project. Additionally, I may thank Mrs. Saalfeld, Mrs. Kuba and Mrs. Haacke for all the instances in which their assistance helped me along the way.

I would also like to acknowledge the *Hydrogen in Metals Group* and the *Theory Group* for suggestions, critic, exchanges of knowledge throughout my graduate stay at the institute and also for the friendly atmosphere. Beyond expressing my gratitude for the acquired knowledge more than my gratitude goes to Joerg, Hamid, Boris, Imad, and Kevin for sharing with me at least 10000 hours in the computer room.

Especially, I may recognize everybody in the Institute of Material Physics who made this experience not only an opportunity to increase my knowledge in physics but remind me that our lives crossed over a path, which has an importance beyond a superficial level of existence which I may remember beyond everything else.

I would also like to acknowledge the DAAD and the Institute of Material Physics for the financial support.

My special thanks goes to Leonie, Johannes and Carsten for being my best and longest friends in Germany, and for sharing with me all good times and also for listening to my complains.

My biggest gratitude is for Kai and Gabriela. For encouraging me to work a lot and for taking me to have some cocktails when I more needed them because without them at my side this would definitely not be possible.

Por ultimo, esta vez este trabajo no se lo dedico al gato. Se lo dedico a mi Madre, Padre y a Tia Loca.

Curriculum Vitae

Personal Data

Name: Diana Marcano
Date of Birth: 10.12.1971
Birthplace: Caracas
Family status: Single
Nationality: Venezuelan

Education

Studies 8/90 – 12/95 Physics studies at Central University,
Caracas, Venezuela.
12/95 Bsc. Physics.
9/98 – 9/2000 M.Sc., Material Engineering at Simon Bolivar
University, Caracas, Venezuela.
Surface Engineering Center
Advisor: Prof. Dr. J. Lira-Olivares
Topic:
*Determination of porosity by means of Dielectric
Permittivity Measurements in ceramics*

since 4/2001 PhD studies at the Institute for
Material physics, Goettingen, in the Group from
Prof. Dr. H. Teichler

Professional Experience

4/96 – 12/97 Petrophysicist
PDVSA, Caracas

1/98 – 9/2000 Research Assistantship, Simon Bolivar University
Caracas

4/2001 – 3/05 DAAD Scholarship, PhD studies at the
Institute for Material physics, Goettingen

since 4/2005 Research Assistantship
Institute for Material Physics in Goettingen